Stony Brook University

PHYSICAL AND CHEMICAL MODIFICATIONS OF SURFACE PROPERTIES LEAD TO ALTERATIONS IN OSTEOBLAST BEHAVIOR

A Dissertation Presented

by

Kathryn Dorst

to

The Graduate School

in Partial Fulfillment of the

Requirements

for the Degree of

Doctor of Philosophy

in

Materials Science and Engineering

Stony Brook University

December 2013

Stony Brook University

The Graduate School

Kathryn Dorst

We, the dissertation committee for the above candidate for the

Doctor of Philosophy degree, hereby recommend

acceptance of this dissertation.

Yizhi Meng – Dissertation Advisor
Assistant Professor, Materials Science and Engineering

Dilip Gersappe - Chairperson of Defense
Professor and Graduate Program Director,
Materials Science and Engineering

Tae Jin Kim
Assistant Professor, Materials Science and Engineering

Michael Hadjiargyrou
Professor and Chair, Life Sciences, New York Institute of Technology

This dissertation is accepted by the Graduate School

Charles Taber

Interim Dean of the Graduate School

Abstract of the Dissertation

Physical and Chemical Modifications of Surface Properties

Lead to Alterations in Cellular Behavior of Osteoblasts

by

Kathryn Dorst

Doctor of Philosophy

in

Materials Science and Engineering

Stony Brook University

2013

Proper formation of the bone extracellular matrix (ECM), or osteoid, depends on the surface properties of pre-existing tissue and the aqueous chemical environment. Both of these factors greatly influence osteoblast migration, cytoskeletal organization, and calcium nodule production, important aspects when considering the biocompatibility of bone implants. By perturbing the physical and/or chemical micro-environment, it may be possible to elucidate effects on cellular function. To examine these factors, murine pre-osteoblasts (MC3T3-E1 subclones 4 and 24) were seeded on polydimethylsiloxane (PDMS) substrates containing "wide" micro-patterned ridges (20 μm width, 30 μm pitch, 2 μm height), "narrow" micro-patterned ridges (2 μm width, 10 μm pitch, 2 μm height), no patterns (flat PDMS), and standard tissue culture (TC) polystyrene as a control. Zinc concentration was adjusted to mimic deficient (0.23 μM), serum-level (3.6 μM), and zinc-rich (50 μM) conditions.

It was found that cells exhibited distinct anisotropic migration in serum-level zinc and zinc-deficient media on the wide PDMS patterns, however this was disrupted under zinc-rich conditions. Production of differentiation effectors, activated metalloproteinase-2 (MMP-2) and transforming growth factor – beta 1 (TGF-β1), was increased with the addition of exogenous zinc. Early stage differentiation, via alkaline phosphatase, was modified by zinc levels on patterned polydimethylsiloxane (PDMS) surfaces, but not on flat PDMS or tissue culture polystyrene (TC). Late stage differentiation, visualized through calcium phosphate nodules, was markedly different at various zinc levels when the cells were cultured on TC substrates. This susceptibility to zinc content can lead to differences in bone mineral production on certain substrates if osteoblasts are not able to maintain and remodel bone effectively, a process vital to successful biomaterial integration.

Dedication Page

I dedicate the work of this dissertation to my parents, Karen Dorst and Anthony Cusano. Their constant love and support has allowed me to be successful in my endeavors and I appreciate all they do and have done for me. I also dedicate this work to my fiancé, Paul Mark, whom has been there for me through all the trials of graduate school and has always believed in me and encouraged me through everything.

Table of Contents

List of Figures

(3.6 μM) and zinc-rich (50 μM) media conditions were isolated on day 8 and 11, normalized to total protein concentration at 17.90 μg/lane.

Figure 4.2. TGF-β1 activation for subclone 4 MC3T3-E1 cell lysates collected on (A) day 8 and (B) day 11, normalized to total protein concentration (A & B) and to percentage of serum-level (3.6 μM) samples (C). A single asterisk (*) indicates a $p<0.01$ level of significance while double asterisks (**) indicate a $p<0.05$ level of significance.

Figure 4.3. ALP production (indicated by dark purple color) by subclone 4 MC3T3-E1 cells in: (A) 3.6 μM zinc, (B) 50μM zinc.

Figure 4.4. Von Kossa staining for calcium phosphate bone nodules (indicated by black areas) of subclone 4 MC3T3-E1 cells on: (A) TC, (B) flat PDMS (C) wide PDMS ridges, (D) narrow PDMS ridges. Images representative of 30 fields of view. Bar = 100 μm.

Figure 4.5. Differentiation timeline on TC, flat PDMS, and patterned PDMS.

Figure 5.1. Cell coverage. Growth of subclone 24, MC3T3-E1 pre-osteoblast cells on various substrates with modifications of Zn concentrations after incubation for 24 hours. Double asterisks (**) indicate a $p<0.01$ difference.

Figure 5.2. Actin Immunofluorescence. Immunofluorescence micrographs of subclone 24 MC3T3-E1 pre-osteoblasts 24 hours after seeding at various Zn concentrations on (A) TC, (B) flat PDMS, (C) wide PDMS FN, (D) narrow PDMS FN. Arrows indicate discrete lamellipodia protrusions while arrowheads in (C) indicate actin clustering on the edge of a micropattern. Bar = 50 μm.

Figure 5.3. (A) Cell spreading area and circularity (B) were computed from fluorescence micrographs in Fig 5.2. A-D. Double asterisks (**) indicate a $p<0.01$ difference.

Figure 5.4. (A) Cell alignment computed from Fig. 5.2 A-D, where 0 degrees indicates complete alignment with patterned ridges/y-axis. (B) Cell shape aspect ratio was calculated from the same set of images and represents the use of ImageJ's ellipse fitting tool

to determine ratio of cell width/length. Double asterisks (**) indicate a $p<0.01$ level of significance.

Figure 5.5. ALP activity (days 7 and 10) of subclone 24 MC3T3-E1 cells on: (A) TC, (B) flat PDMS, (C)wide PDMS ridges, (D) narrow PDMS ridges with modified Zn concentrations.

Figure 5.6. Von Kossa staining for calcified nodules (days 21 and 28) of subclone 24 MC3T3-E1 cells on: (A) TC, (B) flat PDMS (C) wide PDMS ridges, (D) narrow PDMS ridges with modified Zn concentrations. Bar = 100 μm.

List of Abbreviations

ALP – Alkaline phosphatase

ECM – Extracellular matrix

ELISA – Enzyme-linked immunosorbant assay

FN - Fibronectin

GBD - Gelatin binding domain

MEMS – Microelectromechanical systems

MMP-2 – Metalloproteinase-2

MSF - Migration stimulating factor

OCN – Osteocalcin

PBS – Phosphate buffered saline

PDMS - Polydimethylsiloxane

SEM – Scanning electron microscopy

TC - Tissue culture polystyrene

TGF-β1 – Transforming growth factor – beta 1

TβRI – TGF- β receptor (I)

VK – von Kossa

XRD – X-ray diffraction

Acknowledgments

First and foremost, I would like to acknowledge my advisor, Yizhi Meng, for her never-ending guidance throughout my graduate career. I feel very fortunate to be her first grad student, as I learned so much from her first-hand. Her advice and support went beyond the lab, to life and career decisions, and for that I'm very thankful to have had her as my mentor.

Many thanks to Dilip Gersappe and Paul Mark for their patient help with developing random walk models. Thanks also to Derek Rammelkamp for his help in creating Zn-stripped FBS.

Research was carried out, in part, at the Center for Functional Nanomaterials, Brookhaven National Laboratory, which is supported by the U.S. Department of Energy, Office of Basic Energy Sciences, under Contract No. DE-AC02-98CH10886. Kathryn was supported under a GAANN (Graduate Assistance in Areas of National Need) fellowship during the last two years of graduate school. Dilip Gersappe would like to acknowledge support from NSF CBET 1033623.

Publications

This is a list of peer-reviewed publications, book chapters and conference proceedings that were produced during the course of the dissertation.

PEER REVIEWED JOURNAL PUBLICATIONS

K. Dorst, D. Rammelkamp, M. Hadjiargyrou, D. Gersappe, and Y. Meng, "The Effect of Exogenous Zinc Concentration on the Responsiveness of MC3T3-E1 Pre-Osteoblasts to Surface Microtopography: Part I (Migration)" *Materials*, **2013**, *6*, 5517-5532.

K. Dorst, D. Rammelkamp, M. Hadjiargyrou, and Y. Meng, "The Effect of Exogenous Zinc Concentration on the Responsiveness of MC3T3-E1 Pre-Osteoblasts to Surface Microtopography: Part II (Differentiation)" (in preparation)

K. Dorst, D. Rammelkamp, and Y. Meng *et al.*, "Osteoblast clonality determines bone mineral deposition" (in preparation)

Master's Thesis: "Micropatterned Anisotropic Topography Directs Osteoblast Migration and Differentiation" (2012)

CONFERENCE PRESENTATIONS

K. Dorst, E. Farquhar, M. Chance, Y. Meng. "The Role of ECM Proteins in Mediating Osteoblast Motility and Differentiation." International Materials Research Congress XXI, Cancun, Mexico (August 2012).

K. Dorst, C. Zhang, Y. Meng. "Effect of MMP-Mediated Fibronectin Proteolysis on Osteoblast Motility." Materials Research Society Spring 2012 Meeting, San Francisco, CA (April 2012).

C. Zhang, **K. Dorst**, J. Bohon, Y. Meng. "The influence of fibronectin proteolysis on osteoblast mineralization." Materials Research Society Spring 2012 Meeting, San Francisco, CA (April 2012).

K. Dorst, X. Zhao, A. Stein, M. Hadjiargyrou, Y. Meng. "The Role of Physical Modulation of Substrate Properties on Osteoblast Differentiation." Materials Research Society Fall 2011 Meeting, Boston, MA (December 2011).

K. Dorst, J. Horne, Y. Meng. "The Effect of Substrate Properties on Osteoblast Shape, Adhesion, and Motility." Sigma Xi Northeast Regional 2011 Meeting, Stony Brook, NY (April 2011).

CONFERENCE PRESENTATIONS (continued)

K. Dorst, J. Horne, Y. Meng. "A Comparative Study of Osteoblasts and Osteosarcoma Cells in Conditioned Media." American Society of Cell Biology, 50th Annual Meeting, Philadelphia, PA (December 2010).

K. Dorst, Y. Meng. "The Role of Chemical and Physical Modulation of Substrate Properties on Osteoblast Adhesion, Motility and Differentiation." Gordon Research Conference on Biomineralization 2010, New London, NH (August 2010).

K. Dorst, A. Stein, Y. Meng. "Adhesion, Migration and Differentiation Behavior of Osteoblasts on Various Surface Topographies." Poster award at Brookhaven National Lab's Joint National Synchrotron Light Source (NSLS) and Center for Functional Nanomaterials (CFN) Users' Meeting 2010, Upton, NY (May 2010).

K. Dorst, Y. Meng. "Effect of Surface Topography and Chemistry on Osteoblast Biomineralization." Materials Research Society Fall 2009 Meeting. Boston, MA (December 2009).

Chapter 1: Introduction

Background and Significance

Motivation

Advancing medical technologies have provided people with the ability to live longer than ever imagined, while also vastly improving the quality of life for millions. In 2009 the number of people aged 65 and older in the U.S. represented 12.9% of the population, 39.6 million people. In less than 20 years time, by the year 2030, this number is expected to rise to 19% of the population, an astonishing 72 million people in the U.S. alone.[1] Between 1990 and 2000, there was nearly a 25% increase in hip fractures worldwide.[2] One in three women and one in five men over the age of 50 will experience an osteoporotic fracture in their lifetime.[3] These numbers illustrate the dramatic increase in elderly population that will require artificial replacements in the next several decades and beyond. In 2006, more than 450,000 artificial knee replacements and nearly 180,000 artificial hip replacements were performed, according to the National Center for Health Statistics.[4] However, present-day artificial knee and hip implants have several flaws, causing them to only last an average of 15 years. These include rejection by the body's tissues and mechanical failure due to a more physically active population.[5] With a rapidly increasing elderly population, the demand for better strategies in regenerative medicine is expected to rise significantly.

The foundation of better bone implants rests on understanding cell adhesion mechanisms and what influences them. This bottom-up approach focuses on material properties, how proteins adsorb on these materials when cells first interact with them, how cells grow, migrate, and communicate with each other, and finally, how cells organize into the initial layers of bone tissue. The complex, intercalated pathways that occur are still not

widely understood but piece by piece knowledge is gathered and continually added to existing theories that can influence how prosthetics are manufactured in the future.

Osteoblasts and biomaterials interactions

The Extracellular Matrix (ECM)

The study of mechanotaxis (also referred to as durotaxis) among cell lines in the bioMEMS field involves the mimicry of the extracellular matrix (ECM). The ECM is a region of proteins and filaments that interconnects the outside of cells into networks of tissues (**Fig. 1.1**). This organizational scaffold was once thought to be merely structural in use, but now has been recognized as a much more complex player in cell to cell interactions.[6] The ECM is now realized as playing an important role in several vital processes in cell adhesion, survival and differentiation, migration, and proliferation.[6]

Osteoblast differentiation

Osteoblasts are derived from the mesenchymal cell line, along with adipocytes, osteoclasts, chondrocytes, and myocytes. The determination of cell fate is regulated through expression of a series of osteo-specific genes such as that of the bone-morphogenic proteins (BMPs) and the core binding factor a1 (Cbfa1).[7] Additionally, growth factors such as transforming growth factor – beta 1 (TGF-β1) and proteases such as metalloproteinase-2 (MMP-2) play large roles in the intermediate stages of osteoblast maturation.[8] The osteoblast phenotype is demonstrated through the increased production of alkaline phosphatase (ALP), osteocalcin (OCN), and osteopontin (OPN), and finally discrete calcium phosphate (hydroxyapatite) nodules.[7]

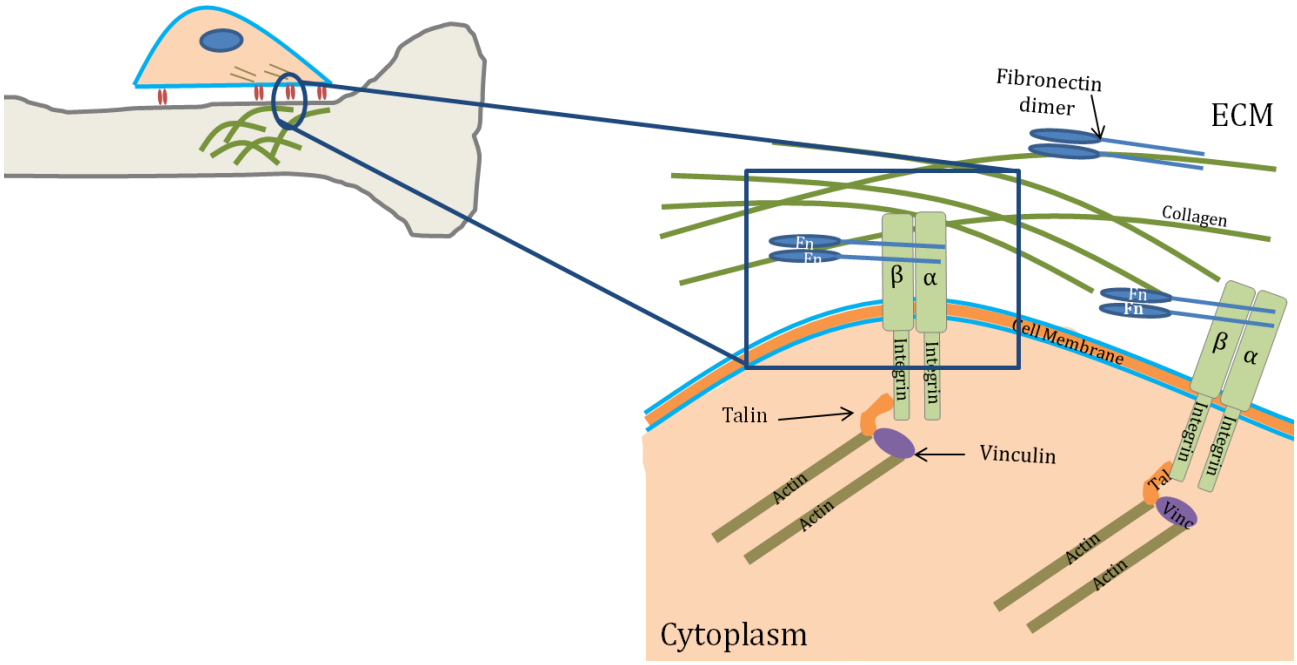

Figure 1.1. Overview of the Extracellular matrix (ECM).
(*Modified from Nature education 2010*)

The production of these phenotypic proteins reflects cells' adherence to the ideal osteoblast maturation sequence. The peak production of these proteins occurs along a strict timeline, where the surge and ebb of production will often determine continuation of the differentiation pathways (**Fig. 1.2**). Osteoblast differentiation can be characterized by three stages: proliferation, maturation of the ECM, and mineralization of the ECM.[9] As cells divide they eventually become confluent, producing copious amounts of collagen in their matrix while mitosis slows to a halt. The tapering of proliferation signals the start of ALP production with a peak observed around day twelve and continuing to day eighteen (**Fig. 1.2**).[9] This enzymatic protein is the main source of inorganic phosphate that is combined with calcium ions from the blood to form hydroxyapatite (calcium phosphate) bone nodules.[10] However, this process does not occur in a single linear step, as cells must loosen their loci to migrate and form multi-layers with collagen fibrils in the ECM, a process regulated by the proteolytic activity of MMPs.[11] The TGF-β1 protein responsible for the mid-late maturation of the ECM is present throughout the early mineralization process but reaches peak levels midway through as MMPs have been found to be one of the maximal activators of this protein.[11,12] As the maturation process continues, the levels of ALP, MMPs, and TGF-β1 decrease around day 21 while several genes, such as osteocalcin, osteopontin, and bone sialoprotein, show increased expression and trigger the final mineralization stage that peaks around twenty-eight days resulting in nodule formation (**Fig. 1.2**).[13]

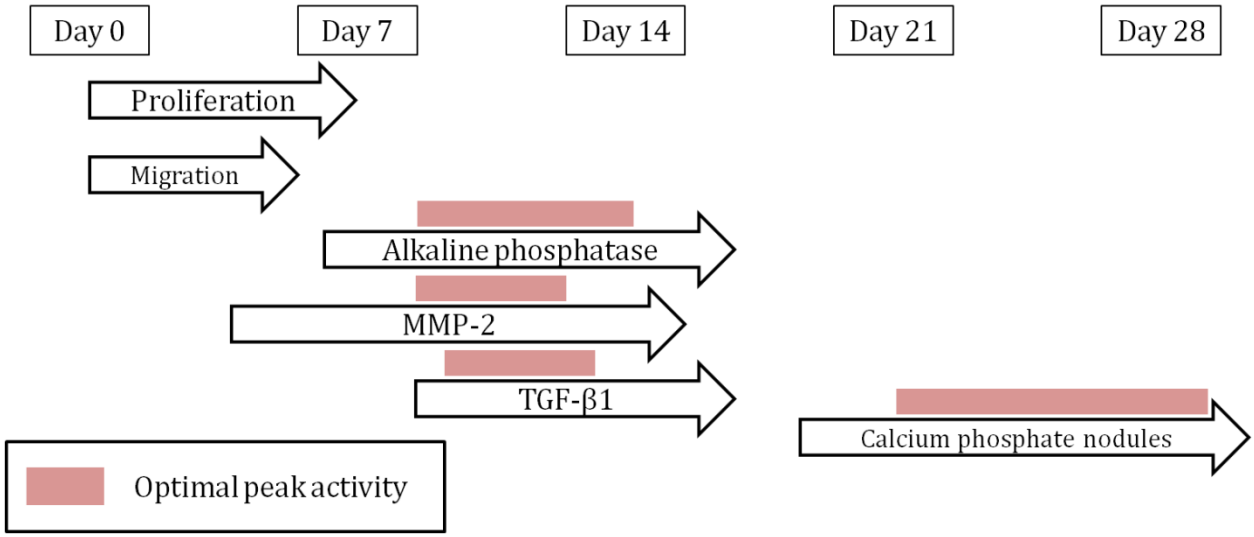

Figure 1.2. Timeline of osteoblast maturation

ECM forces

The mechanical forces the ECM imposes on adhered cells not only can direct cell proliferation, migration, and differentiation but also have shown to have an effect on cell alignment. As the Young's modulus of the ECM increases, cells produce more stress fibers (indicating more force generated by the cells) and additionally align these fibers centripetally from the nucleus.[14] It is proposed that harder surfaces generate more tension in the cell's cytoskeleton that enables the cell's focal adhesion complexes to attach to the surface with better "grip" while softer substrates lead to cells' inability to stretch and form large outward directional cytoskeletal networks due to these complexes losing traction and slipping (**Fig. 1.3**). Thus, with a more rigid substrate surface, cells have a greater spreading area and generate more directed traction and tensional forces.[15] This tension has been found to be necessary to engage the cytoskeleton and to open stretch-activated channels (SAC).[16] These channels allow the influx of calcium ions into the cell, which, through calcium signaling cascades, induces an increase in alkaline phosphatase and osteopontin, important regulators of bone mineralization.[17-20] Repetitive rather than continuous stretching has been found to have more of an inductive effect on cells, modulating the area and density of focal adhesions (such as vinculin and paxillin), increasing tyrosine phosphorylation needed for F-actin polymerization, and increasing the amount of calcium deposition in bone mineral nodules.[21-24]

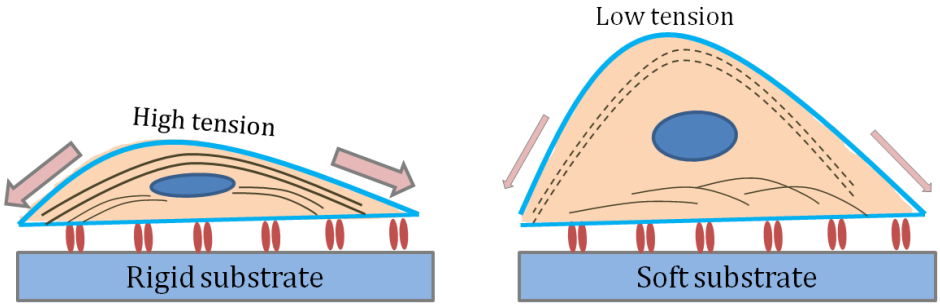

Figure 1.3. Cell tension as a function of cell rigidity.
(*Modified from Kihara et al.*[25])

Substrate rigidity

The rigidity of the ECM (or synthetic cell culture substrate) can induce changes in the organization of the cytoskeleton via signaling of integrins. Khatiwala *et al*. reported an exemplary study of MC3T3-E1 pre-osteoblasts in which the role of the rigidity of substrates was investigated using polyacrylamide hydrogels.[26] It was demonstrated that these pre-osteoblastic cells proliferated and differentiated into osteoblasts that mineralized new bone much faster and to a greater extent on the stiffer substrates. These effects have also been studied previously with smooth muscle cells, as well as fibroblasts, which exhibited faster migration speeds when traveling from softer substrates to stiffer ones.[14,15,27-29]

The preferential migration of osteoblasts toward stiffer substrates supports conclusions from other studies investigating the effect of substrate rigidity on lineage outcomes. Engler *et al.* found that matrix stiffness greatly affected the differentiation outcome of several progenitor cells. Mouse stem cells grown on substrates with varying elastic moduli were found to differentiate (express lineage markers) into neurons, myoblasts, or osteoblasts depending on the rigidity of the substrate material.[30] Other studies confirmed these findings, demonstrating that differentiated neurons are more likely to extend dendritic arms on soft scaffolds, mimicking the small elastic modulus of brain tissue, while optimal cardiomyocyte differentiation has been found to occur on rigid but non-stiff scaffolds that mimic striated muscle fibers.[31, 32]

BioMEMS

In the last decade, synthetic implant technologies have been greatly improved by advancements in the field of bioMEMS (bio-microelectromechanical systems). The MEMS

field, first developed alongside the creation of narrower, more powerful computer microprocessors, has contributed to the evolution of several new technologies in biological roles.[33,34] Using lithographic patterning techniques previously reserved for circuit construction, synthetic biomimetic scaffolds can be rendered to enhance the growth of cells and tissues. Recent studies in this field have used these scaffolds *in vitro* seeking to provide information on how these scaffolds would fare *in vivo*. Of particular interest, are the uses of topography and variation of rigidity via lithographic patterning techniques on these biomimetic scaffolds to understand how cells can be guided by these cues via mechanotaxis.

Patterned substrates

Scaffold rigidity is only one of many factors that have been found to greatly affect the destiny of progenitor cells. A developing technique that has risen to the forefront of bioMEMS technologies is the micro- and nano-patterning of substrate surfaces. These micropatterns are often created using standard photolithography and are then transferred to a predominant material in the field of bioMEMS: polydimethylsiloxane (PDMS). This optically clear, biologically inert, rubber-like polymer is often used as a cell substrate surface because of its gas permeability and biocompatibility.[35, 36] These topographical features mimic those that would be present on the ECM as well as surfaces *in vivo*. The narrow ridges and grooves on the ECM (or in the case of tissue engineering, synthetic substrates mimicking bioscaffolds) have been found to promote cell adherence in several cell lines, including osteoblasts, fibroblasts, and skeletal stem cells.[37-46] These topographical "hills" and "valleys" can be replicated as micropatterns on synthetic bone implant surfaces and may decrease the chance of rejection of an implant *in vivo*. In fact, these patterns have

also been found to not only increase cell adherence but to also induce differentiation in progenitor cell lines and can directly affect gene and protein expression (**Fig. 1.4**).[47-49]

By creating patterns of various shapes (such as rectangles, squares, and rings), studies have also been able to elucidate how these structures create varying amounts of stress and strain on cell morphology.[50] A study by Ruiz *et al.* concluded that cells on outer edges of patterns like squares or rectangles were under high stress while cells adhered to inner edges of patterns such as rings or ellipses were under low stress. These stresses were seen to correlate to cell lineage destiny when given differentiation media: cells under high stress formed osteocytes while those under lower stress formed adipocytes.[51]

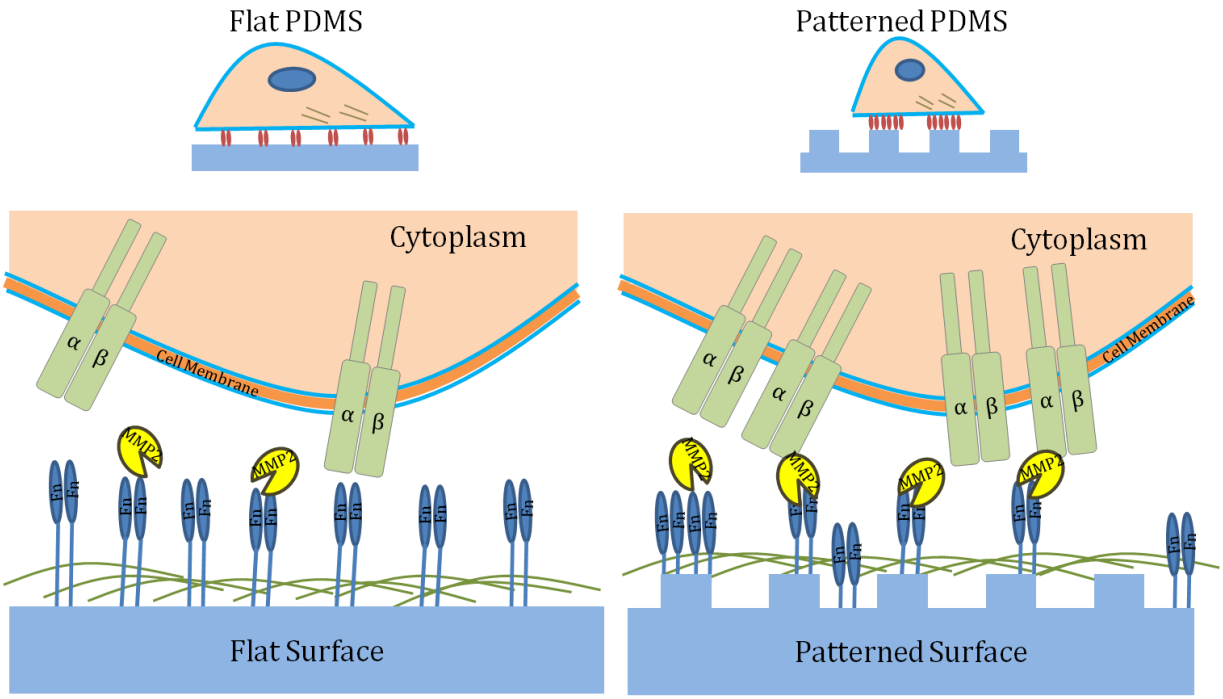

Figure 1.4. Possible scenario of how patterned surfaces may cluster focal adhesion complexes and proteinases.

Topographical effects

Mechanical cues from substrates not only lie in modular characteristics but also in topographical ones as well. Studies of micropatterns of parallel ridges and grooves have elucidated exciting new prospects in the field of regenerative medicine.[15] In a study by Soboyejo *et al*. the integration of linear micropattern gradients on PDMS, by standard photolithography was investigated using osteosarcoma cells.[33,34] Cells were observed to adhere well to the patterns, aligning their actin fibers along the direction of the ridges, as compared to the cells on the non-patterned PDMS surfaces that adhered in random directions. This directional alignment due to contact guidance is important factor in wound healing: less scar formation and immune response from implantation of abiotic materials would be present in materials that were micropatterned in this way according to their findings.[52, 53] Other studies using keratocytes, smooth muscle cells, and epithelial cells have also found this actin directional alignment, resulting in parallel configuration of focal adhesions and traction forces.[34, 54]

The focal adhesion complex

Integrins

Integrins are one of the major components of the focal adhesion complex. In the last decade, it was discovered that these proteins play a role in the communications between the ECM and the underlying cytoskeleton, providing a direct link by which information is exchanged bidirectionally and dynamically (**Fig. 1.5**).[55,56] Composed of α and β subunits, these heterodimeric receptors have been found to be responsible for initial cell adhesion as well as facilitating cell-cell and cell-ECM communications.[57] Integrins not only work directly

as a physical link between the ECM and the outside cell surface, but also play a role in triggering protein kinase pathways (FAK, Src, MAPK), thus indirectly controlling various mitotic functions.[58,59] The inventive use of an arginine-glycine-aspartic acid (RGD) amino acid chain in regenerative tissue engineering studies is commonly employed for changing the surface chemistry of synthetic scaffolds. This residue is of particular importance, as it is an integrin-binding specific peptide sequence present in type 1 collagen.[60] This chain, present in ECM ligands and often functionalized on polymer substrates, serves as an artificial ECM-linking system on the substrate surface and has a high affinity for cell integrins.[61], [62] The integrin receptors, once ligated to the ECM via this RGD sequence, directly link the ECM to the cytoskeleton and provide a pathway which integrates intracellular and extracellular events. Recent studies have shown that ordered RGD ligand dispersion results in better cell spreading and adhesion.[63-69]

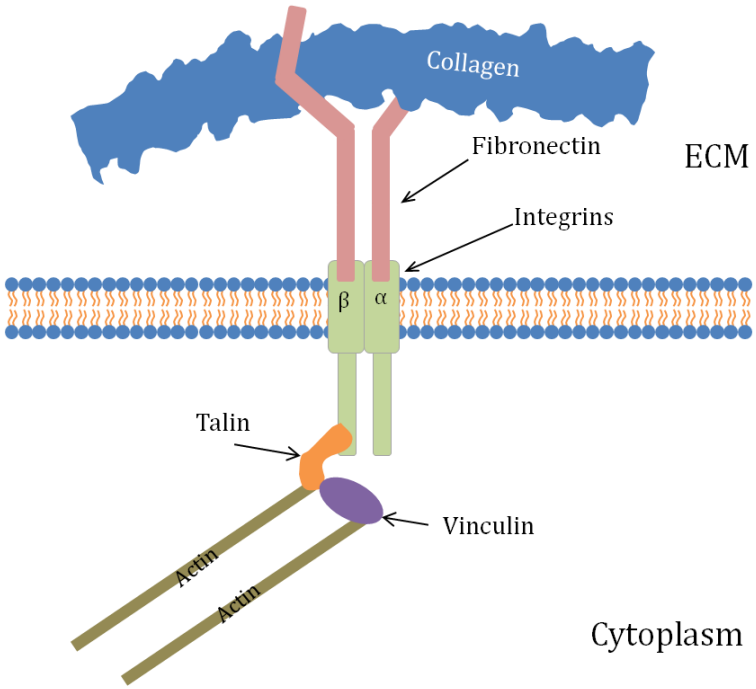

Figure 1.5. The focal adhesion complex.
(*Modified from Nature 2010 education*)

Fibronectin (FN)

Fibronectin (FN) is a 440-500kDa ECM associated protein that is vital to cell adhesion and motility. This protein is generally found *in-situ* as a dimer, composed of two identical monomers. These monomers consist of three repeating modules, FNI, FNII, FNIII. FN exists in two forms in the body: a soluble, globular plasma form in the blood and an insoluble, fibrillar form as a major constituent of the ECM network. The process of fibrillogenesis, transformation from the plasma form to the fibril form, is not completely understood. It is thought that cytoskeletal tension causes FN in the ECM to unwind and expose cryptic sites.[70-72] These sites have been found in several modules, specifically the ^{1}FNIII and ^{2}FNIII domains have been suggested as points of nucleation, where FN fibrillogenesis would initiate.[73] Migration of epithelial cells have shown a biphasic dependence on this fibril formation via the FNIII domains. While matrix polymerization is a requirement for cell adherence and migration, the addition of exogenous amounts of FN after attachment has shown to cause a rapid decrease in migration speeds, perhaps as a feedback mechanism switch reverting from a migration state to a fibrillogenesis state.[74]

Investigations into how FN transforms shape and exposes binding domains have given rise to studies dealing with the fragmentation of FN into grouped and individual domains. These fragments have been found to have proteolytic and motogenic capabilities that are not found in full-length, intact FN.[75] Among these, binding sites for fibrin, heparin, collagen and gelatin, and integrins have been discovered.[76,77] The 70kDa N-terminal fragment containing nine type I modules ($^{1-9}$FNI), two type II modules ($^{1-2}$FNI), and part of the beginning of a type III module (^{1}FNIII) is of particular interest because it has been shown to be necessary for both migration and cell development.[78] This region, called the

migration stimulating factor (MSF), encompasses a 42kDa gelatin binding domain (GBD) and a 25kDa heparin 1 (Hep 1) binding domain (**Fig 1.6**). Within the GBD are two conserved amino acid residues, isoleucine-glycine-aspartic acid (IGD), in the ^{7}FNI and ^{9}FNI modules that have been shown to be implicated in migration in fibroblasts.[78] The IGD sites in the GBD domain have also been shown to be necessary for the phosphorylation of focal adhesion kinase (FAK), a process known to regulate cell migration.[59,79] Interestingly, two other IGD residues also exist in the Hep 1 domain in the ^{3}FNI and ^{5}FNI modules, but have been found to be motogenic only with the addition of vitronectin, suggesting that the $\alpha_v\beta_3$ integrin is important for this activity.[75,79]

The GBD has been found to not only have binding and motogenic activity but also proteolytic (gelatinase) activity as well.[80,81] This domain presents a similar zinc-dependent binding motif as the gelatinase metalloproteinases 2 and 9 (MMP-2 and MMP-9), but has a different inhibition profile and is able to autolyse under certain conditions.[82-85] The gelatinase MMPs and GBD share a HEXXH consensus sequence (a zinc-binding domain) that has been found to be responsible for the degradation of ECM components, a process necessary for migration to occur.[86] The exposure of FNI cryptic sites like GBD could cause matrix degradation through the unwinding of the triple helix of collagen 1 (a major constituent of the ECM), allowing RGD sites to be exposed and bind to $\alpha_v\beta_3$ integrins.[60,87]

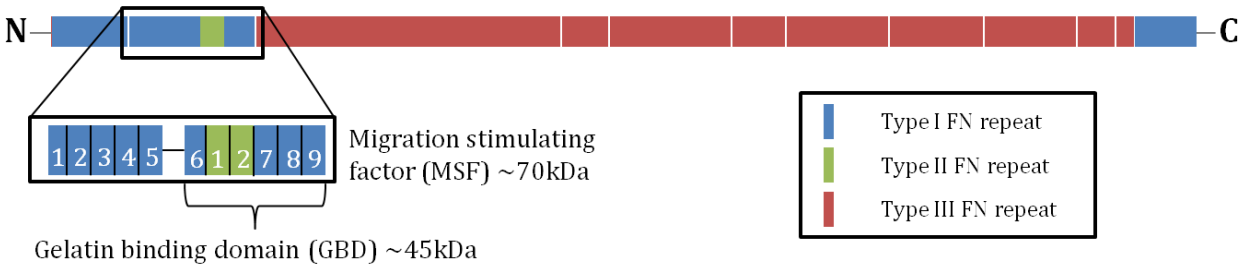

Figure 1.6. A diagram of the domains of fibronectin.
(*Modified from Ellis et al.*[75])

Differentiation effectors

Metalloproteinases (MMPs)

The investigations of FN autoproteolysis lead to the discovery that other proteases can cleave FN into active fragments. The unwinding of the FN molecule allows cryptic sites such as the GBD to be exposed and cleaved by MMP-2.[84,88-90] The MMP-2 site responsible for FN cleavage is located in the C-terminal hemopexin domain (PEX; **Fig. 1.7**).[91] This domain also has an important role in activating MMP-2: binding with tissue inhibitor-2 (TIMP-2; an activator only in small concentrations[92]) during the activation of pro-MMP-2 (precursor to MMP-2) while it is bound to the membrane type 1 MMP (MT1-MMP; aka MMP 14) complex (**Fig. 1.8**).[93,94]

The activation of MMP-2 via MT1-MMP resulting in FN fragmentation down-regulates fibrillogenesis. It has been demonstrated in epithelial cells and fibroblasts that the inhibition of FN fibril formation results in ECM degradation via endocytosis and remodeling and thus cells migrate faster on the existing matrix.[74,88,95] The degradation of the ECM by MMPs lowers the binding activity of MT1-MMP to the matrix via the β_1 integrin, which then down-regulates MT1-MMP, thus lowering MMP-2 activity and decreasing migration (**Fig. 1.9**).[96] One of the substrates of the gelatinase degradation is an inactivated chemokine fragment, monocyte chemoattractant protein 3 (MCP-3).[91] This protein binds to chemokine receptors and impedes migration and calcium signaling.[97] The lowering of MMP-2 activity allows accumulation of the matrix once again which up-regulates MT1-MMP and MMP-2 in a feedback cycle.[98,99]

A similar feedback loop is also seen with MMP-1 degrading collagen-1 via the $\alpha_2\beta_1$ integrin in keratinocytes.[100] Interestingly, a new form of F-actin structures, called invadosomes, have been found to degrade type 1 collagen fibrils and induce MMP-2 activity through the MT1-MMP system, however, they are independent of β_1 integrin.[101]

Needless to say, MMPs are crucial to the proper formation and remodeling of the ECM. In regard to osteogenesis, MMP-2-null and MMP-9-null mice have been found to have skull defects and delayed bone growth.[102,103] MT1-MMP-null mice have shown severe skeletal defects, osteopenia, and fibrosis of soft tissue.[104] Double knockout MMP-2 and MT1-MMP mice resulted in severe vascular defects and postnatal death.[102] Studies of human mesenchymal stem cells and pre-osteoblasts have shown that MT1-MMP is required for production of early differentiation marker alkaline phosphatase (ALP). [105-107] MMP-9 and MMP-13 were shown to regulate murine osteoblast ECM remodeling of soft tissue, collagen and cartilage as well as osteocalcin (OCN), at an earlier timepoint than MMP-2 regulation of mineral nodules during bone repair of a fracture.[108,109] MT1-MMP also transiently regulates bone mineral nodule formation: the persistence of MT1-MMP impairs formation of nodules, while a fluctuating pattern of expression is required for nodule formation.[105,110]

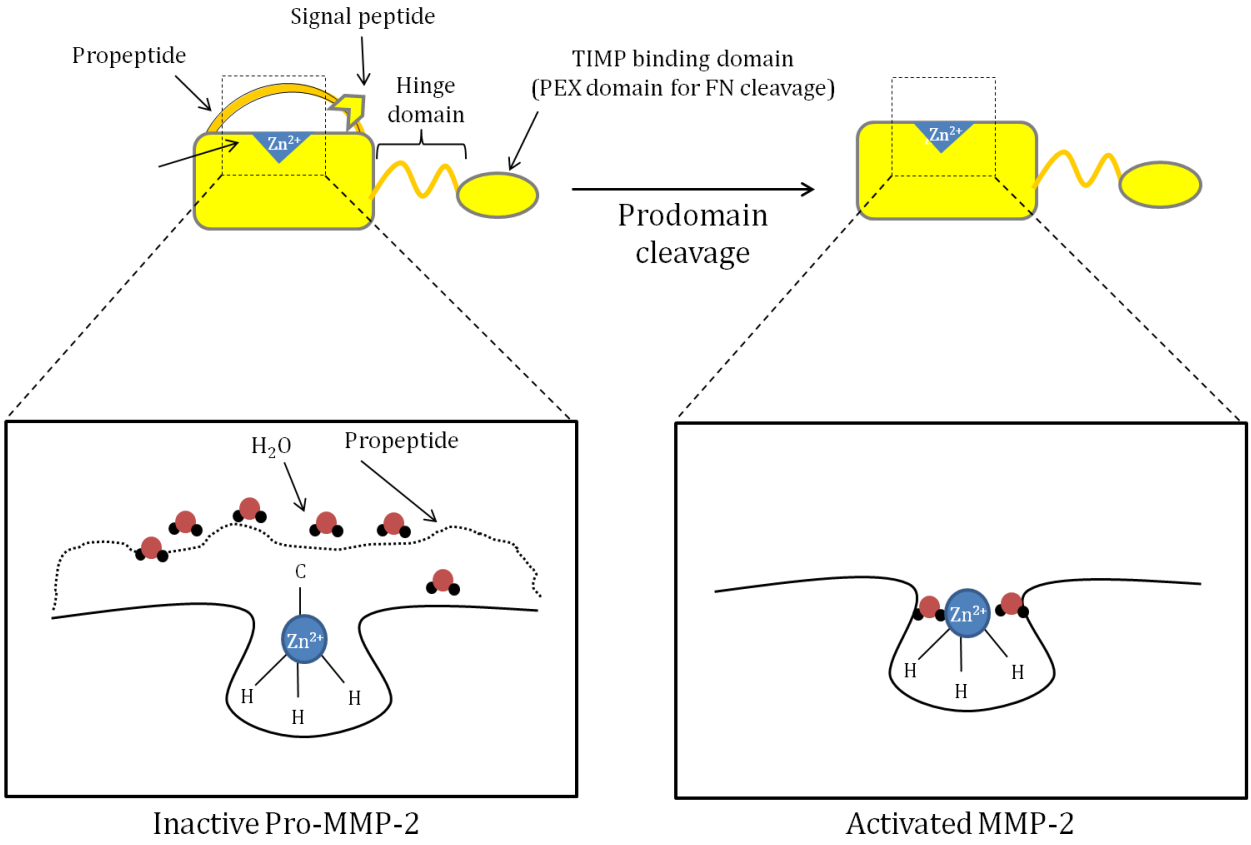

Figure 1.7. The structure and possible model of activation of MMP-2.
(*Modified from Bozzuto et al.*[11])

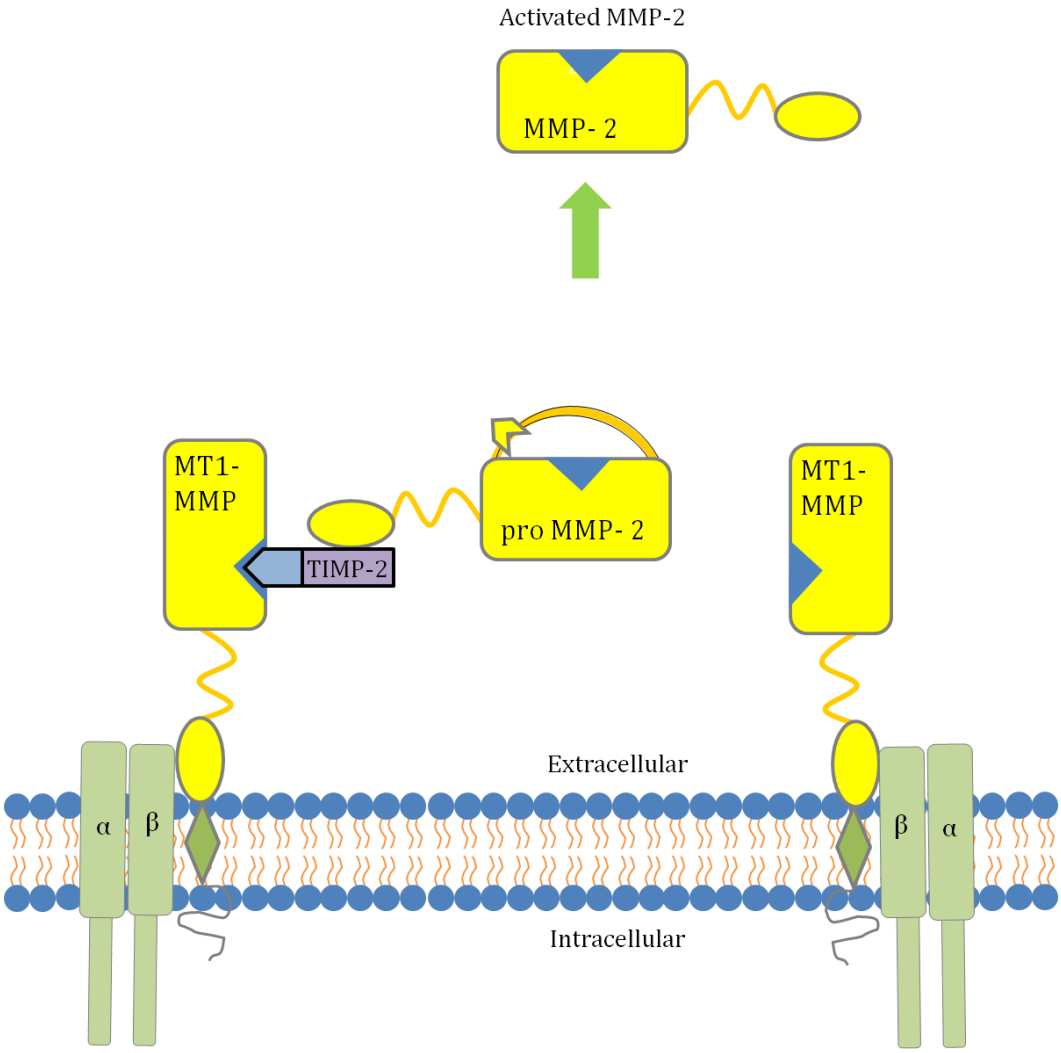

Figure 1.8. The possible model of activation of MMP-2.
(*Modified from Bozzuto et al.*[11])

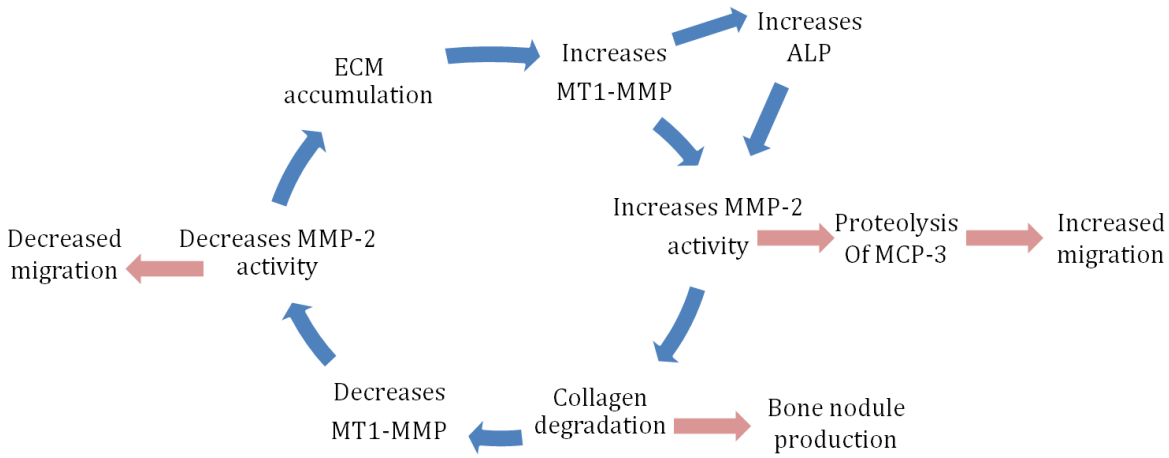

Figure 1.9. The cycle of MMP-2 activation and inhibition during osteoid formation.

Transforming growth factor – beta 1 (TGF-β1)

Not only is MT1-MMP a key regulator of MMP-2 activation but it also serves to regulate activation of a crucial cytokine for bone remodeling, TGF-β1. This growth factor is in the same superfamily as bone morphogenic proteins (BMPs) and is found in three isoforms (β1, β2, and β3).[111] TGF-β1 is the most abundant isoform and is found in high quantities in bone.[112] This factor plays a role in a number of diverse biological processes such as cell migration, proliferation and differentiation. In particular, TGF-β1 is especially important in regulating bone formation and is a known chemoattractant of osteoblasts.[111,113]

Secreted in its latent form, the 390 amino acid protein complex consists of several parts: a 112 amino acid mature peptide, with a latency associated peptide (LAP; 249 AA), and the signal peptide (29 AA).[12,111] The LAP is a non-covalently associated region that confers latency to the mature peptide, shielding the binding site from interacting with TGF-β1 receptors. The term "small latent complex" (SLC) is used to refer to the LAP- TGF-β1 inactive complex. This SLC can covalently attach to the latent TGF-β binding protein (LTBP) to create the large latent complex, LLC, which is the final secreted form (**Fig. 1.10**). This large complex, responsible for the correct folding and secretion of the mature peptide, is then directed to the ECM and stored through binding between the LTBP and the ECM.[111,114] The LTBP forms a network that coincides with the network formed by FN fibrillogenesis during early bone development, with the latter being exclusively necessary to form the prior.[115-117] FN helps to localize the LTBP to the ECM by binding to the hinge domain; FN-null cells minimally activate TGF-β1 and poorly incorporate LTBP-1 into their matrix.[118]

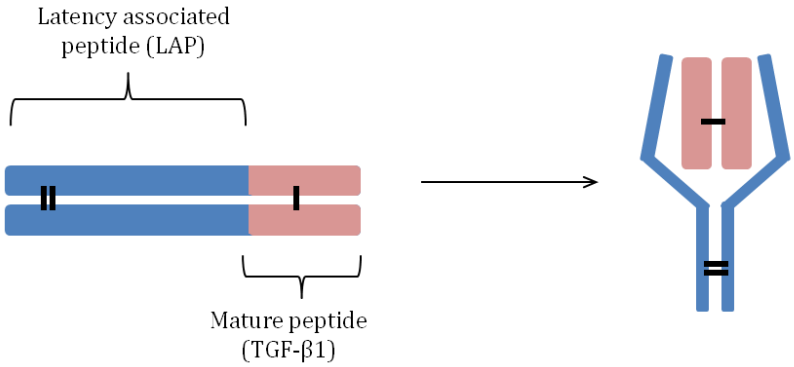

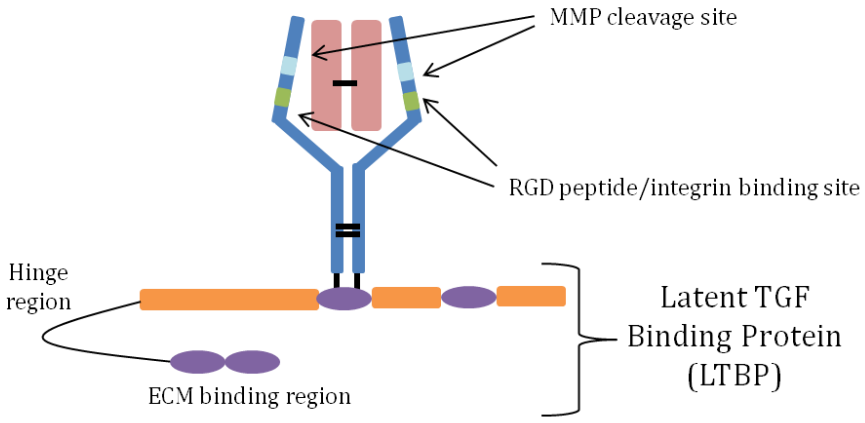

Figure 1.10. Schematic of domains of TGF-β1.
(*Modified from Janssens et al.*[111])

In order to activate the mature TGF-β1 protein, the LTBP-1 and LAP-1 (associated with the β1 structure) must be disassociated from the LLC and SLC.[119] Several theories exist on how this process occurs. The two main conjectures are (1) degradation of the LAP by proteases (**Fig. 1.11**) and (2) induction of a conformational change in the LAP triggered by cell traction forces induced by attachment to a non-compliant surface (**Fig. 1.12**).[12,111] Proteolytic cleavage of the mature TGF from the LAP is thought to occur either through MT-1MMP proximity-association or through the combined actions of MMP-2 and MMP-9.[120-124] These metalloproteinases mediate TGF-β1 activation through interactions with cell surface integrins that they share with the LLC, specifically the families of α_v, α_5, β_1, β_8, and β_3. These integrins recruit the proteases near to where TGF-β1 is being stored and allow for close access to the susceptible LAP-β1 and the ECM-binding hinge region of the LTBP-1.[12,118,125-127] Activated TGF-β1 then freely diffuses to act on the local ECM.

In the second activation method, substrate surface rigidity causes transmission of traction forces throughout the cell membrane, through a similar set of integrins as the previous hypothesis, and onto the LLC, all without proteolytic activity (**Fig. 1.12**).[12,128,129] A mechanically resistant ECM (mimicking the surface it forms on) will exert traction forces onto the LAP-β1 and result in a deformation of the LLC and liberate activated TGF-β1.[130,131] This process occurs only on rigid surfaces; a compliant ECM does not induce any mechanical changes and thus is not responsible for TGF-β1 activation.[130] It is possible that both methods are not mutually exclusive but that one may take place in certain circumstances over the other.

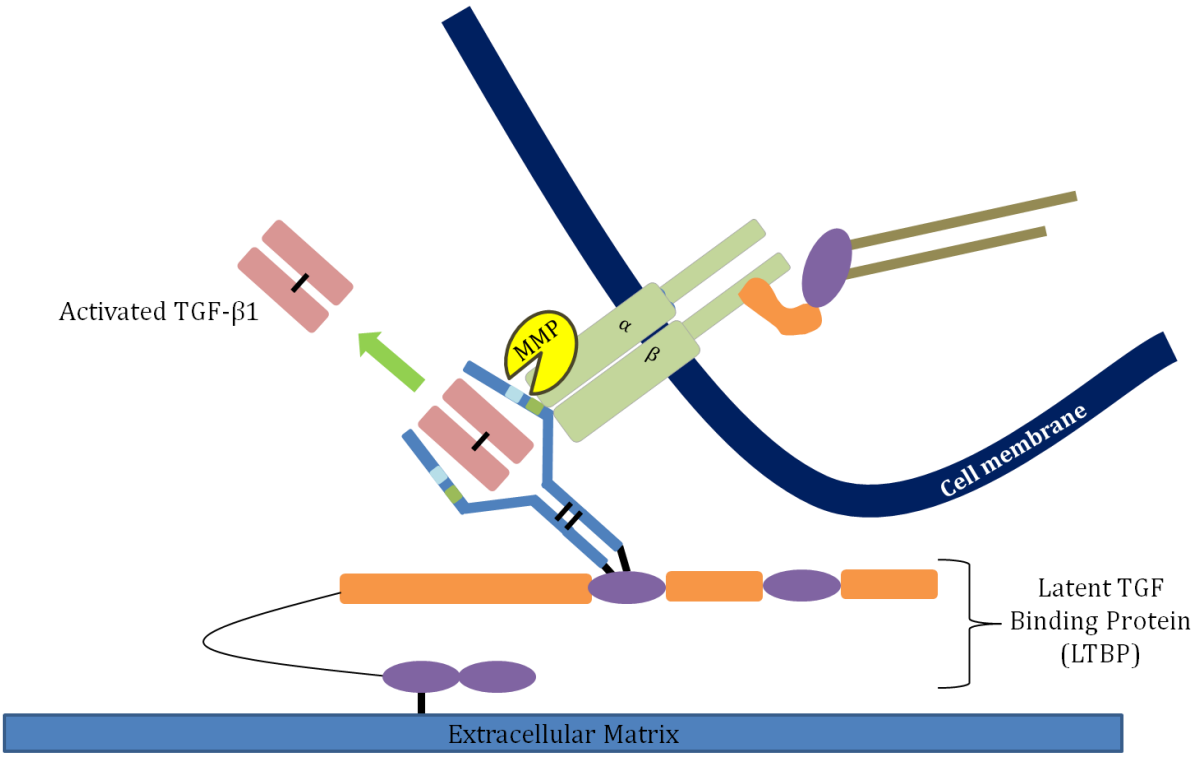

Figure 1.11. Activation of TGF-β1 by MMP-2.
(*Modified from Janssens et al.*[111])

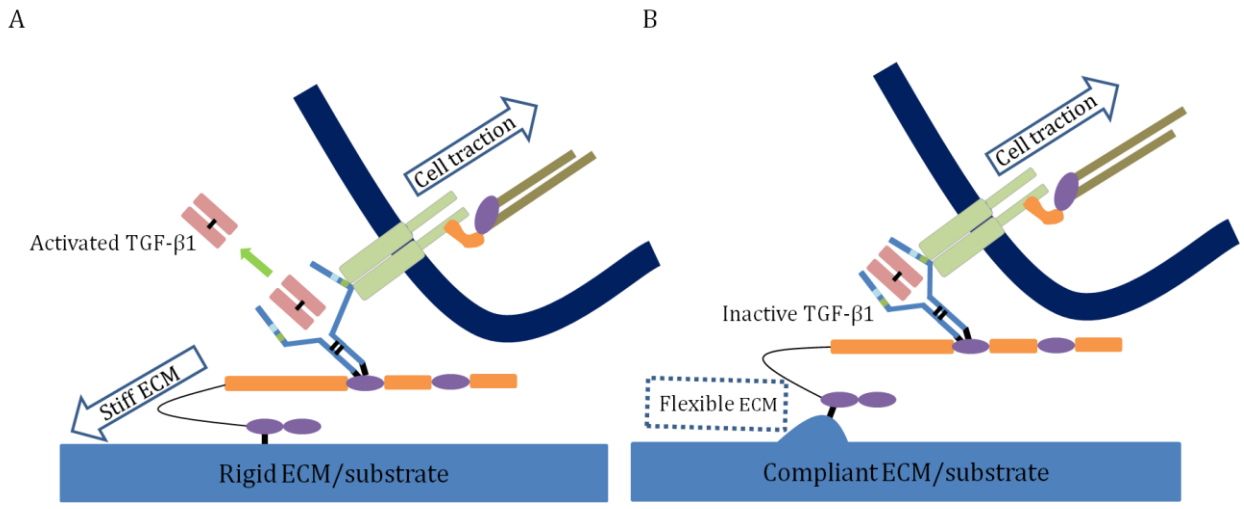

Figure 1.12. Proposed activation of TGF-β1 through surface rigidity (A) on a rigid surface TGF-β1 is activated and released, (B) on a compliant surface TGF-β1 remains inactive.
(*Modified from Janssens et al.*[111])

Once TGF-β1 is activated, it binds to a TGF-β1 receptor (either TβRI, TβRII or both together) and carries out both Smad-dependent and Smad-independent pathways to regulate several cell activities.[111] In the absence of TGF-β1 it has been found that osteoblast proliferation, matrix deposition, and collagen maturity were severely diminished, making this factor crucial for bone and ECM formation.[111,132,133] In studies with MC3T3-E1 pre-osteoblasts, it was found that TGF-β1 activation was at the highest levels during the maturation period (10-16 days after induction media), which coincides with the production of collagen I and alkaline phosphatase (ALP).[113,134-137] The levels of TGF-β1 then start to decrease during the mineralization period (days 16-28). Experimental exogenous additions of this factor during later stages showed cells being less receptive to its effects and it was shown to decrease levels of differentiation markers such as osteocalcin and ALP, possibly suggesting that TGF-β1 has less of a role in later bone mineral production, in an auto-regulatory feedback mechanism.[134,138-141]

Zinc

The zinc-dependent GBD and MMPs highlight how important this cation is to proper cell functioning. The GBD fragment of FN contains seven zinc binding domains in the HEXXH region that are responsible for maintaining the structure of the domain. Addition of exogenous amounts of zinc causes compacting of the GBD at low concentrations and dimer formation of the GBD at high concentrations. This disruption in the structure of FN-GBD caused it to dissociate from a collagen-bound state.[142] It is possible that the exogenous zinc out-competed the GBD for binding sites on the collagen, causing it to dissociate. Zinc in MMPs is part of a highly conserved cysteine switch which is located in the pro-domain.

When present, this domain keeps the MMP in an inactive latent state. Cleavage of the zinc-cysteine bond leads to the loss of the pro-domain and hydrolysis-activation of the MMP.[11]

Zinc deficiency has been shown to impair calcium cell-to-cell signaling and cell proliferation in fibroblasts.[143,144] The intracellular transport of zinc is controlled by zinc-binding storage proteins such as the metallotheioneins (MT) and zinc transporters such as ZnT and Zip.[145-147] ZnT is a transporter protein responsible for decreases in intracellular zinc (transporting it outside the cell), while Zip proteins are responsible for increases in intracellular zinc (transporting it into the cell).[148,149] Zinc deficiency in osteoblasts results in decreased ALP activity (early stage ECM mineralization) and the decline of inorganic phosphate availability.[150] Low ALP levels lead to a poorly calcified ECM, which explains why zinc deficiency results in hindered skeletal growth.[151,152] Zinc has been known to be present in the active site of ALP, and dissociation from this site leads to ALP inactivation.[150] Levels of inorganic phosphate can increase ALP activity by preventing this dissociation.[153] More recently, it has been found that levels of additional late stage osteogenic differentiation factors Runx2 and OCN levels can be depressed with deficiencies in zinc.[148,154]

Computational analysis

Migration analysis

In the absence of external stimuli cells migrate in a random walk fashion.[155] However, when mechanotaxis or chemotaxis is involved cells deviate from this random walk and migrate in a more directed fashion. A simple fit to a random walk model would not showcase the directionality of random walking of cells along topographical patterns.

Therefore, we have used the radius of gyration equation (Eqn. 1 - 4) to determine center of mass in both the *x* and *y* directions and step length (Eqn. 5) to determine if there exists a promoted direction of migration.

$$R_{cm(x)} = \bar{x} = \frac{\sum_{t=1}^{n} x_t}{n} \quad (1)$$

$$Rg_{xt} = \sum_{t=1}^{n} (\bar{x} - x_t)^2 \quad (2)$$

$$Rg_x = \sum (\bar{x} - x_t)^2 \quad (3)$$

$$Rg_x = Rg_{xt} \; when \; n = N$$

These parameters are also determined in the y direction (Rg_y) and the ratio between the radius of gyration in the x and y direction is used to find in which direction the cells prefer to travel:

$$Preferred \; direction \; of \; movement = \frac{Rg_y}{Rg_x} \quad (4)$$

$$SL_x = \overline{|\Delta x|} \quad (5)$$

Step length is reported as the average length of steps in the x and y direction at 6 minute time intervals.

Chapter 2:

Motivation and Objectives of the Research

Objective and hypotheses

The overall objective of this dissertation was to investigate how the exogenous zinc environment modifies interactions between biomaterials and two subclones of pre-osteoblasts and ultimately alters their cellular functions *in vitro*.

This objective was addressed with the following hypotheses and research questions:

Hypothesis 1: The amount of zinc in the environment determines the level of contact guidance demonstrated by MC3T3-E1 subclone 4 pre-osteoblasts on micro-patterns. Initial adhesion stages are driven by ionic surroundings and can modify physical interactions with surface topography.

***Research questions*:**

(1) Is early cell adhesion affected by the topography of the material surface? Is this altered by variations in zinc concentration in the media?

(2) Does varying the surface dimensions of fabricated topographies result in different cell shape from that on an unaltered flat surface? Can this be changed with modified levels of zinc?

(3) Do cell migration patterns and rates differ depending on physical substrate surface features? Does zinc concentration play a role in determining how cells migrate on these surfaces?

(4) Do certain levels of zinc make cells more or less sensitive to the presence of micro-patterns? Can zinc control contact guidance of cells on these patterns?

***Specific aim 1*:** Zinc was investigated as a modifier of cell interactions with physical substrate features. Flat polydimethylsiloxane (PDMS), and micro-patterned PDMS (20 μm wide with a 30 μm pitch and 2 μm height, and 2 μm wide with a 10 μm pitch and 2 μm height) were compared alongside the tissue culture polystyrene gold standard (TC) in regard to morphology and preferential cell migration. These surfaces were seeded with subclone 4 MC3T3-E1 pre-osteoblasts and observed through time-lapse microscopy to determine early stage cell speed, displacement, and directed migration.

Hypothesis 2: Differentiation effects, produced by culturing MC3T3-E1 cells on various substrates, can be modified by zinc levels in the environment. This ionic environment also mediates differentiation effectors, MMP-2 and TGF-β1, which ultimately results in discrepancies in bone nodule formation. The interplay of surface topography and zinc level determines ultimate cell fate.

***Research questions*:**

(1) Do differences in contact guidance predict levels of cell migration factors in mid-stage differentiation? Do variations in zinc levels alter cell response to topography and yield differences in the production of activated MMP-2, responsible for migration and cell multi-layering in early differentiation?

(2) Are variations in MMP-2 levels correlated to differences in production of activated TGF-β1, a factor proposed to be activated by MMP-2?

(3) Does altering of zinc levels yield differences in early stage differentiation on patterned and flat surfaces, as measured by alkaline phosphatase (ALP) *in-situ* staining?

(4) Are differences in media Zn concentration responsible for modifying late stage differentiation, as measured by von kossa (VK) *in-situ* calcium nodule staining?

***Specific aim 2*:** The two biomaterials, golden standard TC and PDMS (flat and patterned), were seeded with a high density of MC3T3–E1 subclone 4 pre-osteoblast cells and given induction media over a period of 0 to 28 days in either serum-levels of zinc or zinc-rich media. The production and activity of the gelatin protease, MMP-2, and TGF-β1 were assessed using gelatin zymography or ELISA, respectively. The levels of early-mid stage differentiation markers (ALP) and late stage (calcium nodules) were determined as indicators of ultimate cell fate on these surfaces.

Hypothesis 3: Alterations in the chemical and physical environment, through introduction of micro-topographies and modified zinc levels, allow for differentiation to occur in otherwise weakly mineralizing subclone 24 pre-osteoblasts.

***Research questions*:**

(1) Is there a difference in cell density and morphology with altered zinc levels across the various surfaces?

(2) Are differences in early stage differentiation markers, as measured by *in situ* staining of ALP, due to physical substrate features? Can these differences be modified through zinc levels?

(3) Are differences in late stage calcium nodule production, as measured by von Kossa, due to physical substrate features? Can these differences be modified through zinc levels?

***Specific aim 3*:** Tissue culture polystyrene, patterned and non-patterned PDMS were used to identify differences in production of differentiation markers using the weakly mineralizing subclone of pre-osteoblasts (MC3T3-E1 subclone 24). Alterations in zinc media content was used to determine the exogenous role of this cation in the production of differentiation markers. Subclone 24 pre-osteoblasts were seeded at confluence and given induction media to promote bone production over a 28 day span. Analysis of early and late stage differentiation markers included *in-situ* staining for ALP and calcium nodules as well as initial cell density and morphology to demonstrate healthy cell growth.

Chapter 3: Migration

3.1 Abstract

Initial cell-surface interactions are guided by the material properties of substrate topography. To examine if these interactions are also modulated by the presence of zinc, we seeded murine pre-osteoblasts (MC3T3-E1, subclone 4) on micro-patterned polydimethylsiloxane (PDMS) containing wide (20 μm width, 30 μm pitch, 2 μm height) or narrow (2 μm width, 10 μm pitch, 2 μm height) ridges, with flat PDMS and tissue culture polystyrene (TC) as controls. Zinc concentration was adjusted to mimic deficient (0.23 μM), serum-level (3.6 μM), and zinc-rich (50 μM) conditions. Significant differences were observed in regard to cell morphology, motility, and contact guidance. We found that cells exhibited distinct anisotropic migration on the wide PDMS patterns under either zinc-deprived (0.23 μM) or serum-level zinc conditions (3.6 μM). However, this effect was absent in a zinc-rich environment (50 μM). These results suggest that the contact guidance of pre-osteoblasts may be partly influenced by trace metals in the microenvironment of the extracellular matrix.

3.2 Introduction

Alterations in physical and chemical characteristics of biomaterial surfaces can modulate cellular behavior via complex events in the extracellular matrix (ECM). In particular, variations in microtopography, mechanical properties (Young's modulus), and surface chemistry can promote cell attachment and migration.[21,47,54,156] The initial formation and development of the ECM can determine cell fate as it undergoes remodeling that is required for tissue homeostasis.

Bone development and regeneration are dynamic processes that are intricately regulated by the interplay between cells and their ECM.[157] These processes are critical in driving osteogenic differentiation by recruiting osteoblast precursor cells from the surrounding tissues.[158-161] Recently, it was shown that the motility of mesenchymal cells was enhanced as soon as one day after treatment with osteogenic medium through the increased activation of the small GTPases, Cdc24 and Rac1, which are critical for mesenchymal cell migration.[162] As such, directional cell migration is crucial to the successful recruitment of these precursor cells, however, its precise role in the regulation of the differentiation of osteoprogenitor cells has not been fully established.

Engineered biomimetic anisotropic topographies (e.g. microscale ridges/grooves) have been shown to promote the adhesion of human osteoblasts,[42,163,164] osteosarcoma cells,[34,156] murine osteoblast-like and mesenchymal stem cells.[53,165] These microfabricated patterns can be designed to induce cell elongation and alignment, resulting in an anisotropic rearrangement of the cell, reorganization of its cytoskeleton, and the re-distribution of the focal adhesions.[166,167] In contrast, the cytoskeleton of cells adhered on a planar surface is randomly structured[168] and they migrate in a random walk fashion.[168] When anisotropy is introduced into the system, such as via a mechanical or chemical gradient, cells deviate from this random walk behavior and exhibit directional migration. Contact guidance, which is bi-directional locomotion along an axis of anisotropy, is one specific example of biased cell migration.[169] Cells that exhibit a directional bias in their motion alter the conformation of their cell body and the distribution of adhesion complexes, which can result in the initiation of signaling events involved in actin polymerization as well as the formation of new focal contacts at the leading edge.[170]

Surface roughness can also modulate cellular response to nutritional factors, such as vitamin D, as shown in an *in vitro* osteoblast model.[171] Because trace metals are essential for bone health,[152] we hypothesized that they may also affect the responsivity of osteoblasts to microtopography. Recently, the homeostatic regulation of zinc has been implicated in impaired skeletal growth,[144,146,147] and zinc deficiency was shown to impede synthesis of bone matrix proteins and calcification of the ECM.[144,150,151] A secondary messenger involved in many signaling pathways,[107,147,150,153,172,173] zinc plays a critical role in cell survival and migration.[86,147,172,173] Zinc homeostasis associated with bone growth is facilitated by transporter proteins from the Slc39/ZIP and Slc30/ZnT families.[145,174,175] Of particular importance are Zip13 and Zip14, which are involved in intracellular zinc distribution and regulation of mammalian systemic growth via the BMP/TGF-β and G-protein coupled receptor (GPCR)-mediated signaling pathways,[145,174] as well as Znt5, which is critical for osteoblast maturation in vitro and maintenance of bone density in vivo.[175] Recent studies have shown that zinc is involved in the late-stage expression of RUNX2, a gene that has been suggested to be essential for recruiting migratory osteoblasts during bone mineralization.[154,176] Therefore early stage migration could be closely linked to ECM turnover and bone mineral production, and could be a useful metric for predicting success of bone formation.

In order to determine the role of exogenous zinc on the migratory behavior of osteoblasts, we cultured MC3T3-E1 cells on micropatterned substrates under zinc-deficient (0.23 μM), serum-level (3.6 μM), and zinc-rich (50 μM) conditions. We hypothesized that early stage (within the first 24 hours) interactions at the cell-material interface are interdependent on both substrate microtopography and zinc serum concentration.

3.3 Materials and Methods

Microfabrication

Using a negative photoresist (SU-8, Microchem, Newton, MA), we fabricated master molds on a silicon substrate at the Center for Functional Nanomaterials (CFN), Brookhaven National Laboratory (BNL, Upton, NY). Silicon wafers (75 mm diameter, single-polished) with <100> orientation were cleaned with acetone and 2-propanol (3000 rpm for 30 seconds) before a 2 μm layer of negative SU-8-2 photoresist (Rohm and Haas; Midland, MI) was deposited by spinning at 2000 rpm for 30 seconds. After prebaking for 1 minute at 65˚C, micropatterns were transferred from a chrome mask to the resist using a 6 second UV exposure on the Karl Suss MJB3 Mask Aligner (277 Watts). The exposed photoresist was post-baked for 1 minute at 95˚C, and the pattern was developed by immersing in propylene glycol monomethyl ether acetate (PGMEA) (Rohm and Haas) for 5-8 minutes and rinsing with DI water, leaving behind raised SU-8 sections (**Fig. 3.1**).

Polydimethylsiloxane (PDMS) replicas containing two patterns (20 μm wide with a 30 μm pitch and 2 μm height, and 2 μm wide with a 10 μm pitch and 2 μm height) were prepared as follows: Sylgard 184 (Dow Corning, Midland, MI) prepolymer was mixed with curing agent at a mass ratio of 10:1, and degassed for 20 minutes. The unpolymerized PDMS was then poured on top of the patterned SU-8 negative master and cured at 65˚C for 1 hour (**Fig. 3.2 & 3.3**). After curing, the positive PDMS patterns were slowly released and plasma etched with 98% oxygen plasma in CFN's Trion Phantom III Reactive Ion Etcher (Clearwater, FL) in order to create silanol groups at the surface of the polymer, rendering it

hydrophilic.[177] Deionized water was added immediately after etching to prevent hydrophobic recovery.

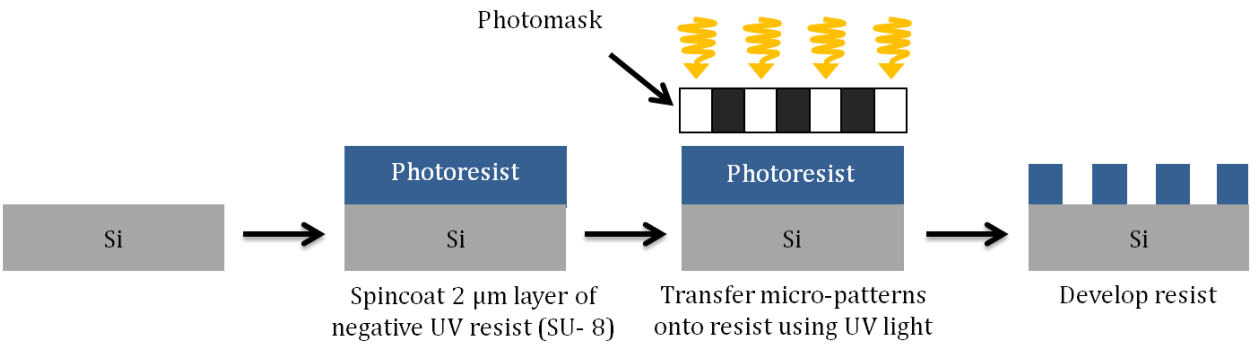

Figure 3.1. Creating a photolithographic pattern on silicon.

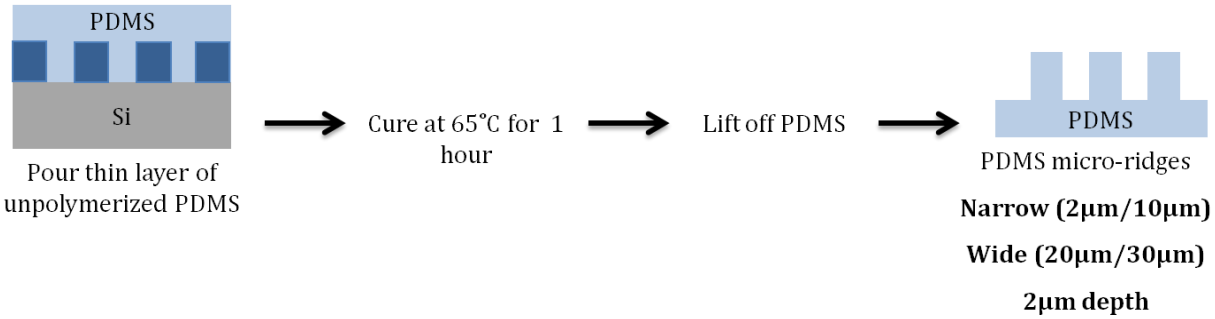

Figure 3.2. Creating PDMS patterns from photolithographic patterns in silicon.

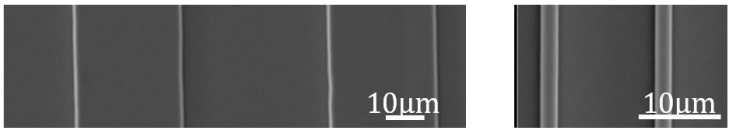

Wide pattern
20 µm wide/30 µm pitch

Narrow pattern
2 µm wide/10 µm pitch

Figure 3.3. SEM micrograph of PDMS patterns: 20 µm wide/30 µm pitch "wide PDMS" ridges, and 2 µm wide/10 µm "narrow PDMS" ridges.

Substrate preparation

Studies utilized 24-well tissue culture (TC) plates (BD Falcon, Bedford, MA) for cell culture. PDMS samples were sterilized by immersion in 70% ethanol for 2 hours in their corresponding wells in the 24-well plate. They were then rinsed twice with Dulbecco's Phosphate Buffered Saline 1x (PBS; Gibco/Invitrogen) before any further substrate preparation. PDMS samples were functionalized with fibronectin, as a 10 μg/mL solution (Sigma Aldrich, St. Louis, MO) in PBS covered the substrates for 30 minutes at room temperature. After subsequent rinsing with PBS, bovine serum albumin (BSA; EMD Chemicals; Gibbstown, NJ) was used to block nonspecific protein binding.

Cell culture and development

Strongly mineralizing MC3T3-E1 pre-osteoblast cells (subclone 4; American Type Culture Collection (ATCC), Manassas, VA) were maintained in 10-cm TC plates (BD Falcon; Franklin Lakes, NJ) using MEM-α (Gibco/Invitrogen, Grand Island, NY) supplemented with 10% fetal bovine serum (FBS; Hyclone/Thermo Fisher Scientific; Logan, UT) and 1% penicillin-streptomycin (Gibco/Invitrogen). Cells were kept in an incubator at 37˚C with 5% CO_2, 95% relative humidity.

Preparation of zinc-deficient and zinc-rich medium

Zinc-deficient medium was prepared by removing zinc from the FBS used in the alpha MEM, similar to the procedure published by Prasad *et al* [178] and Cho *et al.*[179] To prepare zinc-rich medium, the final concentration of zinc was adjusted to 50 μM with zinc sulfate.

Cell coverage

Cells were seeded at a density of 5,000 cells/cm^2 in a 24-well TC plate and incubated (5% CO_2, 95% humidified) at 37˚C for 24 hours. Samples were rinsed with PBS and fixed using 3.7% formaldehyde (J.T. Baker/Mallinckrodt Baker Inc; Phillipsburg NJ) for 15 minutes. The samples were then rinsed with PBS and stained using 2.5 μg/mL of 4', 6-Diamidino-2-Phenylindole Dihydrochloride (DAPI; Sigma) in PBS for 5 minutes covered at room temperature and then rinsed twice with PBS. Approximately 150 fluorescent images were captured for each sample. Images were quantified using ImageJ software and analysis was performed to calculate the average cell density per sample.

Actin analysis

F-actin distribution was visualized with a standard inverted fluorescence microscope (IX51; Olympus Instruments, Melville, NY). Cells seeded at 5,000 cells/cm^2 were maintained at 37˚C for 24 hours to allow complete attachment to the substrate. After fixing with 3.7% formaldehyde, the cells were permeabilized with 0.4% Triton X-100 for 7-8 minutes. The samples were then rinsed with PBS and subsequently stained with 1:100 Alexa Fluor 594 phalloidin (Invitrogen). Using ImageJ, the average spreading area was calculated by converting the number of pixels^2 in the cell area into micrometers^2.

The ImageJ particle measurement plugin was used to fit each cell area to an ellipse shape that represented the ratio of width/length of the cell to determine elongation and alignment to the *y*-axis/patterns. Actin alignment was defined as the angle formed between the major axis of the cell and the direction of the micropattern (*y*-axis), such that a complete, parallel alignment was indicated by 0°. For non-patterned samples, the *y*-axis

was chosen arbitrarily to compare amongst samples. Around 50 cells from three independent experiments were analyzed per sample.

Cell migration: time-lapse microscopy

To capture the migration behavior of cells on the optically transparent substrates, cells were first seeded at 10,000 cells/cm^2 and incubated at 37˚C for 2 hours to allow complete attachment. The medium was then replaced with CO_2-independent medium (supplemented with 10% FBS, 1% penicillin/streptomycin, and 1% L-glutamine, plus zinc additions) and cells were maintained on a 37˚C heated stage. Phase contrast micrographs were captured at 3 minute intervals with a CCD camera attached to the microscope, for a total duration of 2 hours. ImageJ software was used to calculate migration speeds and displacement using a manual tracking plugin.

Numerical analysis of migration

To analyze the directional dependent motility of MC3T3-E1 cells, a Matlab algorithm was used to calculate step length as follows (Eqn. 1 - 2): [180]

$$SL_x = \frac{|x_2 - x_1| + |x_3 - x_2| + \ldots + |x_n - x_{n-1}|}{n - 1} \quad (1)$$

$$SL_y = \frac{|y_2 - y_1| + |y_3 - y_2| + \ldots + |y_n - y_{n-1}|}{n - 1} \quad (2)$$

Where SL_x and SL_y are defined as the step size in the *x*- and *y*-direction, respectively.

Statistics

Each experiment consisted of a minimum of three replicates per treatment group. Statistical analysis was performed using an unpaired student *t*-test to and differences were considered significant at the level of $p<0.01$.

3.4 Results

Cell coverage

At twenty-four hours post-plating, area coverage of MC3T3-E1 pre-osteoblasts in general was similar on both TC and PDMS (**Fig. 3.4**). The only statistically significant increase in cell density was observed when cells were cultured on the flat PDMS at the highest zinc concentration (50 μM). A similar effect, although not statistically significant ($p=0.5$), was also observed for cells on wide PDMS patterns (**Fig. 3.4**). In contrast, cell coverage on the other substrates was not affected by exogenous zinc levels.

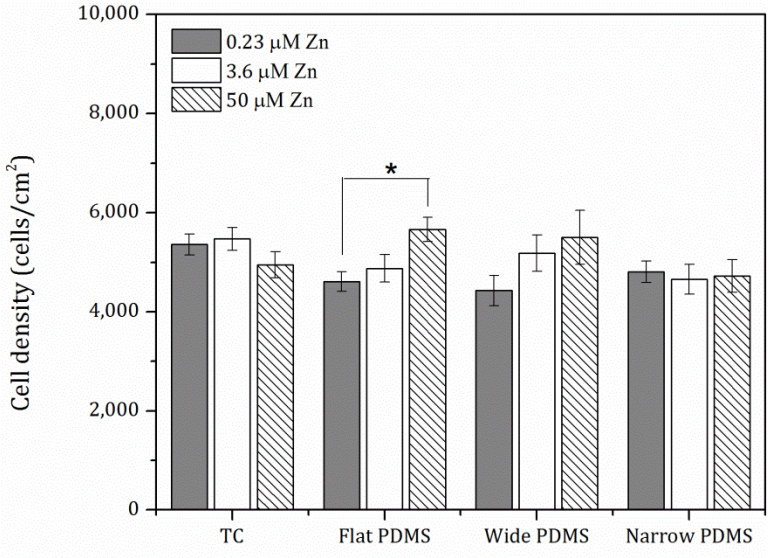

Figure 3.4. Area density of MC3T3-E1 (subclone 4) pre-osteoblast cells on various substrates with modifications of zinc concentrations after incubation for 24 hours. A single asterisk (*) indicates a $p<0.01$ level of significance.

Actin analysis and morphology

Twenty-four hours after seeding, cells had sufficiently adhered to their substrates and F-actin stress fibers were clearly visible on all substrates, as expected (**Fig. 3.5 A-D**). Cell spreading on all the substrates was significantly different: cells on TC and flat PDMS appear to be more spread out and thus larger in area (**Fig. 3.5 A, B & Fig. 3.6**) compared to those on the patterned substrates (**Fig. 3.5 C, D & Fig. 3.6**). Additionally, cells on PDMS surfaces appeared to have more protruding lamellipodia than on TC, typically at the trailing edge (**arrows in Fig. 3.5 B, C, & D**). Analysis of the cell spreading area suggests that zinc concentration only had a significant effect on those cells that were cultured on the wide PDMS pattern, which appeared to be better adhered with increasing zinc (**Fig. 3.6**).

The orientation of the actin cytoskeleton was strongly correlated with the type of substrate and topography (**Fig. 3.7 A**). On the wide PDMS micropatterns (20 μm/30 μm), the actin fibers were most clearly aligned (low theta values) with respect to the longitudinal direction of the pattern (**Fig. 3.5 C and 3.7 A**), whereas those on the narrow PDMS micropatterns (2 μm/10 μm) were not as aligned (higher theta values), as several cells were observed to be oriented diagonally (**Fig. 3.5 D and 3.7 A**). Additionally, actin seemed to cluster on the edges of the wide pattern (**arrowheads in Fig. 3.5 C**). On TC and flat PDMS, the actin fibers were not aligned in any particular orientation, as would be expected for a non-patterned surface (**Fig. 3.5 A, B, and 3.7 A**). Cells on both TC and flat PDMS were also elongated to a similar extent (**Fig. 3.7 B**), but with no statistical differences between substrate type or zinc level.

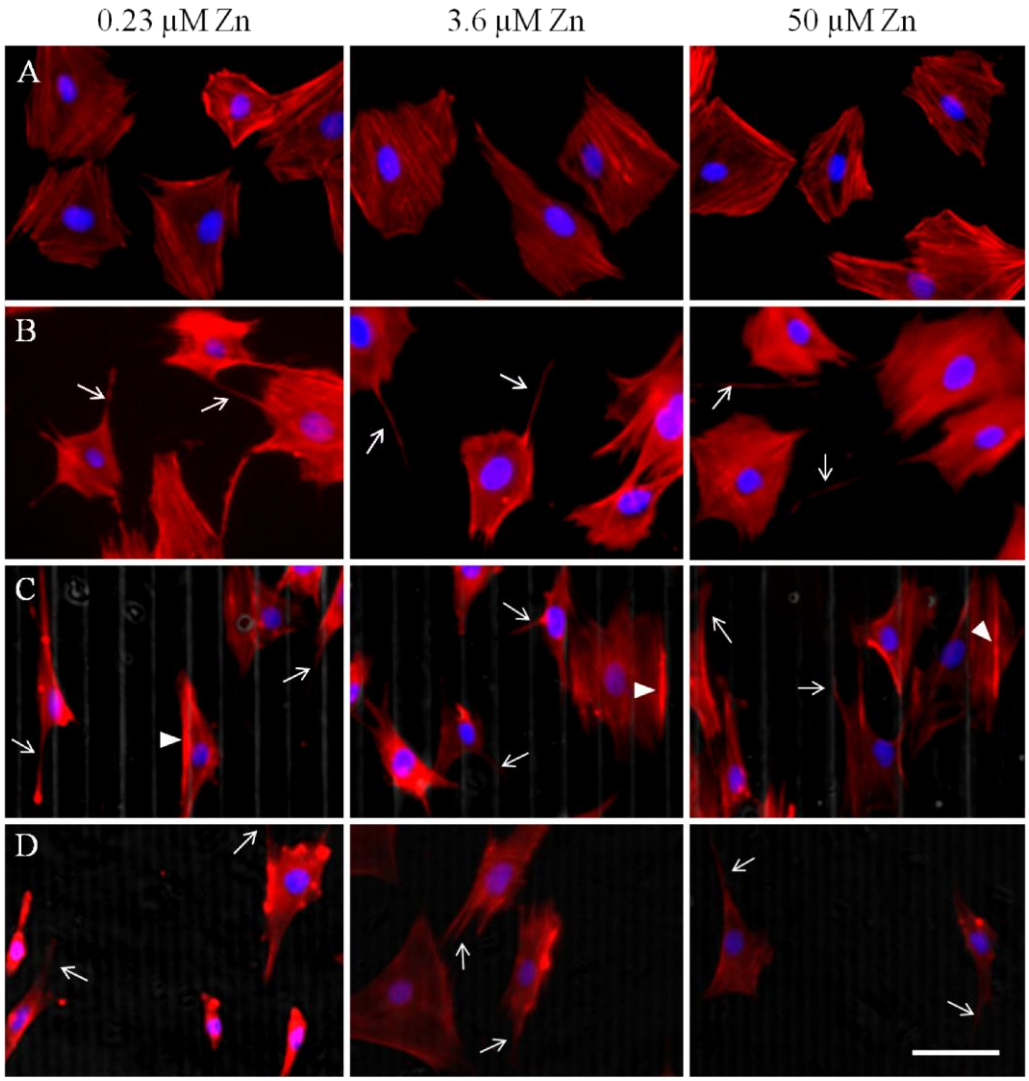

Figure 3.5. Immunofluorescence micrographs of F-Actin (visualized in the red channel) 24 hours after seeding at various zinc concentrations on (A) TC, (B) flat PDMS, (C) wide PDMS pattern and (D) narrow PDMS pattern. Nuclei are visualized in the blue channel. Arrows indicate discrete lamellipodia protrusions while arrowheads in (C) indicate actin clustering on the edge of a micropattern. Bar = 50 µm.

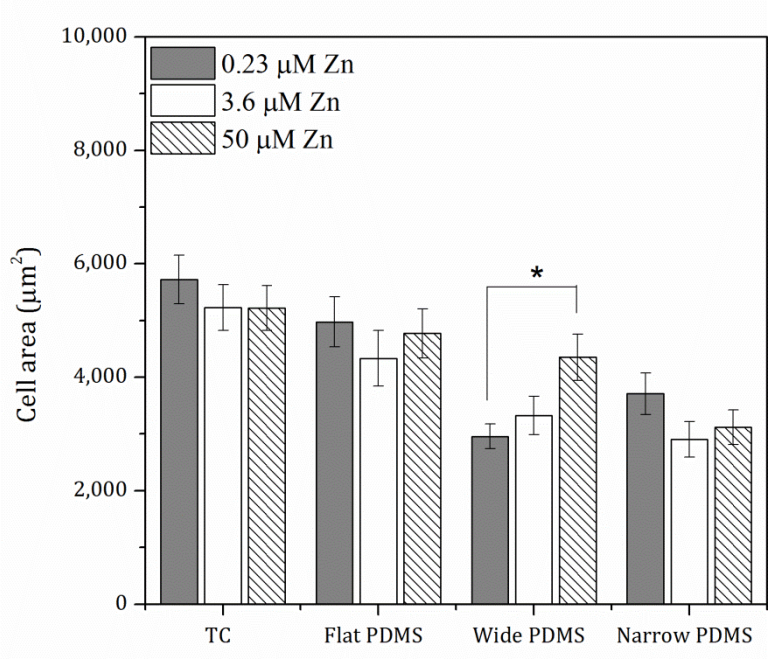

Figure 3.6. Cell spreading area computed from fluorescence micrographs in Fig. 3.2 A-D. A single asterisk (*) indicates a $p<0.01$ level of significance.

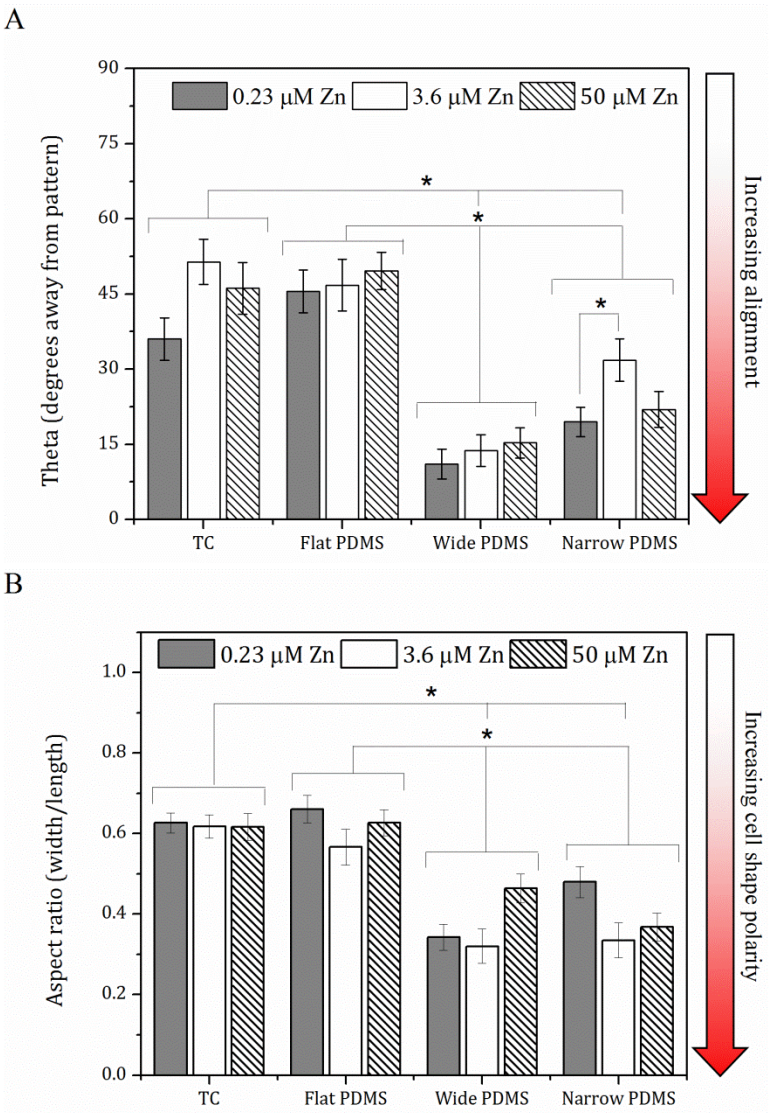

Figure 3.7. (A) Cell alignment computed from Fig. 3.2 A-D, where 0 degrees indicates complete alignment with patterned ridges/y-axis. (B) Cell shape aspect ratio was calculated from the same set of images and represents the use of ImageJ's ellipse fitting tool to determine ratio of cell width/length. A single asterisk (*) indicates a $p<0.01$ level of significance.

Cell migration

Average migration speed, displacement, and directionality of cell movement varied significantly with substrate type. Specifically, cells on TC typically did not travel far from their starting point during the entire two hours of time-lapse video capture (**Fig. 3.8 A**) and migration was randomly directed. Cell migration on flat PDMS (**Fig. 3.8 B**) also took a random pattern, while cells on the wide PDMS patterns traveled much further, in line with the pattern (on top of the ridges; **Fig. 3.8 C**). On the narrow PDMS patterns cell migration appeared more random than on the wide patterns (**Fig. 3.8 D**).

In general, cell migration was noticeably slowest on TC (0.14 – 0.22 μm/min) and was not found to be dependent on zinc (**Fig. 3.8 E**). In contrast, cell migration on flat PDMS was considerably faster (0.27 – 0.44 μm/min) and showed a steady decrease with increasing zinc concentration (**Fig. 3.8 E**). The migratory behavior of MC3T3-E1 cells on flat PDMS is similar to previous reports on breast cancer cells, where the addition of exogenous zinc also attenuated migration.[181,182] Motility of cells on both wide (0.29 – 0.34 μm/min) and narrow (0.28 – 0.36 μm/min) PDMS patterns was similar to that on flat PDMS, however zinc concentration did not have a significant effect (**Fig. 3.8 E**; p=0.35-0.86). Under zinc-deprived (0.23 μM) and serum-level zinc (3.6 μM) conditions, migration on patterned PDMS was reduced compared to flat PDMS, but this reduction was also not significant (p=0.11 - 0.74). Under zinc-rich conditions (50 μM), migration speed did not vary much at all among the three PDMS surfaces. This suggests that cells are less responsive to substrate microtopography when zinc is abundant.

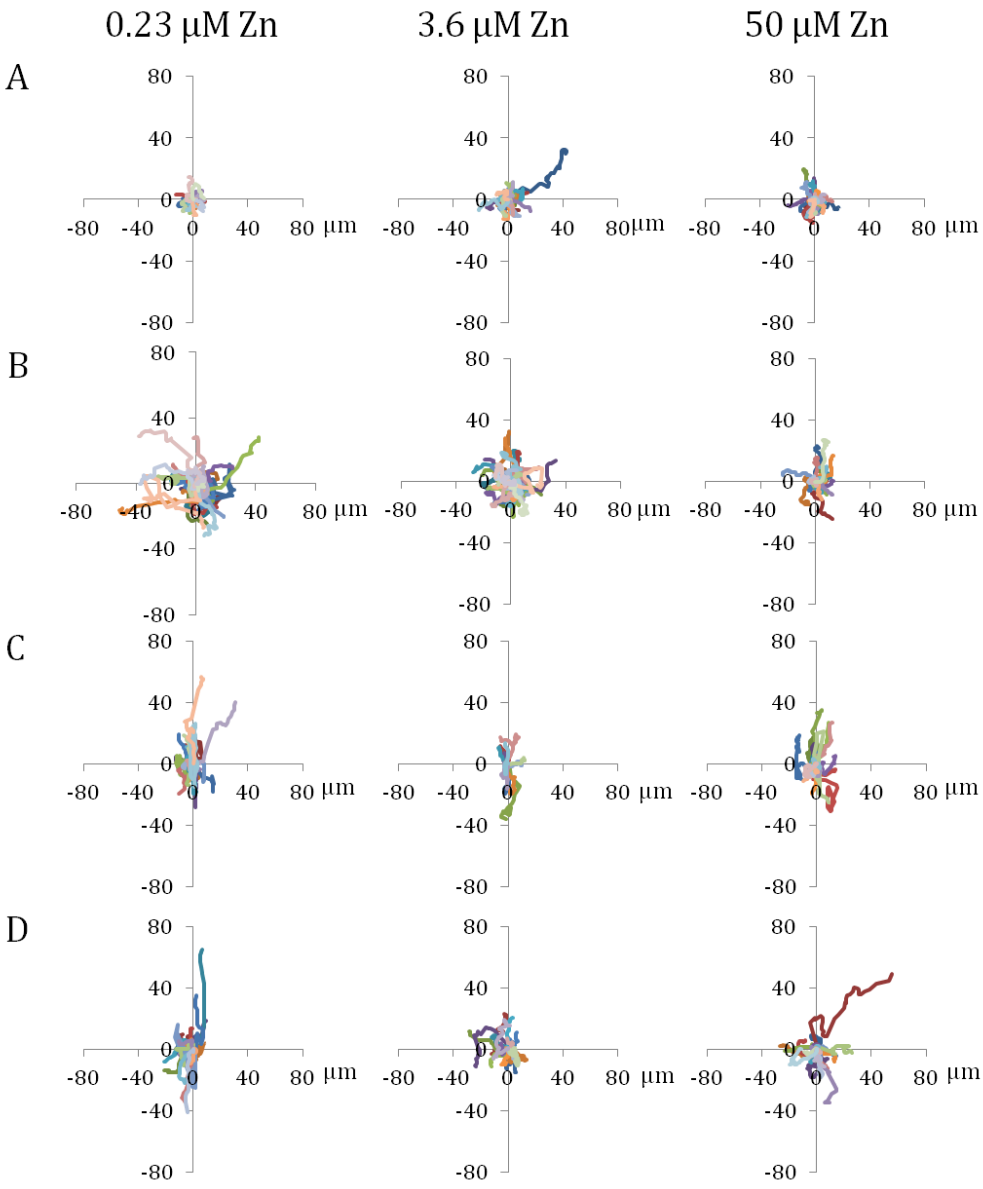

Figure 3.8. Displacement paths of subclone 4 MC3T3-E1 cells in various zinc-modified media after attaching for 2 hours on (A) TC, (B) flat PDMS, (C) 20 µm wide/30 µm wide patterned PDMS ridges, and (D) 2 µm wide/10 µm narrow patterned PDMS ridges. Colored lines represent the migration paths tracked using time-lapse video microscopy.

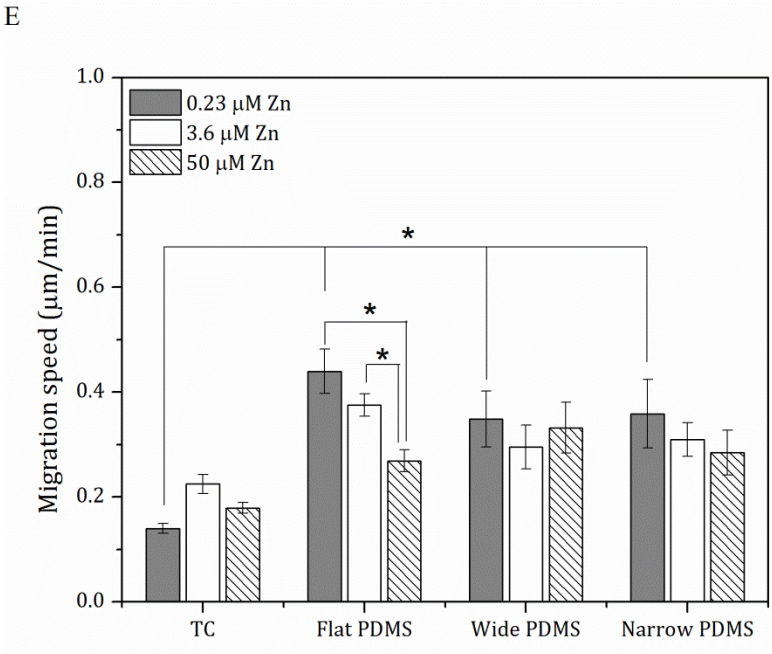

Figure 3.8. (E) Migration speeds of MC3T3-E1 cells on various substrates with modified zinc levels. A single asterisk (*) indicates a $p<0.01$ level of significance.

Contact guidance

At all concentrations of zinc, noticeable differences in cell step size, as well as distinction between step direction in *x* and *y*, were seen (**Fig. 3.9**). At 0.23 μM zinc (zinc-deprived) cells on wide patterned PDMS demonstrated a statistically significant preference for migrating in the *y* direction, along the lengths of the PDMS ridges (**Fig. 3.9 A**). Cells on narrow patterned PDMS also exhibited a slight preference for migrating along the ridges, but not at a significant level (p=0.064). For cells on TC and flat PDMS there was no preference for either direction. At 3.6 μM zinc (serum-level) only cells on the wide PDMS pattern retained their predilection for migration along the ridges, whereas cells on the narrow PDMS pattern behaved as if they were on flat PDMS (**Fig. 3.9 B**). At even higher zinc concentration (50 μM), step size was not significantly different in *x* or *y* direction for cells on all surfaces (**Fig. 3.9 C**).

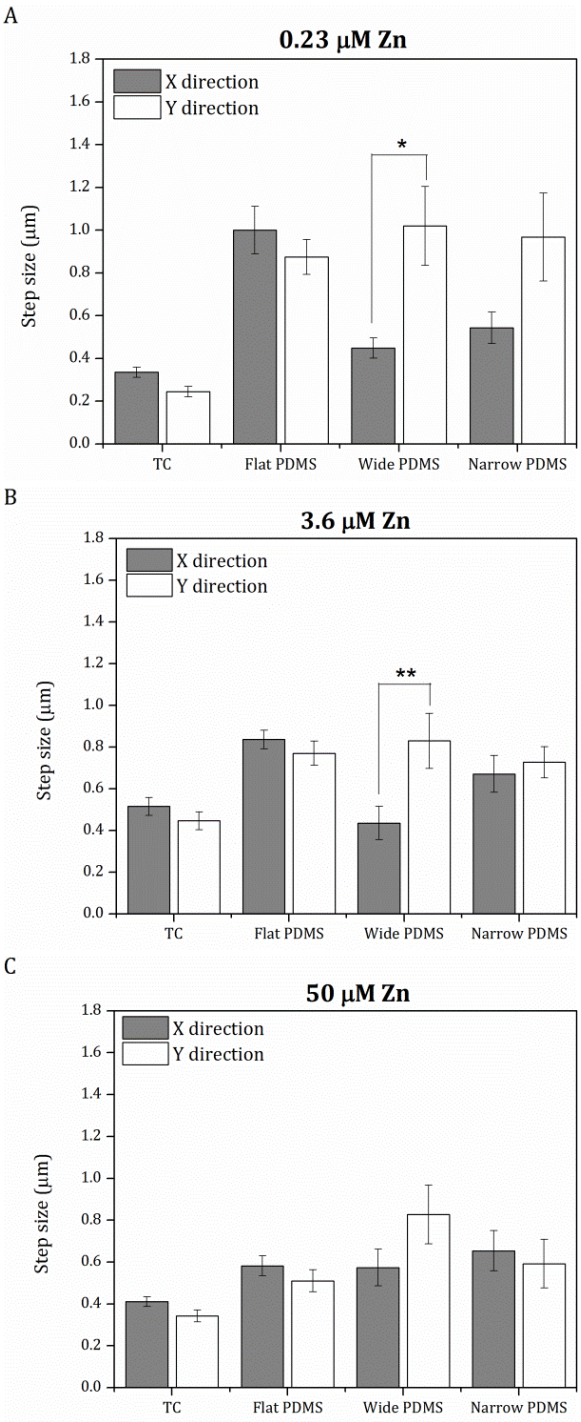

Figure 3.9. Average cell step size in x and y directions with (A) zinc-deprived media, (B) serum-level zinc media, and (C) zinc-rich media. A single asterisk (*) indicates a $p<0.01$ difference while double asterisks (**) indicate a $p<0.05$ difference.

3.5 Discussion

Motility of anchorage-dependent cells is known to be influenced by substrate material properties such as Young's modulus, surface energy, and microtopography. However, the interplay between trace metals and cell migration is not as well understood. In our study, adhesion, morphology and migratory behavior were examined for MC3T3-E1 pre-osteoblasts cultured in various concentrations of exogenous zinc on a microfabricated anisotropic elastomer (PDMS), which has been frequently used to demonstrate contact guidance in cells with a motile phenotype.[167,183] Non-patterned PDMS was also used, as well as standard tissue culture polystyrene as controls.

Cell coverage within 24 hours of seeding was not distinctly different on the four types of surfaces, indicating that neither substrate nor zinc concentration played a significant role in early stage cell survival. The morphology of the MC3T3-E1 cells was round on both of the flat substrates (TC, non-patterned PDMS). In the case of motility, cells on TC did not exhibit a dose dependence on zinc, while migration of the MC3T3-E1 cells on flat PDMS was very sensitive to zinc concentration, similar to previous studies on cancer cell migration.[181,182,184] This suggests that the mode of migration on PDMS is fundamentally different than on TC for the pre-osteoblasts. In contrast, cells cultured on the patterned PDMS surfaces exhibited an elongated spindle-like morphology, typical of mesenchymal cells,[159] and their migration speed was not significantly altered by zinc concentration. The spindle-like morphology has been reported for cells cultured on softer substrates,[185] and therefore we believe that the compliance of the PDMS is partially responsible for the elongation of the MC3T3-E1 cells and their ability to migrate faster than cells on TC. While tracking cell movements, we also observed many more lamellipodia in cells cultured on

PDMS compared to TC, suggesting that the elastomeric substrate is more conducive to the formation of cell protrusions than polystyrene, which could explain the increase in migration speed. In addition, the cells traveling on the larger patterned surfaces had increased numbers of small lamellipodial protrusions, particularly when interacting with the edges of the PDMS ridges. This indicates a more motile phenotype, which is in agreement with the higher migration speeds we observed.

In addition to cell polarity, we observed a significant increase in actin alignment of the MC3T3-E1 cells on patterned PDMS, similar to previous studies of human osteosarcoma cells on PDMS [34,156] as well as murine osteoblast-like and mesenchymal stem cells on micropatterned titanium and silicon.[165,186] The elongation and alignment of the cells results from an anisotropic rearrangement of the cytoskeleton, which re-distributes focal adhesions.[166,167] In our study, the stress fibers of MC3T3-E1 cells on both TC and flat PDMS were randomly oriented, which was expected based on previous studies on flat substrates.[168] There was, however, a visible increase in actin aggregation in the MC3T3-E1 cells along the edges of the wide PDMS ridges, but this clustering was not as pronounced in cells cultured on the narrow PDMS patterns.

Shifts in the spatial distribution of focal adhesions are responsible for regulating cell-substrate adhesion strength [187] and are dependent on both the adhesivity of the ECM and the mechanical compliance of the substrate.[188] A re-distribution of these adhesion complexes would alter the magnitude of cell traction forces, [185] and in turn, would influence cell motility. Previous studies using a rat macrophage model [183] have suggested that ligand clustering on anisotropic surfaces is associated with increased substrate adhesiveness and

is responsible for the contact guidance phenomenon.[167] The migration trajectories of the MC3T3-E1 cells, especially those cultured on wide (20 μm) PDMS micropatterns, exhibited some extent of biased migration along the length of the PDMS micropattern, particularly at the lower zinc concentrations. Step size analysis further confirmed that the wide PDMS micropattern was associated with anisotropic migration, as cells distinctly preferred to migrate parallel to the ridges in the *y* direction. On the other hand, migration in the *y*-direction for cells on the narrow PDMS micropatterns under zinc-deficient conditions was only slightly significantly different (p=0.064) from that in the *x*-direction, indicating that the requirements for contact guidance vary with surface microtopography.

Taken together, these results suggest that the extent to which exogenous zinc levels alter pre-osteoblast motility and directional migration strongly depends on surface dimension. While cell motility on flat PDMS distinctly showed dose dependence on zinc concentration, migration speeds on either patterned PDMS or TC showed no clear trend. Our data also suggest that the anisotropic structure of the PDMS surface was responsible for the directional migration observed in MC3T3-E1 cells, however the contact guidance behavior could be altered under zinc-rich conditions. Because zinc is known to play a role in regulating the binding association between collagen and fibronectin,[142] it is possible that high levels of zinc directly interfered with contact guidance. Extracellular stimuli can trigger zinc-mediated intracellular signaling events either via ZIP transporters or GPCR receptors such as GPR39, which is involved in migration and metabolic activity.[147,189] Further elucidation of the effects of exogenous zinc on the migratory behavior of pre-osteoblasts can enhance our understanding of bone differentiation and mineralization processes, and improve the design of medical devices for enhanced osseointegration.

3.6 Conclusions

Using an *in vitro* model, we demonstrated that modifying the level of exogenous zinc can alter the extent to which pre-osteoblasts respond to surface microtopography. Specifically, contact guidance was exhibited on 20 μm wide PDMS patterns under either zinc-deprived (0.23 μM) or serum-level zinc conditions (3.6 μM), but was absent in a zinc-rich environment (50 μM). These results suggest that trace metals in the microenvironment of the extracellular matrix can interfere with the migratory behavior of pre-osteoblasts, which may have implications in downstream events such as differentiation and mineralization.

3.7 Acknowledgements

I would like to acknowledge P. Mark and D. Gersappe for their aid with Matlab. Thanks also to D. Rammelkamp for his guidance in creating the Zn-stripped FBS.

Chapter 4: Differentiation

4.1 Abstract

Osseointegration of bone implants is a vital part of the recovery process. Numerous studies have shown how patterned geometries can promote cell-substrate associations, strengthening the bond between tissue and implant. Physical interactions at adhesion sites may be manipulated by the aqueous environment of the serum. As demonstrated previously in Chapter 3, zinc levels can be manipulated to render cells more responsive to micropatterns, directing contact guidance. In this chapter, we sought to determine the effect of exogenous zinc on osteoblast differentiation and mineralization of the extracellular matrix. Production of differentiation effectors, activated metalloproteinase-2 and transforming growth factor – beta 1 (TGF-β1), were altered with the addition of exogenous zinc. Early stage differentiation, via alkaline phosphatase, was modified by zinc levels on patterned polydimethylsiloxane (PDMS) surfaces, but not on flat PDMS or tissue culture polystyrene (TC). Late stage differentiation through calcium phosphate nodule production, was markedly different when zinc levels were varied on patterned PDMS and TC substrates. These results suggest that both surface dimension and zinc levels work together in the regulation of osteoblast differentiation to promote bone deposition.

4.2 Introduction

Bone tissue morphogenesis is an intricately regulated process that depends on the interplay between cells and their extracellular matrix (ECM). These interactions can be elucidated by utilizing ECM-mimicking substrates *in vitro.*[157] Small micro-topographies present on the surface of bone have been determined to be an important factor for guiding cell adhesion on the underlying ECM and promoting vital *in vivo* functions.[40,190] Studies have demonstrated that biomimetic topographies (e.g. polymeric microscale

ridges/grooves) can be used to promote the adhesion and differentiation of human osteoblasts.[40,42,46] The presence of these surface features has been shown to induce the expression of bone-specific proteins such as osteocalcin and osteopontin, even in the absence of osteoinductive media.[191,192]

It has been proposed that altered protein expression is due to the re-distribution of focal adhesion complexes and sequestering of integrins along the edges of the topographies.[40,47,63] For reasons that are still not fully understood, this reorganization and clustering leads to changes in gene expression that enhances differentiation of osteoblasts.[193] The grouping of these adhesion complexes to the edges of a pattern results in a more compacted shape as the cell is confined within the boundaries of the ridges. Cells attempt to maintain tensional homeostasis of the cytoskeleton by re-distributing stress fibers which, through the RhoA-ROCK signaling pathway, results in the up-regulation of differentiation genes.[188,194-196] Linear patterns will induce a more elongated shape as the cell stretches along the direction of the feature's dimensions.[41]

Results from Chapter 3 demonstrated that pre-osteoblasts preferentially migrated atop patterned elastomeric ridges which caused them to polarize their shape as they align to the pattern.[197] In this way, the limitation of the cell body area within the confines of the linear pattern acts as an indirect stretching mechanism. Elongation of the cell body has been demonstrated to be important in the mineralization process of osteoblasts. For example, Jansen *et al*. observed that polarization of human fetal pre-osteoblasts decreased early stage differentiation marker, alkaline phosphatase (ALP), activity after 7 days but increased calcium deposition after 21 days.[22] Kim *et al.* observed that polarizing stretch of

human mesenchymal stem cells increased osteopontin but decreased osteocalcin gene expression.[198] Ultimately, substrate surface topography, as an effector of cell shape, is one of the critical factors directing mesenchymal cell fate.[37,195]

Additionally, it has been shown that micro-textured surfaces can also enhance cell responsivity to certain differentiation co-factors, modifying cell function.[171,181] We have previously demonstrated in Chapter 3 that levels of zinc in the microenvironment alter cell interactions with topographical surface features in regard to actin organization and contact guidance.[197] Alcantara *et al.* determined that depriving pre-osteoblasts of physiological concentrations of zinc resulted in a decrease in both early (ALP) and late stage differentiation (calcium phosphate nodules).[150] Zinc is present in the active site of ALP and dissociation from this site leads to inactivation of the enzyme, resulting in a decrease production of inorganic phosphate.[150] The decline of inorganic phosphate availability propagates a poorly calcified ECM, resulting in hindered skeletal growth.[151]

The zinc-dependent metalloproteinase-2 (MMP-2) represents another factor vital to pre-osteoblast differentiation and ECM remodeling. Secreted in its inactive form, a cysteine-rich pro-domain prevents hydrolysis of the zinc binding site until phosphorylation by ALP renders the protease active during early-mid stage differentiation.[11,107] The proteinase acts to turn over the local ECM in order to allow for the multi-layering of cells that is required for large bone nodule formation.[11] Studies have shown that block the activation of MMP-2 resulted in bone defects and delayed mineralization of the ECM.[102,103]

MMP-2 perpetuates pre-osteoblast differentiation as a known activator of another critical component, transforming growth factor – beta 1 (TGF-β1).[111] TGF-β1 is found in

high quantities in bone and plays a role in a number of diverse biological processes such as cell migration, proliferation and differentiation.[111,112] In particular, TGF-β1 is especially important in regulating bone formation and is a known chemoattractant of osteoblasts.[111-113] In the absence of TGF-β1, it was found that osteoblast proliferation, matrix deposition, and collagen maturity were severely diminished, making this factor crucial for bone formation and ECM mineralization.[111,132,133] Ma *et al*. demonstrated that increased levels of zinc stimulated TGF-β1 production and activation using *in vivo* rat skeletal studies.[199] Investigations using MC3T3-E1 pre-osteoblasts found that TGF-β1 activation levels were highest during the maturation period (10-16 days after induction media), which coincides with the production of collagen I and alkaline phosphatase (ALP), while levels dwindle during the mineralization period (days 16-28).[113,135,136] Exogenous addition of this activated factor during the mineralization stage was shown to decrease levels of differentiation markers such as osteocalcin and ALP and prohibit bone formation, suggesting that TGF-β1 has less of a direct presence in later bone mineral production.[139-141]

Increasing the level of exogenous zinc from 3.6 μM to 50 μM disrupted early stage directional migration of pre-osteoblasts on polydimethylsiloxane (PDMS) micropatterns, as shown in Chapter 3.[197] This study provided motivation to investigate whether osteogenic differentiation is also affected at the same zinc conditions. To this end, PDMS micropatterns were fabricated as previously described,[197] containing either wide (20 μm width, 30 μm pitch, 2 μm height) or narrow (2 μm width, 10 μm pitch, 2 μm height) linear ridges. Flat PDMS was used as a non-patterned control and tissue culture polystyrene (TC) was provided as the biological golden standard.

Based on the previous results of early stage pre-osteoblast migration on anisotropic surfaces, it was hypothesized that exogenous zinc would also have an effect on topography-guided osteogenic differentiation and biomineralization. More specifically, varying the zinc level in the microenvironment would alter MMP-2 activation, TGF-β1 production and calcium nodule formation. Knowledge regarding the physicochemical factors that orchestrate the interactions between ECM substrates and their ionic environment can advance the understanding of bone differentiation and, ultimately, tissue regeneration.

4.3 Materials and Methods

Substrate fabrication

The fabrication of micropatterns in PDMS was described in Chapter 3.[197] Briefly, standard photolithography was used to create sections of negative resist from which PDMS replicas containing two patterns (20 μm wide with a 30 μm pitch and 2 μm height, and 2 μm wide with a 10 μm pitch and 2 μm height) were created. PDMS substrates were rendered hydrophilic using plasma oxygen.[177] As a control, planar 24-well tissue culture (TC) plates (BD Falcon, Bedford, MA) were used. PDMS substrates were functionalized with fibronectin, at 10 μg/mL (Sigma Aldrich, St. Louis, MO) followed by bovine serum albumin (EMD Chemicals; Gibbstown, NJ) to block nonspecific protein binding.

Cell culture and development

Pre-osteoblast MC3T3-E1 cells (subclone 4; American Type Culture Collection (ATCC), Manassas, VA) were maintained using MEM-α (Gibco/Invitrogen, Grand Island, NY) supplemented with 10% fetal bovine serum (FBS; Hyclone/Thermo Fisher Scientific; Logan, UT) and 1% penicillin-streptomycin (Gibco/Invitrogen) at 37˚C with 5% CO_2, 95%

relative humidity. Media was supplemented with 4 mM glycerol 2-phosphate (Sigma) and 50 μg/mL sodium L-ascorbate (Sigma) and replaced every 2-3 days. Subclone 4 MC3T3-E1 pre-osteoblasts were chosen due to their demonstrated ability to produce copious amounts of calcium phosphate nodules on TC.[200]

As described in chapter three,[197] zinc levels were varied using a standardized process by Prasad *et al.*[178] and levels of zinc were reported to be 3.6 μM (serum-level).[179] Zinc-rich conditions of 50 μM were used to mimic zinc supplementation to a deficient system.

Alkaline phosphatase production (ALP)

Twenty-four hours after seeding at 50,000 cells/cm^2, cells were given induction medium (supplemented with glycerol 2-phosphate and sodium L-ascorbate) for 7 days or 10 days. At each time point, fresh ALP substrate buffer was prepared using 2-amino-2-(hydroxymethyl)-1,3-propanediol (Tris base, Applied Science; Indianapolis, IN), sodium chloride (Sigma), and magnesium chloride (Sigma), with the pH adjusted to 9.5 using hydrochloric acid. Samples were rinsed with Tris-Buffered Saline Tween-20 (TBST) before starting the assay. A working reagent of nitro blue tetrazolium (NBT, Sigma) and 5-bromo-4-chloro-3-indolyl phosphate (BCIP, Sigma) was prepared fresh and added to each sample and allowed to incubate for 10 minutes at room temperature. Color development was stopped by rinsing the samples with deionized water. Images were captured using a color photo scanner.

Calcium phosphate nodules (von Kossa)

Cells used for von Kossa assay were cultured in induction medium for 21 and 28 days after seeding at 50,000 cells/cm^2. At each time point the samples were rinsed twice with PBS and fixed using formaldehyde in PBS for 10 minutes. Following a water rinse, the cells were covered with a silver nitrate solution and exposed to UV light for 20 minutes. The samples were then rinsed with water and covered with sodium thiosulfate (Electron Microscopy Sciences, EMD; Hatfield, PA) for 3 minutes, followed by final water rinse. A color photo scanner was used to capture images.

MMP-2 activity: gelatin zymography

Twenty-four hours after seeding at 50,000 cells/cm^2, cells were given induction medium (supplemented with glycerol 2-phosphate and sodium L-ascorbate) for a period through 11 days. At each timepoint, the samples were serum starved for 24 hours before supernatant was removed from the cell sample and lysis buffer (Tris-HCl, Triton X-100) was added and the plate frozen at -80˚C. Samples were taken through several freeze-thaw cycles to release the cell layer from the sample. Additional cell layer removal was done by scraping and the lysates were then transferred to individual tubes. Next they were passed through a needle several times before adding to a QIAShredder (Qiagen; Hilden, Germany) containing a filter and a collection tube and then centrifuged to remove any cell structural components.

Using a Nanodrop-1000 spectrophotometer (Wilmington, DE), protein concentration in the samples was normalized to by the addition of Tris-Glycine SDS sample buffer (Tris-HCl, glycerol, SDS, bromophenol blue, DI water) before being electropohoresed

on a pre-made acrylamide gel containing 10% gelatin (Biorad, Hercules, CA). Tris-Glycine SDS running buffer (Tris base, glycine, SDS, DI water) was used as reservoir buffer in the gel box and a constant voltage of 125 V was maintained. Subsequent to running the gel, samples were then incubated for 30 minutes in zymogram renaturing buffer consisting of 2.5% (v/v) Triton-X-100. The renaturing buffer was then decanted and developing buffer (Tris base, Tris-HCl, NaCl, $CaCl_2$, Brij 35, DI water) was added to the gel for 30 minutes. The developing buffer was then replaced with fresh developing buffer and incubated with the gel at 37˚C overnight. The developing buffer was then removed and a Coomassie Blue stain was incubated with the gel at room temperature for 30 minutes and subsequently decanted and rinsed with destaining solution over several hours until bands were clear. Areas of protease activity appeared as clear bands against a dark blue background where the protease has digested the substrate. Images were captured using a color photo scanner.

TGF-β1 ELISA

Cell lysates were prepared similarly to that of the MMP-2 samples. Briefly, Cells were seeded at 50,000 cells/cm^2 and given induction medium (supplemented with glycerol 2-phosphate and sodium L-ascorbate) for 8 or 11 days and serum-starved for 24 hrs before adding lysis buffer and freezing at -80˚C. Additional cell layer removal was done by scraping and the lysates were then transferred to individual tubes. Next they were passed through a 21 gauge needle several times before adding to a QIAShredder containing a filter and a collection tube and then centrifuged to remove any cell structural components. Using a Nanodrop-1000 spectrophotometer samples were analyzed for protein concentration.

Activated TGF-β1 was determined using the TGF-β1 E_{max} ImmunoAssay System (Promega Co., Madison, WI). The assay was performed according to the manufacturer's instructions. Briefly, samples were diluted with PBS to an appropriate range for in vitro cell culture samples and split into two sets. The first set was diluted again to the final concentration for use, these samples contained only naturally processed TGF-β1 and represented the amount of activated TGF-β1. The second set was acid treated with hydrochloric acid and then neutralized with sodium hydroxide to activate all the TGF-β1 in the samples, representing total amount of both activated and latent TGF-β1. Samples were normalized to average mass of total protein amount.)

Statistics

Each experiment consisted of a minimum of three replicates per treatment group. Statistical analysis was performed using an unpaired student *t*-test to and differences were considered significant at the level of $p<0.01 – 0.05$.

4.4 Results

Metalloproteinase-2 (MMP-2)

Results from gelatin zymography showed distinct bands for both latent pro-MMP-2 (72 kDa) and the active form of MMP-2 (68 kDa) for some, but not all, of the substrates (**Fig. 4.1**). At serum-level (3.6 μM) zinc, total MMP-2 production on either day 8 or 11 was high in cultures extracted from TC and patterned PDMS, as can be seen by bright bands at 72 kDa and 68 kDa (**Fig. 4.1**). The intensity of the 68 kDa activated MMP-2 band in the TC lane is noticeably stronger, particularly in 3.6μM zinc media. In contrast, cells cultured on flat PDMS produced almost no MMP-2 at serum-level zinc (faint or absent bands in **Fig.**

4.1). This coincides with the inability to exhibit contact guidance.[197] At 50 μM zinc, however, both bands were clearly observed for cultures on flat PDMS. Additionally, there was not a visible difference in MMP-2 production/activation between any of the substrates under zinc-rich conditions (**Fig. 4.1**). Interestingly under these same zinc-rich conditions, contact guidance was also absent for all treatment groups.[197]

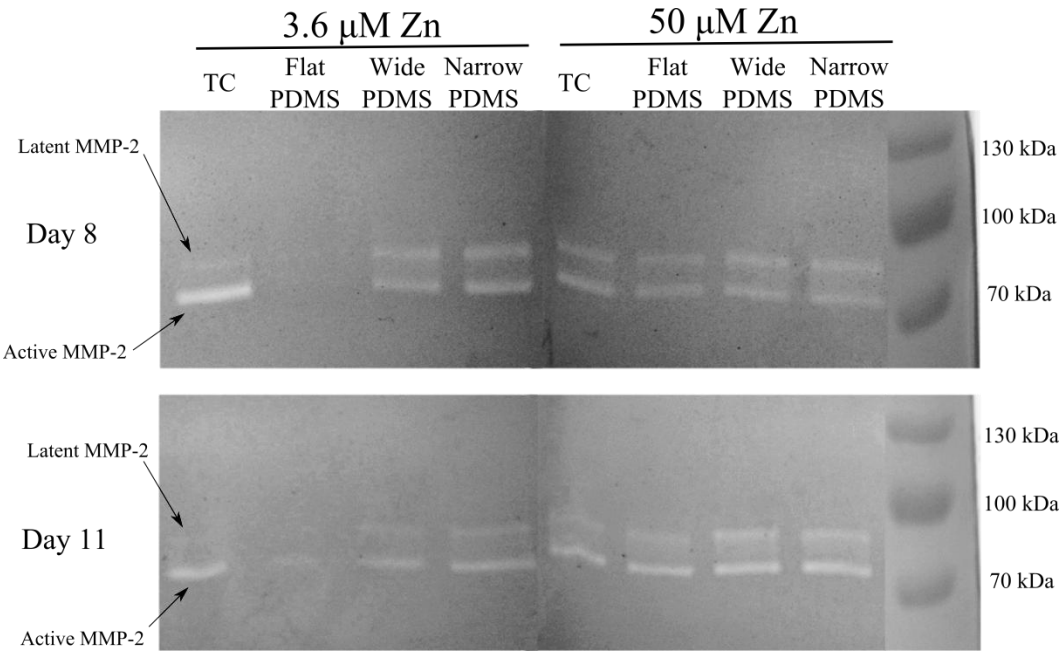

Figure 4.1. Gelatin zymogram demonstrating MMP-2 activity (indicated by bright bands). Subclone 4 MC3T3-E1 cell protein samples on PDMS and TC surfaces in serum level zinc (3.6 μM) and zinc-rich (50 μM) media conditions were isolated on day 8 and 11, normalized to total protein concentration at 17.90 μg/lane.

Transforming Growth Factor – Beta 1 (TGF-β1)

Activated TGF-β1 levels were found to be influenced by exogenous zinc only when cells were cultured on either TC or patterned PDMS (**Fig. 4.2 A & B**). Increasing exogenous zinc concentration from 3.6 μM to 50 μM resulted in a significant increase in TGF-β1 activation only in MC3T3-E1 cells cultured on either TC or patterned PDMS (**Fig. 4.2 A & B**). Specifically, TGF-β1 activation on TC increased by 450% (by day 8) and 150% (by day 11) (**Fig. 4.2**), similar to published findings in the literature.[111] In contrast, TGF-β1 activation for cells on flat PDMS either decreased (by ~25% on day 8) or was unaltered (day 11) with the increase of exogenous zinc concentration (**Fig. 4.2**). When cells were cultured on wide PDMS micropatterns, TGF-β1 activation increased on both day 8 (200%) and day 11 (67%), but to a lesser extent compared to cells on TC. On the narrow PDMS micropatterns, activation increased by 67% on day 8 and 100% by day 11. The most demonstrated difference in increase of activated TGF-β1 between the two zinc concentrations over time was found on TC surfaces as compared to cells on the other substrates (**Fig. 4.2 C**).

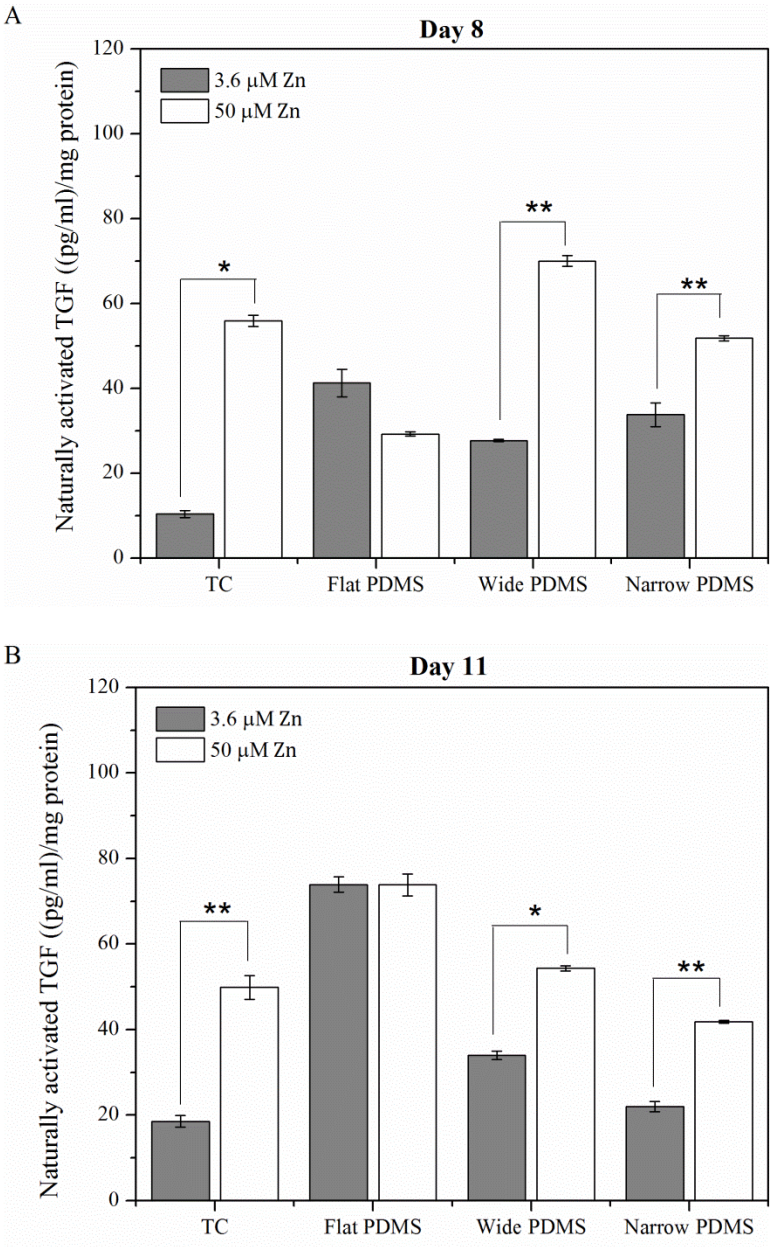

Figure 4.2. TGF-β1 activation for subclone 4 MC3T3-E1 cell lysates collected on (A) day 8 and (B) day 11, normalized to total protein concentration (A & B) and to percentage of serum-level (3.6 μM) samples (C). A single asterisk (*) indicates a $p<0.01$ level of significance while double asterisks (**) indicate a $p<0.05$ level of significance.

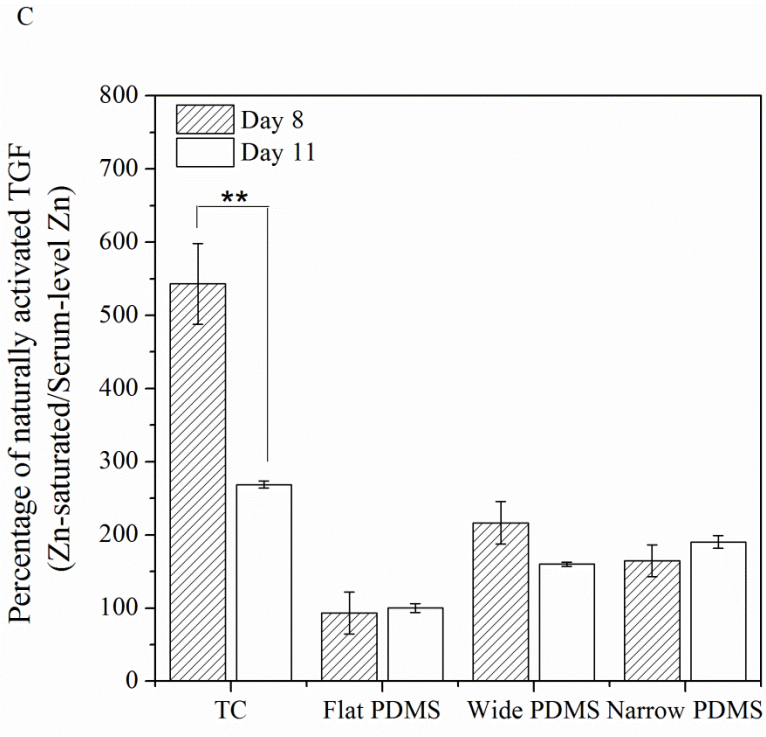

Figure 4.2 cont. TGF-β1 activation for subclone 4 MC3T3-E1 cell lysates collected on (A) day 8 and (B) day 11, normalized to total protein concentration (A & B) and to percentage of serum-level (3.6 μM) samples (C). A single asterisk (*) indicates a $p<0.01$ level of significance while double asterisks (**) indicate a $p<0.05$ level of significance.

Alkaline phosphatase (ALP)

ALP production was strongly positive for cells cultured up to 10 days on TC at both serum-level zinc and zinc-rich conditions, as indicated by the dark purple coloration (**Fig. 4.3).** This was expected of the subclone 4 of the MC3T3-E1 cell line, whose ALP production typically peaks around 14days.[200,201] For cells that were cultured on flat PDMS, ALP activity was negative irrespective of zinc concentration (**Fig. 4.3**). On the patterned PDMS surfaces, ALP was positive at serum-level zinc (3.6 μM; but not at elevated zinc (50 μM); **Fig. 4.3 B**), coincident with contact guidance behavior.[197] It was previously observed that contact guidance was absent in cells cultured on PDMS under zinc-rich conditions, regardless of surface microtopography.[197] This indicates that, while patterns in the PDMS sustained cell ability to start differentiating on a soft hydrophilic surface, this effect was zinc concentration-dependent. However, the modification of zinc did not interfere with cells' ability to undergo early differentiation on TC (**Fig. 4.3 A & B**).

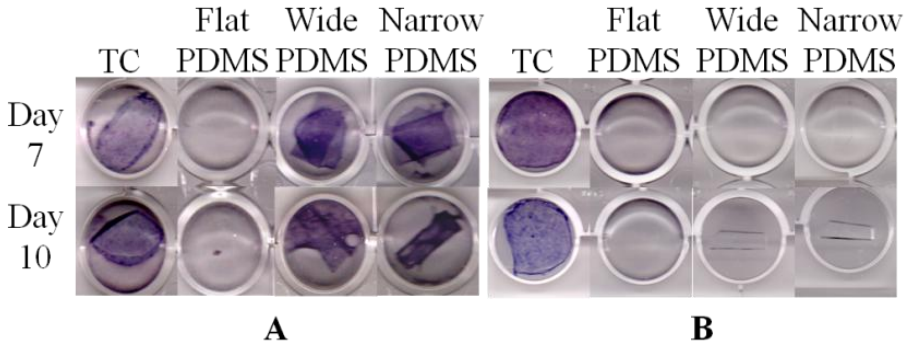

Figure 4.3. ALP production (indicated by dark purple color) by subclone 4 MC3T3-E1 cells in: (A) 3.6 μM zinc, (B) 50μM zinc.

Von Kossa

Von Kossa staining revealed an abundance of dark, punctate nodules in MC3T3-E1 cultured on TC for up to 28 days at serum-level zinc (3.6 μM; **Fig. 4.4 A**).[200] At elevated levels of zinc (50 μM), the von Kossa staining was lighter and more diffuse in color (**Fig. 4.4 A**). On either flat or patterned PDMS, calcium deposition appeared to be completely absent regardless of zinc concentration, except for the cells on wide micropatterns on day 28 (images representative of 30 fields of view), which produced a few small calcified clusters (**Fig. 4.4 B - D**). While cells on patterned PDMS had previously produced ALP in serum-level zinc conditions, this differentiation effect was not continued through late stage differentiation (**Fig. 4.4 C & D**). Increased zinc levels not only prevented cells on patterned PDMS from incurring ALP and bone nodules, it disrupted the cells' ability to differentiate on the rigid TC samples as well (**Fig. 4.4 A**; 50 μM).

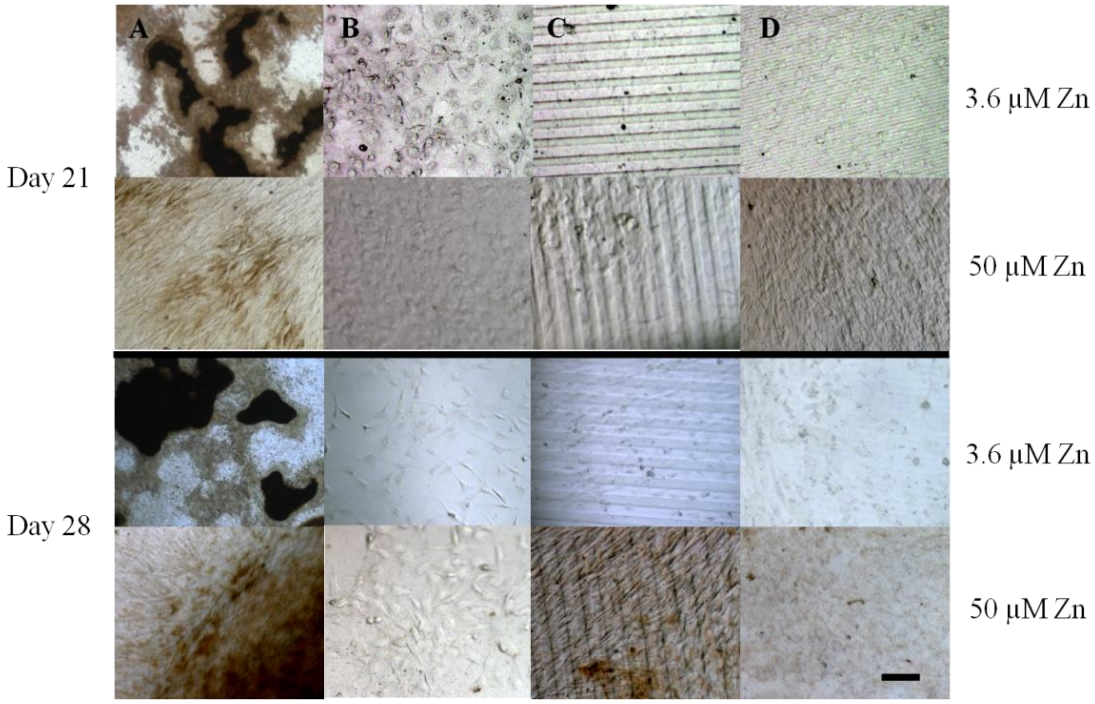

Figure 4.4. Von Kossa staining for calcium phosphate bone nodules (indicated by black areas) of subclone 4 MC3T3-E1 cells on: (A) TC, (B) flat PDMS (C) wide PDMS ridges, (D) narrow PDMS ridges. Images representative of 30 fields of view. Bar = 100 µm.

4.5 Discussion

Cell differentiation is a process which requires precise timing and convergence of factors that influence regulatory pathways. Thus, I sought to observe early and late stage osteoblast differentiation as well as the activity levels of transforming growth factor – beta 1 (TGF-β1) and metalloproteinase-2 (MMP-2), both of which are known to be instrumental in guiding the fate of differentiating osteoblast.[171]

It has been determined that both the chemical and physical factors in the environment contribute to the success of osteoblastic differentiation and new bone growth.[152,190] Previous studies have demonstrated that surface microtopographical features, achieved via micro-abrasion or lithographic patterning, alter cell growth, migration, and differentiation.[38,171,193] As shown previously in chapter three, anisotropic micropatterns fabricated in PDMS result in the directional migration of pre-osteoblasts.[197] This effect was mediated by levels of exogenous zinc, which could either enhance or diminish contact guidance of the cells. Much is still unknown about the effects of exogenous zinc on osteogenic differentiation and mineralization, a concern when considering the ossointegration of biomaterial implants.

Wojciak *et al*. first suggested that alignment of cells to ridges/grooves may depend on tyrosine phosphorylation of actin binding proteins, such as focal adhesion kinase (FAK) which is believed to be involved in signaling pathways leading to osteogenic differentiation.[183,202] On flat substrata the actin of rat macrophages was densest around the periphery of the cell, whereas on patterned substrata, actin, integrins and vinculins aggregated along the ridge/groove boundaries. Actin clustering at the edges of the PDMS

ridges was also observed in our previous study, particularly in those cell populations that exhibited contact guidance.[197]

The process of ligand clustering on anisotropic surfaces increases the local rigidity of microfilaments, raising cytoskeletal tension, which has been found to alter signaling pathways during the differentiation process.[167,194,195] However, the distinction between patterned and flat PDMS was present only in serum-levels of zinc, as depleting or increasing this cation abrogated all ALP production on the patterned surfaces. Cells on TC produced high amounts of ALP, without regard to zinc levels. The clear differences in early stage differentiation between patterned and flat PDMS were not upheld through late stage differentiation. Cells on TC continued the mineralization process through 28 days but only in serum-levels of zinc. Studies by Fukada *et al.* and Yamaguchi *et al.* have demonstrated that zinc is a crucial element for regulating bone health and homeostasis; deficiencies in this ion have resulted in diminished skeletal growth[144,146,147] and poor calcification of the ECM.[150] Zinc has been shown to act as a signaling molecule that is involved in several regulatory pathways.[172,173] The balance of intra- and extra- cellular zinc concentrations is governed by transporter proteins such as Slc39/ZIP and Slc30/ZnT.[145,174,175] Presence of the Zip13 and Zip 14 proteins have been shown to be factors in the coordination of mammalian cell growth through BMP/TGF-β and G-protein coupled receptor (GPCR)-mediated signaling pathways.[145,174] A study by Ma et al. showed that zinc levels directly determine production of TGF-β1 in newborn rats.[199] Znt5 has been presented as a regulator of osteoblast maturation and is required for the maintenance of bone density.[175]

In order to better understand the processes that govern differentiation, we investigated the role of the zinc-dependent metalloproteinase, MMP-2, in this system. This protein is responsible for increasing cell motility through localized ECM remodeling, a process which is required for multi-cell layering during mineralization.[11,96] It is secreted in its latent form and is then preferentially activated by a cell membrane-tethered MMP, MT1-MMP. Studies have shown that up-regulation of MT1-MMP results in increased ECM turnover, which is essential for osteoblast differentiation.[11,92,95] The activity of MMP-2 can also be mediated by ALP via phosphorylation.[107] In this study, we showed that cells on patterned PDMS produced similar amounts of MMP-2 and ALP as compared to cells on TC and yet they were much more motile on the former.[197] Cells on flat PDMS in serum-level zinc conditions (3.6 μM) had little to no MMP-2 production while yielding the fastest cell migration rate.[197] This effect is counterintuitive, as MMP-2 has been previously shown to be a promoter of cell migration.[11] It is interesting to note the lack of both MMP-2 and ALP on this flat PDMS surface in serum-level zinc conditions while zinc-rich (50 μM) media remarkably raised the levels of MMP-2 production to that of both patterned PDMS and TC while having little effect on ALP production. Thus, it was not increased ALP presence that propagated the increase in MMP-2 production, as it has previously been thought that ALP is an activator of MMP-2.[107] This may point to a discrepancy in how MMP-2 is activated or engaged on soft flat surfaces. A chemical imbalance via increased zinc levels on flat PDMS produced the same effect on MMP-2 activation as interaction with a patterned physical substrate.

We sought to further investigate this finding by observing TGF-β1 activation levels since zinc has been shown to promote secretion of this protein.[199] MMP-2 is also a known

effector of TGF-β1: the ECM-bound latency-associated peptide-1 (LAP-1) which renders TGF-β1 inactive, contains a metalloproteinase cleavage site for activation.[111] The LAP-1 associates with αvβ3 integrins, localizing it to the cell surface, and forming a triplex with MMP-2. This bridges MMP-2 to the ECM, which cleaves the LAP-1 (activating TGF-β1) and increases localized ECM remodeling as required for bone formation.[12] A substantial increase in the production of this activated growth factor was observed in the presence of exogenous zinc (50 μM) as compared to serum-levels on both TC and patterned PDMS surfaces, in agreement with other studies.[199] In all instances this increase was at least twice that of levels in serum conditions, while in the case of TC on day 8 this increase was nearly five-fold. In contrast, zinc-rich conditions on flat PDMS either caused a decrease or maintenance of similar amounts of activated TGF-β1 compared to serum conditions on days 8 and 11, respectively.

The precisely-timed activation of TGF-β1 is critical in the bone mineralization process and mis-alignment of timing could result in disruption of the mineralization of the ECM.[132,133,141] We have shown that patterned PDMS substrates supported TGF-β1 activation to similar extent and timing as TC in both serum-level zinc and zinc-rich conditions. Of note, flat PDMS produced the maximal amount of activated TGF-β1 on both days 8 and 11 in serum-level zinc (3.6 μM) media. Additionally, both TC and patterned PDMS surfaces yielded a decrease in levels of activated TGF-β1 from day 8 to day 11, while cells on flat PDMS increased in production during the same time frame. This could indicate that there exist differences in the timing of differentiation factors when cells are cultured on the various surfaces. Addition of exogenous activated TGF-β1 to cells at times beyond necessary has shown to decrease the levels of differentiation markers such as ALP and

results in the halt of bone mineral production later.[111,134,138] Thus, the distinctions in the timing of activated TGF-β1 could be responsible for the differences in ALP and calcium nodule production on soft non-patterned substrates. Presence of micropatterns in the PDMS substrate resulted in a more timely accumulation of TGF-β1, similar to that of TC, resulting in early, but not late stage differentiation of cells in serum-levels of zinc. This suggests that directional migration/contact guidance could be a critical step during early osteogenic differentiation.

As early as 7 days after induction with osteogenic media, distinct differences in ALP generation were seen between the substrates in the various zinc levels. The activity of this vital enzyme is an indicator of how well the cells generate inorganic phosphate to be used for late stage mineral production. Levels of ALP production on patterned PDMS partially complimented the trend seen in the activation of MMP-2. Patterns in PDMS were able to induce cells to generate substantial amounts of ALP, resembling that produced by cells on TC substrates (golden standard) in serum-levels of zinc. This effect was in stark contrast to that seen on flat PDMS, which rendered cells unable to produce visible ALP at any zinc level. The increase in ALP production may be explained from the clustering of actin fibers seen previously during contact guidance.[197] The process of ligand clustering on anisotropic surfaces increases the local rigidity of microfilaments, raising cytoskeletal tension, which has been found to alter signaling pathways during the differentiation process.[167,194,195] This response may be owed to the inherent substrate rigidity of TC, which generates high levels of cytoskeletal tension that promotes osteoblast differentiation.[30,195]

Von Kossa calcium phosphate staining revealed that patterns in PDMS could not sustain ECM mineralization through 21 days: all PDMS substrates were devoid of bone nodules regardless of zinc level. It is possible that the total cytoskeletal force exerted on the ECM was not sufficient to foster certain signaling events needed for complete osteogenic differentiation.[188] It has been suggested that there may be interacting TGF-β1 activation pathways that require attachment of cells to a non-compliant surface.[12] In this manner, integrins are engaged that are responsible for mechanically coupling cytoskeletal tension with TGF-β1 activation.[12,95] This indicates that this tightly regulated long-term process requires a certain level of zinc presence and cannot be sustained even when a high level of cytoskeletal force is maintained: late stage differentiation must then be regulated through an interplay of both substrate physical features and the trace metal conditions of the environment. Our results collectively indicate that anisotropy, surface compliance, and zinc levels in the extracellular fluid are all critical interdependent elements in directing the secretion of activated factors, which have a pivotal role in the regulation of osteogenic differentiation (**Fig. 4.5**).

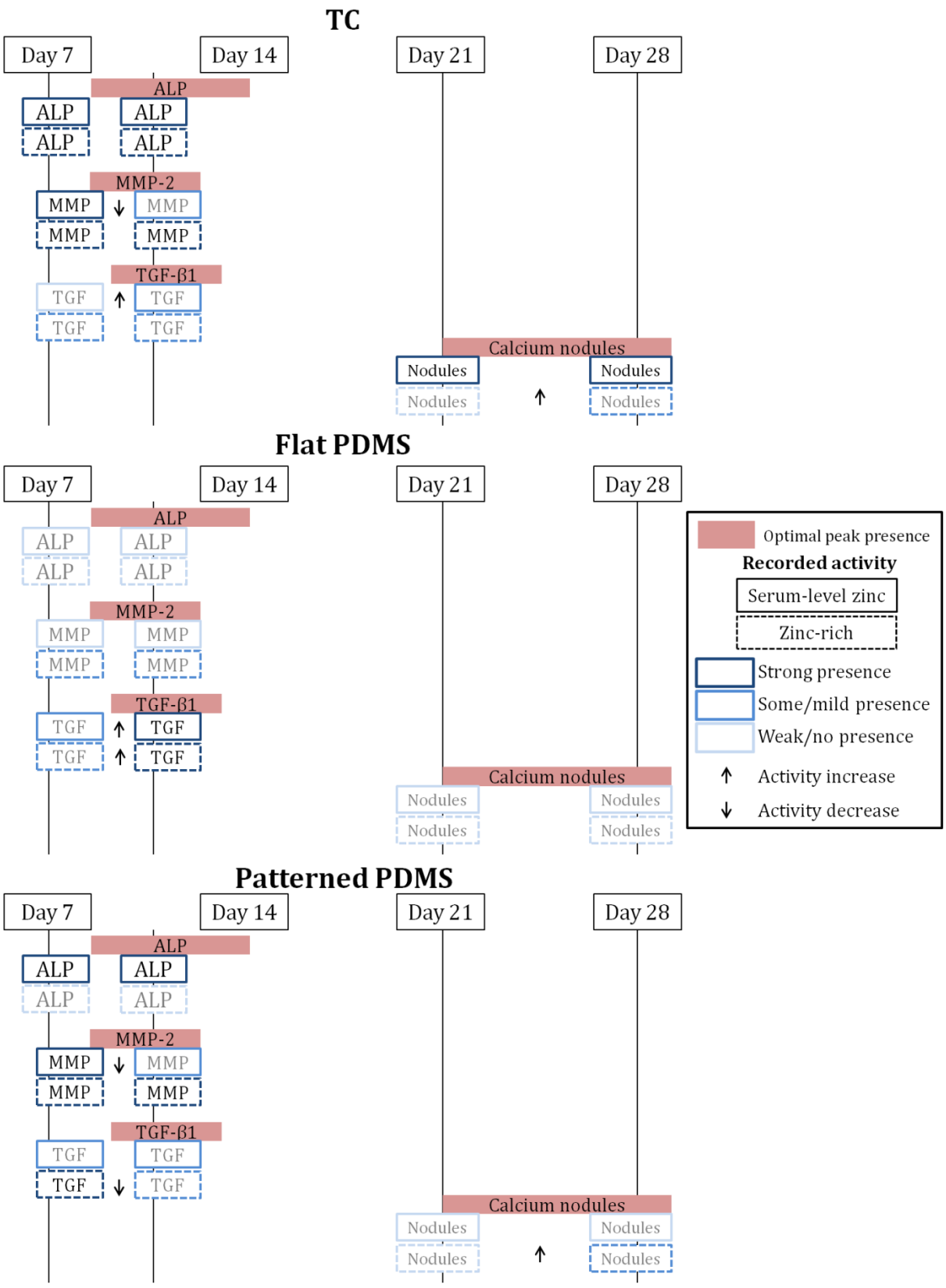

Figure 4.5. Differentiation timeline on TC, flat PDMS, and patterned PDMS

4.6 Conclusions

Compliant substrates delay growth factor secretion, leading to a disruption in late stage differentiation of pre-osteoblasts. The use of micropatterns in soft elastomers can help re-align the timing of early- to mid-stage differentiation to that of the ideal osteoblast phenotype. Without the aid of patterns this timing can be moderately re-aligned by utilizing a zinc-rich environment to produce an increase in levels of activated MMP-2.

4.7 Acknowledgements

Thanks to D. Rammelkamp for his guidance in creating the Zn-deprived FBS.

Chapter 5: Clonality

5.1 Abstract

Osteoblast phenotype is not only determined by origin and cell line, but can also be influenced by subcloning of a particular cell line. In Chapter 4, subclone 4 MC3T3-E1 cells demonstrated the ability to produce robust calcium nodules in the presence of serum-levels of zinc on TC substrates. In this chapter, another subclone of MC3T3-E1 pre-osteoblasts, subclone 24, is investigated in various substrate-ionic environments. This subclone has been determined to weakly mineralize the ECM in the presence of serum-zinc levels on TC, a direct opposite result as subclone 4. With altered zinc levels, cells were observed to produce a distinct positive result in terms of calcium nodule production. It was determined that growth and morphology were not hindered by modifying zinc levels, while early (ALP) and late stage (calcium nodules) differentiation processes were altered greatly. Therefore, zinc may play an important role in determining the mis-differentiation of this subclone.

5.2 Introduction

MC3T3-E1 cells are a unique cell line in that two distinct subclones have been identified, 4 and 24, which produce starkly different quantities of calcified nodules.[203] It is known that subclone 24 MC3T3-E1 cells are a weakly mineralizing clone of pre-osteoblasts.[184] While the intricate differentiation process is not fully understood, some research has shown that differences in collagen production may be at the root of the discrepancies in bone mineral production.[150] A study by Tang *et al*. found that mis-functional subclones, like subclone 24, behave much like their cancerous counterpart (osteosarcoma) by failing to produce bone mineral nodules.[204]

Alcantara *et al*. demonstrated that subclone 24 naturally produced higher levels of ALP, an enzyme required for the production of inorganic phosphate, a component of the calcium phosphate nodules that comprise bone.[150] This study also found that deprivation of zinc in the fluid environment resulted in decreased collagen synthesis, ALP activity, and calcium nodule production in both subclones 4 and 24.[150] With an increase in zinc, subclone 24 cells increased their ALP activity significantly, while subclone 4 cells had moderate increases. This study preliminarily demonstrates the differences between the subclones, as a factor of zinc content in the environment.

Subclone 24 cells' lessened ability to differentiate and produce minerals may possibly be due to sensitivity to ionic environmental factors, such as zinc. Chapters 3 and 4 highlighted the importance of zinc in the progression of early and mid-stage differentiation in subclone 4 cells. The demonstrated increase in MMP-2 and TGF-β1 activity in zinc-rich conditions of subclone 4 cells suggests that addition of exogenous zinc may be able to rescue the subclone 24 osteoblastic phenotype. The zinc-modified differentiation factors that aid in subclone 4 mineralization may be regulated differently under varied conditions to propel the mineralization of subclone 24 cells.

5.3 Materials and Methods

Substrate fabrication

The fabrication of micropatterns in PDMS was described in Chapters 3 and 4.[197] Briefly, standard photolithography was used to create sections of negative resist from which PDMS replicas containing two patterns (20 μm wide with a 30 μm pitch and 2 μm height, and 2 μm wide with a 10 μm pitch and 2 μm height) were created. PDMS substrates

were rendered hydrophilic using plasma oxygen.[177] As a control, unaltered 24-well tissue culture (TC) plates were used. PDMS substrates were functionalized with fibronectin, at 10 μg/mL followed by bovine serum albumin to block nonspecific protein binding.

Cell culture and development

Pre-osteoblast MC3T3-E1 cells (subclone 24; American Type Culture Collection (ATCC), Manassas, VA) were maintained using MEM-α supplemented with 10% fetal bovine serum (FBS) and 1% penicillin-streptomycin at 37˚C with 5% CO_2, 95% relative humidity. Media was supplemented with 4 mM glycerol 2-phosphate and 50 μg/mL sodium L-ascorbate and replaced every 2-3 days. Subclone 24 MC3T3-E1 pre-osteoblasts were chosen to compare with subclone 4 MC3T3-E1 cells used in Chapters 3 and 4, which demonstrated ability to produce copious amounts of calcium phosphate nodules on TC.[200]

As described in Chapters 3 and 4,[197] zinc levels were varied using a standardized process by Prasad *et al.* [178] and levels of zinc were reported as 3.6 μM (serum-level) and 0.23 μM (deficient chelexed FBS).[179] Zinc-rich conditions of 50 μM were used to mimic zinc supplementation to a deficient system.

Cell culture and development

Similarly to subclone 4 cells, subclone 24 weakly mineralizing MC3T3-E1 pre-osteoblast cells were maintained in MEM-α supplemented with 10% FBS and 1% penicillin-streptomycin. Cells were kept in an incubator at 37˚C with 5% CO_2, 95% relative humidity. For differentiation assays, medium was supplemented with 4 mM glycerol 2-phosphate and 50 μg/mL sodium L-ascorbate. The medium was replaced every 2-3 days. Chelexed FBS was produced as before and Zn levels were replenished using $ZnSO_4$.

Cell coverage

Cells were seeded at a density of 5,000 cells/cm^2 in a 24-well TC plate and incubated (5% CO_2, 95% humidified) at 37˚C for 24 hours. As described in Chapter 3, at each time point the samples were rinsed with PBS and fixed using 3.7% formaldehyde and stained using DAPI. Approximately 150 fluorescent images were captured for each sample. Images were quantified using ImageJ software and statistical analysis was performed to calculate the average cell density per sample.

Actin analysis

As described in Chapter 3, F-actin distribution was visualized with a standard inverted fluorescence microscope. Cells seeded at 5,000 cells/cm^2 were maintained for 24 hours to allow complete attachment to the substrate. After fixing with formaldehyde, cells were permeabilized and stained with Alexa Fluor 594 phalloidin. Using ImageJ, the average spreading area was calculated by converting the number of pixels in the cell area into micrometers^2.

The ImageJ particle measurement plugin was used to fit each cell area to an ellipse shape that represented the ratio of width/length of the cell to determine elongation and alignment to the *y*-axis/patterns. Actin alignment was defined as the angle formed between the major axis of the cell and the direction of the micropattern (*y*-axis), such that a complete, parallel alignment was indicated by 0°. For non-patterned samples, the *y*-axis was chosen arbitrarily to compare amongst samples. Around 50 cells were analyzed per sample.

Alkaline phosphatase production (ALP)

Twenty-four hours after seeding at 50,000 cells/cm^2, cells were given induction medium (supplemented with glycerol 2-phosphate and sodium L-ascorbate) for 7 days or 10 days. As described in Chapter 4, freshly prepared NBT and BCIP were added to each sample and allowed to incubate for 10 minutes at room temperature. Color development was stopped by rinsing the samples with deionized water. Images were captured using a color photo scanner.

Calcium phosphate nodules (von Kossa)

Cells used for von Kossa assay were cultured in induction medium for 21 and 28 days after seeding at 50,000 cells/cm^2. As described in Chapter 4, cells were covered with a silver nitrate solution and exposed to UV light for 20 minutes. The samples were then rinsed with water and covered with sodium thiosulfate. A color photo scanner was used to capture images.

Statistics

Each experiment consisted of a minimum of three replicates per treatment group. Statistical analysis was performed using an unpaired student t-test to and differences were considered significant at the level of $p<0.01 – 0.05$.

5.4 Results

Cell coverage

Across all surfaces and zinc concentrations, cell density did not vary much after 24 hours (**Fig. 5.1**). Thus, any subsequent results are not due to inability of the surfaces to support cell growth.

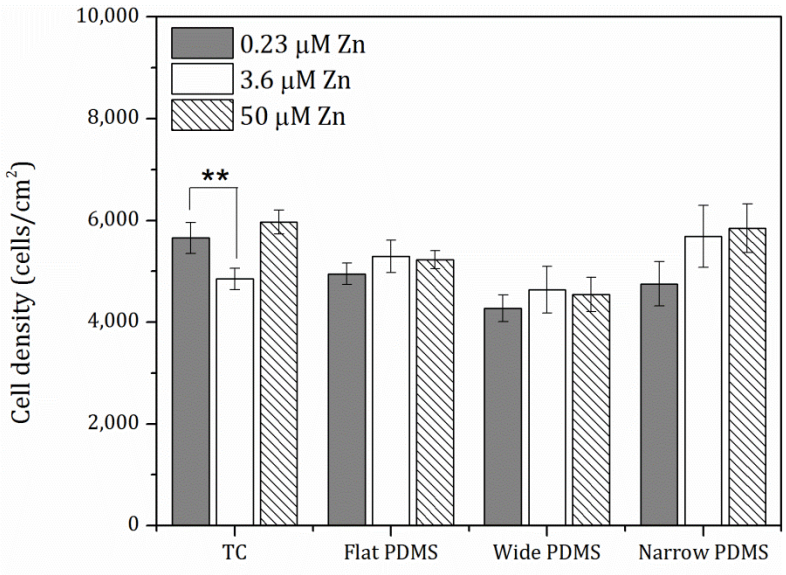

Figure 5.1. Cell coverage. Growth of subclone 24, MC3T3-E1 pre-osteoblast cells on various substrates with modifications of Zn concentrations after incubation for 24 hours. Double asterisks (**) indicate a $p<0.01$ difference.

Actin analysis

Twenty-four hours after seeding, cells had sufficiently adhered to their substrates and F-actin stress fibers were clearly visible in the cytoskeleton of cells on all substrates, as expected (**Fig. 5.2**). Non-patterned surfaces (TC and flat PDMS; **Fig 5.2 A & B and 5.3**) elicited a more spread out cell area than the patterned surfaces (wide and narrow PDMS; **Fig. 5.2 C & D and 5.3**), in a manner similar to subclone 4 cells seen in Chapter 3. Also reminiscent of subclone 4 cells, subclone 24 cells cultured on PDMS displayed increased lamellipodia protrusions as indicated by white arrows (**Fig. 5.2 B-D**). There was not distinguishable trend in cell shape due to fluctuations in zinc content. On wide PDMS patterns, actin accumulated along the ridges of the pattern (**arrowheads in Fig. 5.2 C**), much like that seen in subclone 4 cells.

The orientation of the actin cytoskeleton was dependent on topographical features, with actin fibers most clearly aligned with respect to the longitudinal direction of the pattern (**Fig. 5.2 C and 5.4 A**). Cells on the narrower PDMS micropatterns (2 μm/10 μm) were not as aligned, as several cells were oriented diagonally (**Fig. 5.2 D and 5.4 A**). On the non-patterned substrates, i.e. TC and flat PDMS, cell orientation was quite random (**Fig. 5.2 A & B and 5.4 A**). Elongation values, derived from comparing cell shape to an ellipse, supported the morphological observations, where cells on flat surfaces took on more rounded shapes (**Fig. 5.4 B**). Modification of zinc levels on a particular substrate did not statistically alter cell shape on each surface, indicating that the process of cell spreading is tightly controlled by physical features of the surface and not as affected by varied zinc concentrations (**Fig. 5.4 B**).

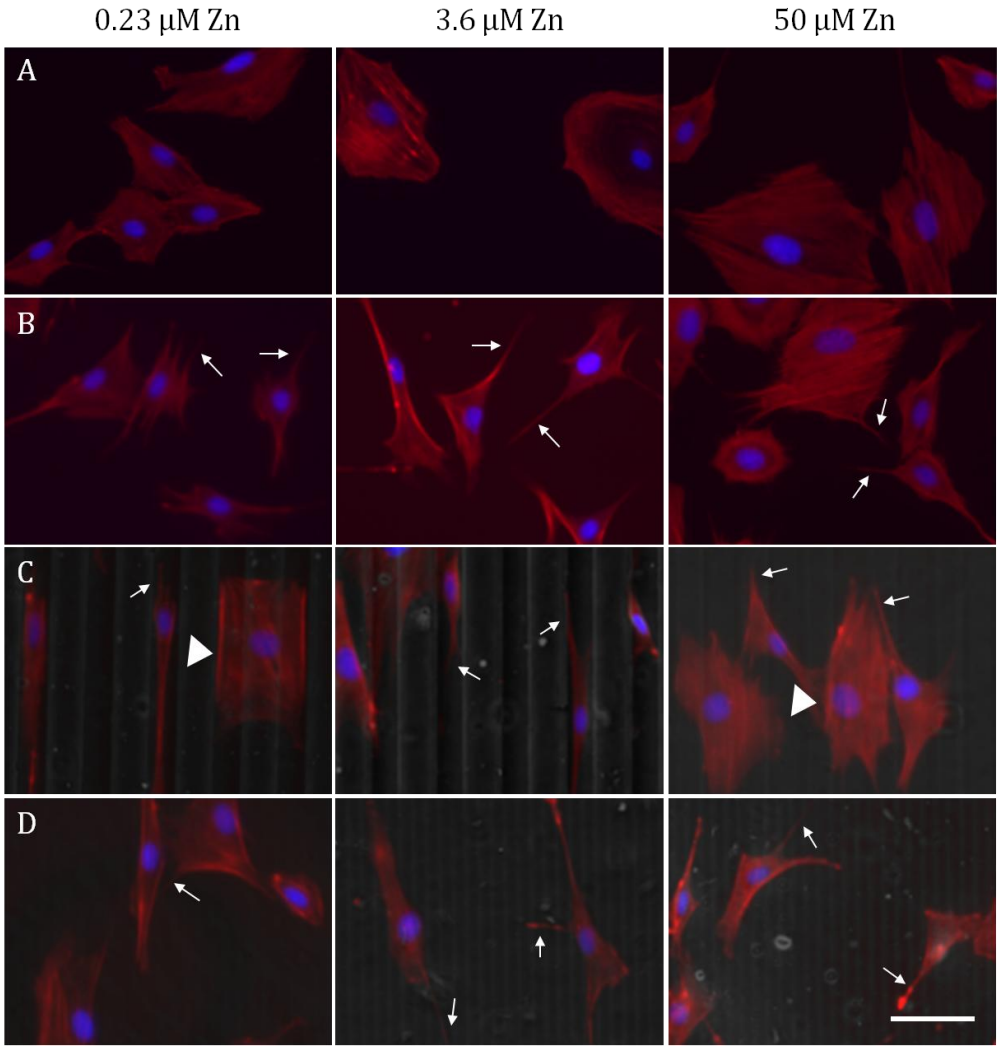

Figure 5.2. Actin Immunofluorescence. Immunofluorescence micrographs of subclone 24 MC3T3-E1 pre-osteoblasts 24 hours after seeding at various Zn concentrations on (A) TC, (B) flat PDMS, (C) wide PDMS FN, (D) narrow PDMS FN. Arrows indicate discrete lamellipodia protrusions while arrowheads in (C) indicate actin clustering on the edge of a micropattern. Bar = 50 µm.

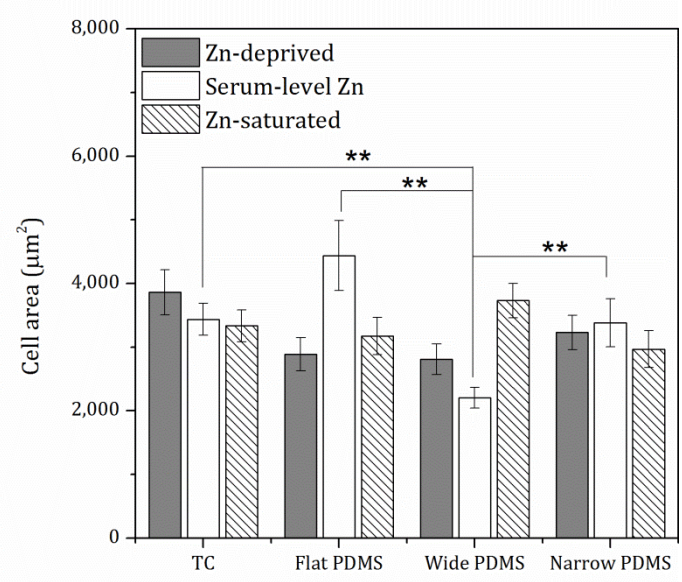

Figure 5.3. Cell spreading area computed from fluorescence micrographs in Fig 5.2. A-D. Double asterisks (**) indicate a $p<0.01$ difference.

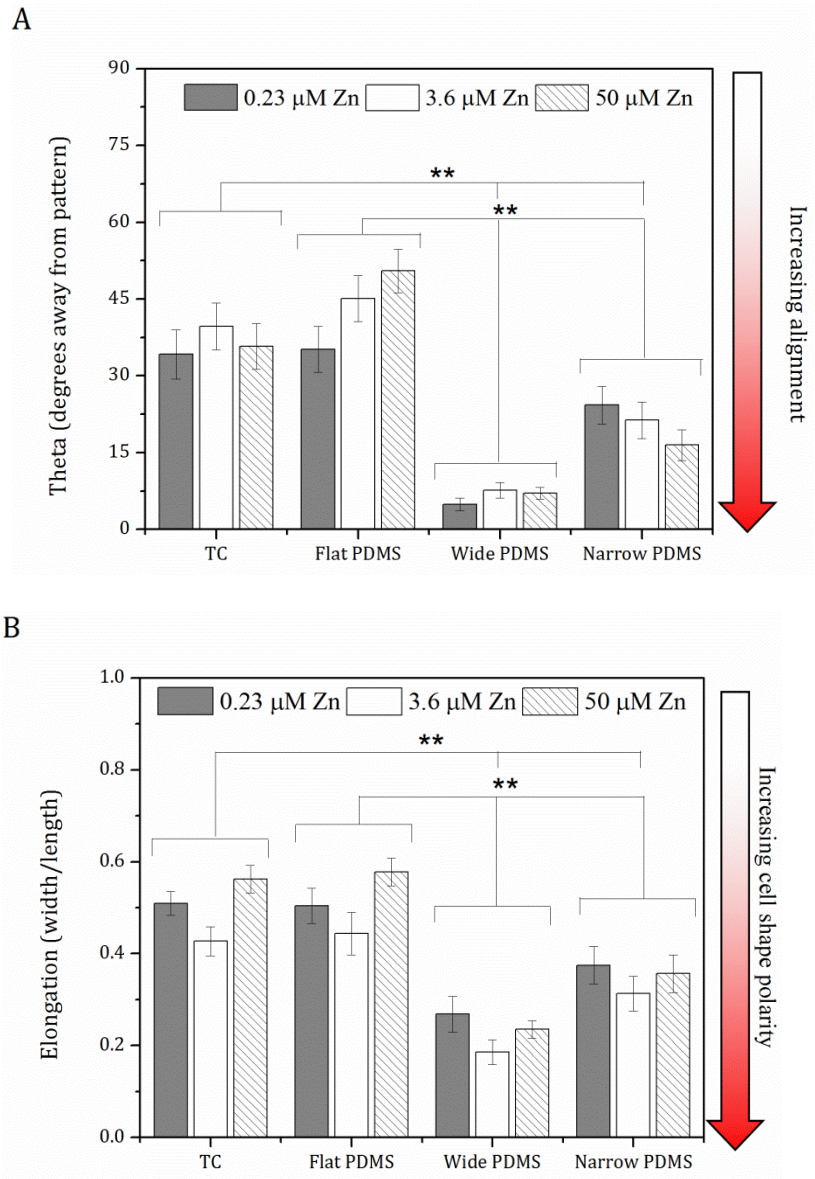

Figure 5.4. (A) Cell alignment computed from Fig. 5.2 A-D, where 0 degrees indicates complete alignment with patterned ridges/y-axis. (B) Cell shape aspect ratio was calculated from the same set of images and represents the use of ImageJ's ellipse fitting tool to determine ratio of cell width/length. Double asterisks (**) indicate a $p<0.01$ level of significance.

Alkaline phosphatase (ALP) production

In a manner similar to subclone 4 cells, distinct differences in ALP production by subclone 24 cells were seen across the various substrates after stimulation with ascorbic acid and glycerol 2-phosphate (**Fig. 5.5**). Cells on TC and patterned PDMS produced a vivid dark purple color by day 7 in serum-levels of zinc, indicating robust ALP activity (**Fig. 5.5 A & C-D**). However, on patterned PDMS, this effect was not continued through modified zinc levels (0.23 μM and 50 μM), while ALP levels remained constant on TC throughout zinc variations (**Fig. 5.5 A**). In contrast to subclone 4 cells' inability to produce ALP on flat PDMS at any zinc level, subclone 24 cells did produce minor amounts of ALP on flat PDMS in both zinc-deprived (0.23 μM) and zinc-rich media (50 μM; **Fig. 5.5 B**) but failed to produce visible amounts of ALP in serum levels (3.6 μM).

Calcium nodules (von Kossa)

While cells produced small sparse calcium nodules (black areas) on TC after 28 days of incubation in induction media at serum level Zn (3.6 μM), much larger nodules were seen with altered levels of Zn at either 0.23 μM or 50 μM (**Fig. 5.6 A**). Of note, while cells produced ALP at all zinc levels on TC, only at modified levels of Zn did cells produce calcified nodules on this surface. In contrast, subclone 4 cells did not produce bone nodules when cultured in modified levels of zinc on TC, the opposite effect seen with subclone 24 cells. All PDMS surfaces, both flat and patterned, failed to produce visible calcium nodules at any zinc level (**Fig. 5.6 B - D**), despite signs of successful early differentiation (**Fig. 5.5**).

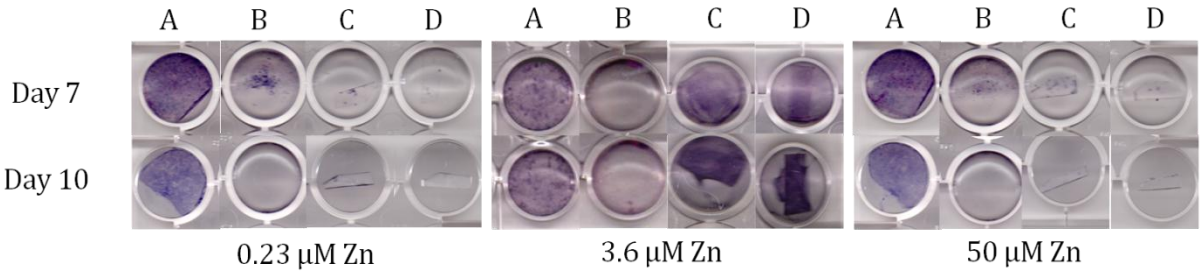

Figure 5.5. ALP activity (days 7 and 10) of subclone 24 MC3T3-E1 cells on: (A) TC, (B) flat PDMS, (C)wide PDMS ridges, (D) narrow PDMS ridges with modified Zn concentrations.

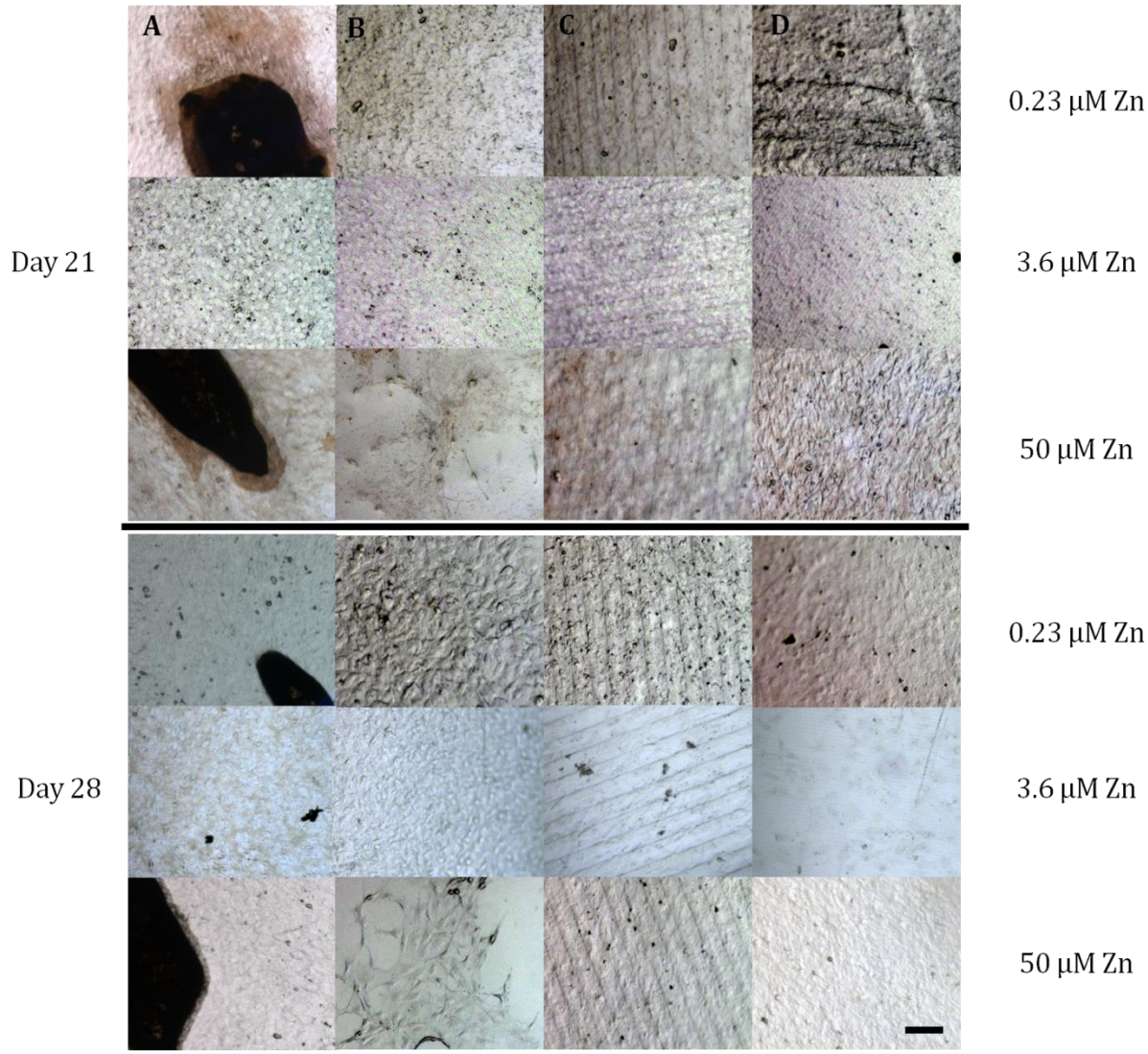

Figure 5.6. Von Kossa staining for calcified nodules (days 21 and 28) of subclone 24 MC3T3-E1 cells on: (A) TC, (B) flat PDMS (C) wide PDMS ridges, (D) narrow PDMS ridges with modified Zn concentrations. Bar = 100 μm.

5.5 Discussion

Previous studies have found that mis-functional cells, such as subclone 24 MC3T3-E1 non-mineralizing pre-osteoblasts, behave much like their cancerous counterpart (osteosarcoma) in that they fail to properly undergo complete differentiation while over-expressing other differentiation factors.[150,204] A study by O'Dell *et al.* demonstrated that zinc deficiency resulted in decreased proliferation of cells,[143] however we have shown that both subclone 4 and 24 maintained their cell density, despite alterations in zinc levels.[197] Morphologically, the subclone 24 cells appeared similar to the subclone 4 cells, indicating that the divergence between the two subclones occurs at a later point in the differentiation pathway.

Examination of early stage differentiation also indicated comparable results between the subclones, as cells on TC and patterned PDMS produced large amounts of ALP in serum-level zinc conditions. While sharing similarities in ALP production, these subclones then diverged, indicating a break in the parallel pathways of differentiation. I hypothesized that since additional levels of zinc were able to alter growth factor and proteinase activity in subclone 4 cells that this cation could play a part in changing levels of differention in subclone 24 cells. By modifying zinc levels, subclone 24 cells were able to undergo late stage differentiation which was impossible in serum-level zinc. Studies have indicated that osteosarcoma cells produce a superfluous amount of MMP-2, resulting in excessive amounts of ECM turnover, disrupting later differentiation.[204] It is possible that subclone 24 cells also share this excess in MMP-2 production, although not investigated in this study, and this may halt differentiation but would be disrupted by zinc level modification.

Alcantara *et al*. demonstrated the importance of zinc in their studies of both subclone 4 and 24 MC3T3-E1 cells.[150] It was found that by depriving both subclones of zinc, production of ALP and subsequent collagen production and differentiation was halted, a result supported by others.[148,154] Zinc has been determined to be a potent regulator of ALP and collagen-I production: Zn is a co-factor of ALP and when it is dissociated from the enzymatic protein it results in inactivation of the enzyme.[179,205] Thus, it was unexpected to observe ALP production in our zinc-deprived (0.23 μM Zn) and zinc-saturated (50 μM Zn) TC samples. Nagata *et al*. demonstrated that while zinc deficiency resulted in poor calcified nodules, that this deprivation is time sensitive.[148] In their study, early differentiation was promoted with addition of exogenous zinc, while zinc deprivation at a later stage seemed to have less of an effect on mineralization, concurring with our results of subclone 24 cells.[148]

The intracellular transport of zinc is controlled by zinc-binding storage proteins such as the metallotheioneins (MT) and zinc transporters such as ZnT and Zip.[145,146,174] ZnT is a transporter protein responsible for decreases in intracellular zinc (transporting it outside the cell), while Zip proteins are responsible for increases in intracellular zinc (transporting it into the cell).[148,149] It is possible that these pathways are regulated differently between the subclones of pre-osteoblasts, which may be why zinc alters differentiation in distinct ways. This hypothesis may be extended to other cells with mis-functional differention pathways, such as osteosarcoma. Altering trace metal levels therefore may be a possible means to rectify differentiation-based diseases.

5.6 Conclusions

Strongly mineralizing subclone 4 and weakly mineralizing subclone 24 display similarities in growth and morphology when grown on various surfaces and in modified zinc media. The parallels between the subclones continue through early-mid stage differentiation, as shown by similarities in ALP production. However, distinctions arise at later stages of differentiation, where calcium nodule production is dissimilar. Modifications in exogenous zinc levels determined that the subclones are affected by the cation in dissimilar ways, producing bone nodules under opposite conditions. Zinc plays a critical role in late differentiation of pre-osteoblasts and may regulate this process in different ways in cells with mis-functional differentiation.

5.7 Acknowledgements

Thanks to D. Rammelkamp for his guidance in creating the Zn-stripped FBS.

Chapter 6: Summary

6.1 Final discussion

Centuries ago, early medicine utilized the first materials that interacted with body tissues and organs. Often accompanied by high rates of failure, these primitive means propelled the desire to understand biocompatibility. The modern field of biomaterials is relatively new and only now, with recent technologies, are we able to begin to elucidate the interactions that take place when a foreign material meant for long-term use is placed into a cellular system.

Cell behavior depends on small-scale interactions between focal adhesions and proteins adsorbed on the surface of a substrate. Material properties have been shown to influence this initial protein adsorption and ultimately determine how cells attach and survive on the substrate. In their natural *in vivo* environment, proteins expressed on surrounding tissues are presented to the focal adhesions of cells in a specific manner. It is the goal of biomaterials to elicit a similar protein adsorption response and to successfully develop the ECM of the external cell environment, a requirement for successful integration.

The purpose of this dissertation was to provide a better understanding of how physical and mechanical properties of biomaterials (such as topography and rigidity) can affect and produce very specific changes in regard to cell migration and differentiation. Alterations in the ionic aqueous environment can mediate these changes to a large extent, indicating that not only the physical but chemical surroundings must be considered. Furthermore, cellular response to changes in the ionic environment can differ not only by cell type or origin, but also within a single cell line, between subclones.

Micro-topographies were utilized in this work to distinguish cell behaviors that are affected by physical features, while maintaining constant surface chemistry and mechanical properties. Two subclones of the same cell line of pre-osteoblasts were chosen due to well-known contrasts in differentiation. In order to better understand the implications of the aqueous environment on cell-substrate interactions, variations in zinc content were used to demonstrate deficient (0.23 μM), surplus (50 μM), or serum-levels (3.6 μM) of this ion. Time-points were selected to demonstrate adhesion, spreading, migration, and production of differentiation markers, all critical components of biomaterial integration.

The first indicator of successful material biocompatibility is the ability to maintain and grow cells. Both subclones maintained cell coverage across the varied surfaces, indicating that these substrates supported cell adhesion to the same extent as the golden standard, tissue culture polystyrene. Additionally, modification of zinc content did not interfere with cell coverage or modulate cell morphology. However, cell morphology was highly dependent on materials' Young's modulus and possibly surface chemistry. Both subclone 4 and 24 cells on PDMS substrates had far more lamellipodial protrusions than cells on rigid TC. Organization of the actin fibers within the cell body was varied based on topographical features of the surfaces. Both flat PDMS and TC promoted more rounded, less polarized cell spreading in a random fashion, while patterned PDMS surfaces encouraged cell growth along the axis of the pattern, in a much more elongated, linear shape in both subclones. Zinc levels only slightly modulated shape and alignment but not to a significant amount and not with a distinguishable trend.

Migration rates and displacement patterns were found to be different at the various zinc levels. Increase in zinc content resulted in significant decreases in cell speed on flat PDMS, but did not elicit a discernible trend on cells migrating on the other surfaces. Augmentation of zinc levels hindered the significant contact guidance that was demonstrated by cells on the wide PDMS patterns. This indicates that the chemical environment plays a significant role in how cells interact with material substrates. Contact guidance is considered the one of the first steps of integration of cells to topographies which may eventually control later distribution of growth factors and alignment of the cytoskeleton. This can be extended to biomaterial integration as a whole, where alignment can lead to less scar tissue formation.[206]

As osteoblastic cells proliferate and become confluent, they develop their ECM in preparation for the start of the mineralization process, which is indicative of properly differentiating cells. Growth factors and proteases are mediators of the ECM development stage and are secreted and activated in response to the physical and chemical environment. Integrins of the focal adhesion complex are responsible for sequestering these factors to the cell surface for localized activity. These integrins were initialized during attachment of the cell to the substrate and the combination of the alpha and beta units and their availability varies throughout the differentiation process. The specific integrins responsible for sequestration of growth factors and proteases is still not clear, and it is possible that groupings of several different alpha-beta pairs may compensate for more variability within certain environments.

In this work, it was also demonstrated that the increased availability of zinc ions resulted in substantially more MMP-2 and TGF-β1 activation. This was most noticeable on flat PDMS, which failed to produce significant amounts of MMP-2 in serum-levels of zinc, but was able to support MMP-2 activation to the same extent as the golden standard, TC, in zinc-rich conditions. The micro-topographies in PDMS produced a similar effect, where levels of MMP-2 were comparable to TC in both serum and increased zinc levels. Activation of TGF-β1 was also modified by both topography and zinc content, most noticeably on TC and patterned PDMS surfaces.

In a similar manner to MMP-2 activation, patterns in PDMS induced cells to produce TGF-β1 to the same extent as cells on TC. Additionally, zinc-rich conditions promoted increased TGF-β1 production on both TC and patterned PDMS surfaces. Increased zinc levels decreased TGF-β1 activation on flat PDMS by day 8 and had no effect by day 11 on the same surface. However, TGF-β1 production on flat PDMS was the highest among all the surfaces at serum-zinc levels, indicating that this substrate may induce overproduction of this growth factor. Increased levels of TGF-β1 at late stages has been indicated as a mineralization deterrent in other studies.[111] The peak timing of TGF-β1 occurred on day 8 for cells on both patterned PDMS and TC in serum-levels of zinc, but occurred on day 11 for cells on these substrates in zinc-rich media. The delay of TGF-β1 activation in both zinc-rich conditions and on flat PDMS may have deterred late-stage mineralization of the ECM, resulting in the inability for subclone 4 cells to produce bone nodules on non-patterned soft substrates and those in surplus zinc environments.

Early-mid stage differentiation, in the form of ALP production, was increased on patterned PDMS samples to and raised to the same level as cells on TC in serum-level zinc. However, this effect was disrupted when cells on patterned PDMS were placed in a zinc-rich environment. Both flat PDMS and TC were unaffected by zinc concentration, but produced stark contrasts in production of this enzymatic protein. Cells on flat PDMS failed to produce any visible ALP at any zinc level while TC maintained continuous substantial production. This effect could be explained through the differences in material rigidity, as mentioned before, substrate compliance will often not provide enough cytoskeletal tension in order to continue differentiation processes. The effect on ALP was consistent among both subclone 4 and 24 cells but their parallel pathways diverged during late stage differentiation. Both increased and decreased zinc content produced calcium nodules on TC in subclone 24 cells, which are notoriously weakly mineralizing in serum-levels of zinc. In contrast, subclone 4 cells only produced calcium nodules in serum-levels of zinc on TC and altering the zinc content disrupted this effect. Both subclones failed to produce significant calcium nodules on all PDMS surfaces, with only a small increase seen on subclone 4 wide patterns in zinc-rich conditions. This indicates that while patterns can increase early stage differentiation markers such as MMP-2, TGF-β1, and ALP this effect is not carried through to late stage differentiation and substrate rigidity and a specific ionic environment may be the ultimate determinates of cell differentiation fate.

6.2 Limitations

No body of research is without its limitations and while this work endeavored to not include biases, a few restrictions must be noted.

Physical limitations, such as the inability to pattern TC without changing surface chemistry and wettability, resulted in an incomplete set of both rigid and soft substrates with micro-topographies. Additionally, fabricating patterns in PDMS may induce micro-rigidity which may be responsible for the increased differentiation effects seen on these substrates. Overcoming this limitation would involve making several sets of variations in PDMS and determining micro-mechanical properties using an AFM. Beyond this, actin and focal adhesion clustering could also create micro-tension by the spatial distribution of the integrins along patterns.

Another limiting aspect is the inability to decouple surface chemistry from inherent material properties. The surface compositions of TC and PDMS are vastly different and cannot be compared directly. Some studies have tried to maintain surface chemistry while adjusting material rigidity by utilizing various cross-linked polyacrylamide gels but this requires this use of different amounts of cross-linking agent, which would still modify surface chemistry. In regard to chemical limitations, this work uses small resin chelex beads to remove zinc (and other metals) from FBS. This method is established, but there is a lack of information on determining the actual content (ions, proteins, etc.) of FBS before and after using chelex resin. This is especially difficult to characterize due to the inherent variability of FBS from batch to batch, thus samples were incubated in the same set of media to minimize batch-to-batch variation.

6.3 Future work and outlook

Additional experiments that would complete this work would include investigations of MMP-2 and TGF-β1 activation in subclone 24 as to compare with subclone 4 levels and

to determine if their parallel pathways diverge during this stage. A complete screening of integrins responsible for differentiation effects would elucidate the molecular means which lead to the changes seen in TGF-β1 and MMP-2 due to Zn levels.

The studies in this dissertation were primary investigations into how cells and materials interact on an interfacial level. To take this work beyond the lab and be more applicable to available medical implants, other materials would need to be considered. Most implants are created from metals and alloys, and are much more rigid surfaces than the TC and PDMS surfaces utilized in this work. As a bridge to new investigations in the medical realm, the same micropatterns created in PDMS could be fabricated in single crystalline <100> silicon to observe effects of patterns on very rigid surfaces.

The signaling of integrins, as controlled by the organization of the cytoskeleton is heavily influenced by the rigidity of the ECM or ECM-mimicking substrates. One study demonstrated that pre-osteoblasts proliferated and differentiated into full-phenotype osteoblasts that mineralized bone to a much greater extent and in a faster many on stiffer substrates.[26] Other cell lines, such a smooth muscle cells and fibroblasts have exhibited faster migration speeds when traveling on softer rather than more rigid substrates.[14,15,27-29] These findings are in agreement with our own results, where the fastest migration took place on flat PDMS and the slowest was on the rigid TC. This observation could be used to determine how cells interact with their implanted metal substrate – a faster cell may not anchor itself as well as a slower moving cell.

Demonstrated preferential migration, or mechanotaxis, of osteoblasts toward stiffer substrates supports conclusions from other studies investigating the effect of substrate

rigidity on lineage outcomes. Engler *et al.* found that matrix stiffness greatly affected the differentiation outcome of several progenitor cells. Mouse stem cells grown on substrates with varying elastic moduli were found to differentiate (express lineage markers) into neurons, myoblasts, or osteoblasts depending on the rigidity of the substrate material.[30] Other studies confirmed these findings, demonstrating that differentiated neurons are more likely to extend dendritic arms on soft scaffolds, mimicking the small elastic modulus of brain tissue, while optimal cardiomyocyte differentiation has been found to occur on rigid scaffolds that mimicked striated muscle fibers.[31,32] Thus, a stiffer surface should be considered in investigations on how patterns induce pre-osteoblast differentiation.

This work has sought to increase understanding of cell-material interactions within a set of physiologically relevant environments. *In vitro* results, demonstrating modified contact guidance and differentiation factors, can be extended to imply significance of these factors for consideration when progressing toward *in vivo* implantation of biomaterials.

References

1. Aging Ao. Aging Statistics. Volume 2010.

2. Johnell O, Kanis JA. An estimate of the worldwide prevalence and disability associated with osteoporotic fractures. Osteoporos Int 2006;17(12):1726-33.

3. Melton LJ, 3rd, Atkinson EJ, O'Connor MK, O'Fallon WM, Riggs BL. Bone density and fracture risk in men. J Bone Miner Res 1998;13(12):1915-23.

4. Freid VM, Bernstein AB, National Center for Health S. Health care utilization among adults aged 55-64 years : how has it changed over the past 10 years? Hyattsville, MD: U.S. Dept. of Health and Human Services, Centers for Disease Control and Prevention, National Center for Health Statistics; 2010.

5. Bozic KJ, Rubash HE, Berry J, J. SK, Durbhakula SM. Hip and Knee Replacement. April 2010.

6. Daley WP, Peters SB, Larsen M. Extracellular matrix dynamics in development and regenerative medicine. Journal of Cell Science 2012;121(3):255-264.

7. Yamaguchi A, Komori T, Suda T. Regulation of osteoblast differentiation mediated by bone morphogenetic proteins, hedgehogs, and Cbfa1. Endocr Rev 2000;21(4):393-411.

8. Roman-Roman S, Garcia T, Jackson A, Theilhaber J, Rawadi G, Connolly T, Spinella-Jaegle S, Kawai S, Courtois B, Bushnell S and others. Identification of genes regulated during osteoblastic differentiation by genome-wide expression analysis of mouse calvaria primary osteoblasts in vitro. Bone 2003;32(5):474-82.

9. Lian JB, Stein GS. Development of the osteoblast phenotype: molecular mechanisms mediating osteoblast growth and differentiation. Iowa Orthop J 1995;15:118-40.

10. Balcerzak M, Hamade E, Zhang L, Pikula S, Azzar G, Radisson J, Bandorowicz-Pikula J, Buchet R. The roles of annexins and alkaline phosphatase in mineralization process. Acta Biochim Pol 2003;50(4):1019-38.

11. Bozzuto G, Ruggieri P, Molinari A. Molecular aspects of tumor cell migration and invasion. Ann Ist Super Sanita 2010;46(1):66-80.

12. Wipff PJ, Hinz B. Integrins and the activation of latent transforming growth factor beta1 - an intimate relationship. Eur J Cell Biol 2008;87(8-9):601-15.

13. Beck GR, Jr., Zerler B, Moran E. Gene array analysis of osteoblast differentiation. Cell Growth Differ 2001;12(2):61-83.

14. Engler A, Bacakova L, Newman C, Hategan A, Griffin M, Discher DE. Substrate Compliance versus Ligand Density in Cell on Gel Responses. Biophysical Journal 2004;86(1):617-628.

15. Lo CM, Wang HB, Dembo M, Wang YL. Cell movement is guided by the rigidity of the substrate. Biophys J 2000;79(1):144-52.

16. Charras GT, Horton MA. Determination of cellular strains by combined atomic force microscopy and finite element modeling. Biophysical Journal 2002;83(2):858-879.

17. Formigli L, Meacci E, Sassoli C, Chellini F, Giannini R, Quercioli F, Tiribilli B, Squecco R, Bruni P, Francini F and others. Sphingosine 1-phosphate induces cytoskeletal reorganization in C2C12 myoblasts: physiological relevance for stress fibres in the modulation of ion current through stretch-activated channels. Journal of Cell Science 2005;118(6):1161-1171.

18. Gomes ME, Sikavitsas VI, Behravesh E, Reis RL, Mikos AG. Effect of flow perfusion on the osteogenic differentiation of bone marrow stromal cells cultured on starch-based three-dimensional scaffolds. Journal of Biomedical Materials Research Part A 2003;67A(1):87-95.

19. Batra NN, Li YJ, Yellowley CE, You LD, Malone AM, Kim CH, Jacobs CR. Effects of short-term recovery periods on fluid-induced signaling in osteoblastic cells. Journal of Biomechanics 2005;38(9):1909-1917.

20. Holtorf HL, Jansen JA, Mikos AG. Flow perfusion culture induces the osteoblastic differentiation of marrow stromal cell-scaffold constructs in the absence of dexamethasone. Journal of Biomedical Materials Research Part A 2005;72A(3):326-334.

21. Chiquet M. Regulation of extracellular matrix gene expression by mechanical stress. Matrix Biology 1999;18(5):417-426.

22. Jansen JHW, Eijken M, Jahr H, Chiba H, Verhaar JAN, van Leeuwen J, Weinans H. Stretch-Induced Inhibition of Wnt/beta-Catenin Signaling in Mineralizing Osteoblasts. Journal of Orthopaedic Research 2010;28(3):390-396.

23. Cunningham JJ, Linderman JJ, Mooney DJ. Externally applied cyclic strain regulates localization of focal contact components in cultured smooth muscle cells. Annals of Biomedical Engineering 2002;30(7):927-935.

24. Katanosaka Y, Bao J, Komatsu T, Suemori T, Yamada A, Mohri S, Naruse K. Analysis of cyclic-stretching responses using cell-adhesion-patterned cells. Journal of Biotechnology 2008;133(1):82-89.

25. Kihara T, Haghparast SMA, Shimizu Y, Yuba S, Miyake J. Physical properties of mesenchymal stem cells are coordinated by the perinuclear actin cap. Biochemical and Biophysical Research Communications 2011;409(1):1-6.

26. Khatiwala CB, Peyton SR, Putnam AJ. Intrinsic mechanical properties of the extracellular matrix affect the behavior of pre-osteoblastic MC3T3-E1 cells. Am J Physiol Cell Physiol 2006;290(6):C1640-50.

27. Pelham RJ, Wang Y-l. Cell locomotion and focal adhesions are regulated by substrate flexibility. Proceedings of the National Academy of Sciences 1997;94(25):13661-13665.

28. Peyton SR, Putnam AJ. Extracellular matrix rigidity governs smooth muscle cell motility in a biphasic fashion. J Cell Physiol 2005;204(1):198-209.

29. Wong JY, Velasco A, Rajagopalan P, Pham Q. Directed Movement of Vascular Smooth Muscle Cells on Gradient-Compliant Hydrogels†. Langmuir 2003;19(5):1908-1913.

30. Engler AJ, Sen S, Sweeney HL, Discher DE. Matrix elasticity directs stem cell lineage specification. Cell 2006;126(4):677-89.

31. Flanagan LA, Ju YE, Marg B, Osterfield M, Janmey PA. Neurite branching on deformable substrates. Neuroreport 2002;13(18):2411-5.

32. Jacot JG, McCulloch AD, Omens JH. Substrate stiffness affects the functional maturation of neonatal rat ventricular myocytes. Biophys J 2008;95(7):3479-87.

33. Bustillo JM, Howe RT, Muller RS. Surface micromachining for microelectromechanical systems. Proceedings of the IEEE 1998;86(8):1552-1574.

34. Fu G, Soboyejo WO. Cell/surface interactions of human osteo-sarcoma (HOS) cells and micro-patterned polydimelthylsiloxane (PDMS) surfaces. Materials Science and Engineering: C 2009;29(6):2011-2018.

35. Belanger MC, Marois Y. Hemocompatibility, biocompatibility, inflammatory and in vivo studies of primary reference materials low-density polyethylene and polydimethylsiloxane: a review. J Biomed Mater Res 2001;58(5):467-77.

36. Charati SG, Stern SA. Diffusion of Gases in Silicone Polymers: Molecular Dynamics Simulations. Macromolecules 1998;31(16):5529-5535.

37. Chen CS, Mrksich M, Huang S, Whitesides GM, Ingber DE. Geometric Control of Cell Life and Death. Science 1997;276(5317):1425-1428.

38. Lee SW, Kim SY, Lee MH, Lee KW, Leesungbok R, Oh N. Influence of etched microgrooves of uniform dimension on in vitro responses of human gingival fibroblasts. Clin Oral Implants Res 2009;20(5):458-66.

39. Lee SW, Kim SY, Rhyu IC, Chung WY, Leesungbok R, Lee KW. Influence of microgroove dimension on cell behavior of human gingival fibroblasts cultured on titanium substrata. Clin Oral Implants Res 2009;20(1):56-66.

40. Lim JY, Dreiss AD, Zhou Z, Hansen JC, Siedlecki CA, Hengstebeck RW, Cheng J, Winograd N, Donahue HJ. The regulation of integrin-mediated osteoblast focal adhesion and focal adhesion kinase expression by nanoscale topography. Biomaterials 2007;28(10):1787-97.

41. Maeda YT, Inose J, Matsuo MY, Iwaya S, Sano M. Ordered Patterns of Cell Shape and Orientational Correlation during Spontaneous Cell Migration. PLoS ONE 2008;3(11).

42. Martinez E, Engel E, Lopez-Iglesias C, Mills CA, Planell JA, Samitier J. Focused ion beam/scanning electron microscopy characterization of cell behavior on polymer micro-/nanopatterned substrates: a study of cell-substrate interactions. Micron 2008;39(2):111-6.

43. Miller C, Shanks H, Witt A, Rutkowski G, Mallapragada S. Oriented Schwann cell growth on micropatterned biodegradable polymer substrates. Biomaterials 2001;22(11):1263-1269.

44. Pesen D, Haviland DB. Modulation of Cell Adhesion Complexes by Surface Protein Patterns. ACS Applied Materials & Interfaces 2009;1(3):543-548.

45. Sjöström T, Dalby MJ, Hart A, Tare R, Oreffo ROC, Su B. Fabrication of pillar-like titania nanostructures on titanium and their interactions with human skeletal stem cells. Acta Biomaterialia 2009;5(5):1433-1441.

46. Su W-T, Yang J-Y, Lin C-D, Chu I-M. Control Cell Behavior on Physical Topographical Surface. Japanese Journal of Applied Physics Part 1-Regular Papers Short Notes & Review Papers 2004;43(6B):3806- 3809.

47. Cavalcanti-Adam EA, Aydin D, Hirschfeld-Warneken VC, Spatz JP. Cell adhesion and response to synthetic nanopatterned environments by steering receptor clustering and spatial location. HFSP J 2008;2(5):276-85.

48. Kim EJ, Boehm CA, Mata A, Fleischman AJ, Muschler GF, Roy S. Post microtextures accelerate cell proliferation and osteogenesis. Acta Biomater 2010;6(1):160-9.

49. Mussig E, Schulz S, Spatz JP, Ziegler N, Tomakidi P, Steinberg T. Soft micropillar interfaces of distinct biomechanics govern behaviour of periodontal cells. Eur J Cell Biol 2010;89(4):315-25.

50. Nelson CM, Jean RP, Tan JL, Liu WF, Sniadecki NJ, Spector AA, Chen CS. Emergent patterns of growth controlled by multicellular form and mechanics. Proceedings of the National Academy of Sciences of the United States of America 2005;102(33):11594-11599.

51. Ruiz SA, Chen CS. Emergence of patterned stem cell differentiation within multicellular structures. Stem Cells 2008;26(11):2921-7.

52. Matsuzaka K, Walboomers XF, Yoshinari M, Inoue T, Jansen JA. The attachment and growth behavior of osteoblast-like cells on microtextured surfaces. Biomaterials 2003;24(16):2711-9.

53. Soboyejo W, Nemetski B, Allameh S, Marcantonio N, Mercer C, Ricci J. Interactions between MC3T3-E1 cells and textured Ti6Al4V surfaces. Journal of Biomedical Materials Research 2002;62(1):56-72.

54. Kim DH, Wong PK, Park J, Levchenko A, Sun Y. Microengineered platforms for cell mechanobiology. Annu Rev Biomed Eng 2009;11:203-33.

55. Hynes RO. Integrins: bidirectional, allosteric signaling machines. Cell 2002;110(6):673-87.

56. Arnaout MA, Mahalingam B, Xiong JP. Integrin structure, allostery, and bidirectional signaling. Annu Rev Cell Dev Biol 2005;21:381-410.

57. Hynes RO. Integrins: versatility, modulation, and signaling in cell adhesion. Cell 1992;69(1):11-25.

58. Schwartz MA, Baron V. Interactions between mitogenic stimuli, or, a thousand and one connections. Curr Opin Cell Biol 1999;11(2):197-202.

59. Schlaepfer DD, Mitra SK. Multiple connections link FAK to cell motility and invasion. Current Opinion in Genetics & Development 2004;14(1):92-101.

60. Taubenberger AV, Woodruff MA, Bai H, Muller DJ, Hutmacher DW. The effect of unlocking RGD-motifs in collagen I on pre-osteoblast adhesion and differentiation. Biomaterials 2010;31(10):2827-35.

61. Milburn C, Chen J, Cao Y, Oparinde GM, Adeoye MO, Beye A, Soboyejo WO. Investigation of effects of Argenine–Glycine–Aspartate (RGD) and nano-scale titanium coatings on cell spreading and adhesion. Materials Science and Engineering: C 2009;29(1):306-314.

62. Garcia AJ. Get a grip: integrins in cell-biomaterial interactions. Biomaterials 2005;26(36):7525-9.

63. Cavalcanti-Adam EA, Micoulet A, Blummel J, Auernheimer J, Kessler H, Spatz JP. Lateral spacing of integrin ligands influences cell spreading and focal adhesion assembly. Eur J Cell Biol 2006;85(3-4):219-24.

64. Huang J, Gräter SV, Corbellini F, Rinck S, Bock E, Kemkemer R, Kessler H, Ding J, Spatz JP. Impact of Order and Disorder in RGD Nanopatterns on Cell Adhesion. Nano Letters 2009;9(3):1111-1116.

65. Kong HJ, Hsiong S, Mooney DJ. Nanoscale Cell Adhesion Ligand Presentation Regulates Nonviral Gene Delivery and Expression. Nano Letters 2006;7(1):161-166.

66. Koo LY, Irvine DJ, Mayes AM, Lauffenburger DA, Griffith LG. Co-regulation of cell adhesion by nanoscale RGD organization and mechanical stimulus. Journal of Cell Science 2012;115(7):1423-1433.

67. Lee KY, Alsberg E, Hsiong S, Comisar W, Linderman J, Ziff R, Mooney D. Nanoscale Adhesion Ligand Organization Regulates Osteoblast Proliferation and Differentiation. Nano Letters 2004;4(8):1501-1506.

68. Massia SP, Hubbell JA. An RGD spacing of 440 nm is sufficient for integrin alpha V beta 3-mediated fibroblast spreading and 140 nm for focal contact and stress fiber formation. J Cell Biol 1991;114(5):1089-100.

69. Poole K, Khairy K, Friedrichs J, Franz C, Cisneros DA, Howard J, Mueller D. Molecular-scale Topographic Cues Induce the Orientation and Directional Movement of Fibroblasts on Two-dimensional Collagen Surfaces. Journal of Molecular Biology 2005;349(2):380-386.

70. Oberhauser AF, Badilla-Fernandez C, Carrion-Vazquez M, Fernandez JM. The mechanical hierarchies of fibronectin observed with single-molecule AFM. J Mol Biol 2002;319(2):433-47.

71. Barthelemi S, Robinet J, Garnotel R, Antonicelli F, Schittly E, Hornebeck W, Lorimier S. Mechanical forces-induced human osteoblasts differentiation involves MMP-2/MMP-13/MT1-MMP proteolytic cascade. J Cell Biochem 2012;113(3):760-72.

72. Adhikari AS, Chai J, Dunn AR. Mechanical Load Induces a 100-Fold Increase in the Rate of Collagen Proteolysis by MMP-1. Journal of the American Chemical Society 2011;133(6):1686-1689.

73. Vakonakis I, Staunton D, Rooney LM, Campbell ID. Interdomain association in fibronectin: insight into cryptic sites and fibrillogenesis. EMBO J 2007;26(10):2575-83.

74. Hocking DC, Chang CH. Fibronectin matrix polymerization regulates small airway epithelial cell migration. Am J Physiol Lung Cell Mol Physiol 2003;285(1):L169-79.

75. Ellis IR, Jones SJ, Staunton D, Vakonakis I, Norman DG, Potts JR, Milner CM, Meenan NA, Raibaud S, Ohea G and others. Multi-factorial modulation of IGD motogenic potential in MSF (migration stimulating factor). Exp Cell Res 2010;316(15):2465-76.

76. Hynes R. Molecular biology of fibronectin. Annu Rev Cell Biol 1985;1:67-90.

77. Yamada KM. Fibronectins: structure, functions and receptors. Curr Opin Cell Biol 1989;1(5):956-63.

78. Schor SL, Ellis IR, Jones SJ, Baillie R, Seneviratne K, Clausen J, Motegi K, Vojtesek B, Kankova K, Furrie E and others. Migration-stimulating factor: a genetically truncated onco-fetal fibronectin isoform expressed by carcinoma and tumor-associated stromal cells. Cancer Res 2003;63(24):8827-36.

79. Schor SL, Ellis I, Banyard J, Schor AM. Motogenic activity of IGD-containing synthetic peptides. J Cell Sci 1999;112 (Pt 22):3879-88.

80. Keil-Dlouha V, Planchenault T. Potential proteolytic activity of human plasma fibronectin. Proc Natl Acad Sci U S A 1986;83(15):5377-81.

81. Lambert Vidmar S, Lottspeich F, Emod I, Imhoff JM, Keil-Dlouha V. Collagen-binding domain of human plasma fibronectin contains a latent type-IV collagenase. European Journal of Biochemistry 1991;201(1):79-84.

82. Pagano M, Reboud-Ravaux M. Cryptic activities of fibronectin fragments, particularly cryptic proteases. Frontiers in Bioscience-Landmark 2011;16:698-706.

83. Pagano M, Clodic G, Bolbach G, Michiel M, Haddag S, Reboud-Ravaux M. Liberation of an N-terminal proline-rich peptide from the cryptic proteinase of fibronectin by auto-proteolysis. Archives of Biochemistry and Biophysics 2008;479(2):158-162.

84. Boudjennah L, Dalet-Fumeron V, Pagano M. Expression of collagenase/gelatinase activity from basement-membrane fibronectin--isolation after limited proteolysis of a bovine lens capsule and molecular definition of this thiol-dependent zinc metalloproteinase. Eur J Biochem 1998;255(1):246-54.

85. Houard X, Monnot C, Dive V, Corvol P, Pagano M. Vascular smooth muscle cells efficiently activate a new proteinase cascade involving plasminogen and fibronectin. J Cell Biochem 2003;88(6):1188-201.

86. Houard X, Germain S, Gervais M, Michaud A, van den Brule F, Foidart JM, Noel A, Monnot C, Corvol P. Migration-stimulating factor displays HEXXH-dependent catalytic activity important for promoting tumor cell migration. Int J Cancer 2005;116(3):378-84.

87. Millard CJ, Ellis IR, Pickford AR, Schor AM, Schor SL, Campbell ID. The role of the fibronectin IGD motif in stimulating fibroblast migration. J Biol Chem 2007;282(49):35530-5.

88. Fukai F, Ohtaki M, Fujii N, Yajima H, Ishii T, Nishizawa Y, Miyazaki K, Katayama T. Release of biological activities from quiescent fibronectin by a conformational

change and limited proteolysis by matrix metalloproteinases. Biochemistry 1995;34(36):11453-9.

89. Watanabe K, Takahashi H, Habu Y, Kamiya-Kubushiro N, Kamiya S, Nakamura H, Yajima H, Ishii T, Katayama T, Miyazaki K and others. Interaction with heparin and matrix metalloproteinase 2 cleavage expose a cryptic anti-adhesive site of fibronectin. Biochemistry 2000;39(24):7138-44.

90. Steffensen B, Chen Z, Pal S, Mikhailova M, Su J, Wang Y, Xu X. Fragmentation of fibronectin by inherent autolytic and matrix metalloproteinase activities. Matrix Biol 2011;30(1):34-42.

91. Bauvois B. New facets of matrix metalloproteinases MMP-2 and MMP-9 as cell surface transducers: Outside-in signaling and relationship to tumor progression. Biochim Biophys Acta 2012;1825(1):29-36.

92. Bernardo MM, Fridman R. TIMP-2 (tissue inhibitor of metalloproteinase-2) regulates MMP-2 (matrix metalloproteinase-2) activity in the extracellular environment after pro-MMP-2 activation by MT1 (membrane type 1)-MMP. Biochem J 2003;374(Pt 3):739-45.

93. Strongin AY, Collier I, Bannikov G, Marmer BL, Grant GA, Goldberg GI. Mechanism of cell surface activation of 72-kDa type IV collagenase. Isolation of the activated form of the membrane metalloprotease. J Biol Chem 1995;270(10):5331-8.

94. Strongin AY, Marmer BL, Grant GA, Goldberg GI. Plasma membrane-dependent activation of the 72-kDa type IV collagenase is prevented by complex formation with TIMP-2. J Biol Chem 1993;268(19):14033-9.

95. Shi F, Sottile J. MT1-MMP regulates the turnover and endocytosis of extracellular matrix fibronectin. Journal of Cell Science 2011.

96. Rodriguez D, Morrison CJ, Overall CM. Matrix metalloproteinases: what do they not do? New substrates and biological roles identified by murine models and proteomics. Biochim Biophys Acta 2010;1803(1):39-54.

97. McQuibban GA, Gong JH, Tam EM, McCulloch CA, Clark-Lewis I, Overall CM. Inflammation dampened by gelatinase A cleavage of monocyte chemoattractant protein-3. Science 2000;289(5482):1202-6.

98. Ellerbroek SM, Wu YI, Overall CM, Stack MS. Functional Interplay between Type I Collagen and Cell Surface Matrix Metalloproteinase Activity. Journal of Biological Chemistry 2001;276(27):24833-24842.

99. Gilles C, Polette M, Seiki M, Birembaut P, Thompson EW. Implication of collagen type I-induced membrane-type 1-matrix metalloproteinase expression and matrix

metalloproteinase-2 activation in the metastatic progression of breast carcinoma. Lab Invest 1997;76(5):651-60.

100. Pilcher BK, Dumin JA, Sudbeck BD, Krane SM, Welgus HG, Parks WC. The activity of collagenase-1 is required for keratinocyte migration on a type I collagen matrix. J Cell Biol 1997;137(6):1445-57.

101. Juin A, Billottet C, Moreau V, Destaing O, Albiges-Rizo C, Rosenbaum J, Génot E, Saltel F. Physiological type I collagen organization induces the formation of a novel class of linear invadosomes. Molecular Biology of the Cell 2011.

102. Loffek S, Schilling O, Franzke CW. Series "matrix metalloproteinases in lung health and disease": Biological role of matrix metalloproteinases: a critical balance. Eur Respir J 2011;38(1):191-208.

103. Mosig RA, Dowling O, DiFeo A, Ramirez MC, Parker IC, Abe E, Diouri J, Aqeel AA, Wylie JD, Oblander SA and others. Loss of MMP-2 disrupts skeletal and craniofacial development and results in decreased bone mineralization, joint erosion and defects in osteoblast and osteoclast growth. Hum Mol Genet 2007;16(9):1113-23.

104. Holmbeck K, Bianco P, Caterina J, Yamada S, Kromer M, Kuznetsov SA, Mankani M, Robey PG, Poole AR, Pidoux I and others. MT1-MMP-deficient mice develop dwarfism, osteopenia, arthritis, and connective tissue disease due to inadequate collagen turnover. Cell 1999;99(1):81-92.

105. Manduca P, Castagnino A, Lombardini D, Marchisio S, Soldano S, Ulivi V, Zanotti S, Garbi C, Ferrari N, Palmieri D. Role of MT1-MMP in the osteogenic differentiation. Bone 2009;44(2):251-265.

106. Lu C, Li X-Y, Hu Y, Rowe RG, Weiss SJ. MT1-MMP controls human mesenchymal stem cell trafficking and differentiation. Blood 2010;115(2):221-229.

107. Sariahmetoglu M, Crawford BD, Leon H, Sawicka J, Li L, Ballermann BJ, Holmes C, Berthiaume LG, Holt A, Sawicki G and others. Regulation of matrix metalloproteinase-2 (MMP-2) activity by phosphorylation. FASEB J 2007;21(10):2486-95.

108. Lieu S, Hansen E, Dedini R, Behonick D, Werb Z, Miclau T, Marcucio R, Colnot C. Impaired remodeling phase of fracture repair in the absence of matrix metalloproteinase-2. Dis Model Mech 2011;4(2):203-11.

109. D'Alonzo RC, Kowalski AJ, Denhardt DT, Nickols GA, Partridge NC. Regulation of collagenase-3 and osteocalcin gene expression by collagen and osteopontin in differentiating MC3T3-E1 cells. J Biol Chem 2002;277(27):24788-98.

110. Filanti C, Dickson GR, Di Martino D, Ulivi V, Sanguineti C, Romano P, Palermo C, Manduca P. The expression of metalloproteinase-2, -9, and -14 and of tissue

inhibitors-1 and -2 is developmentally modulated during osteogenesis in vitro, the mature osteoblastic phenotype expressing metalloproteinase-14. J Bone Miner Res 2000;15(11):2154-68.

111. Janssens K, ten Dijke P, Janssens S, Van Hul W. Transforming growth factor-beta1 to the bone. Endocr Rev 2005;26(6):743-74.

112. Seyedin SM, Thomas TC, Thompson AY, Rosen DM, Piez KA. Purification and characterization of two cartilage-inducing factors from bovine demineralized bone. Proc Natl Acad Sci U S A 1985;82(8):2267-71.

113. Ehnert S, Baur J, Schmitt A, Neumaier M, Lucke M, Dooley S, Vester H, Wildemann B, Stockle U, Nussler AK. TGF-beta1 as possible link between loss of bone mineral density and chronic inflammation. PLoS ONE 2010;5(11):e14073.

114. Miyazono K, Olofsson A, Colosetti P, Heldin CH. A role of the latent TGF-beta 1-binding protein in the assembly and secretion of TGF-beta 1. EMBO J 1991;10(5):1091-101.

115. Dallas SL, Sivakumar P, Jones CJ, Chen Q, Peters DM, Mosher DF, Humphries MJ, Kielty CM. Fibronectin regulates latent transforming growth factor-beta (TGF beta) by controlling matrix assembly of latent TGF beta-binding protein-1. J Biol Chem 2005;280(19):18871-80.

116. Todorovic V, Rifkin DB. LTBPs, more than just an escort service. J Cell Biochem 2012;113(2):410-8.

117. Sivakumar P, Czirok A, Rongish BJ, Divakara VP, Wang YP, Dallas SL. New insights into extracellular matrix assembly and reorganization from dynamic imaging of extracellular matrix proteins in living osteoblasts. J Cell Sci 2006;119(Pt 7):1350-60.

118. Fontana L, Chen Y, Prijatelj P, Sakai T, Fassler R, Sakai LY, Rifkin DB. Fibronectin is required for integrin alphavbeta6-mediated activation of latent TGF-beta complexes containing LTBP-1. FASEB J 2005;19(13):1798-808.

119. Gentry LE, Webb NR, Lim GJ, Brunner AM, Ranchalis JE, Twardzik DR, Lioubin MN, Marquardt H, Purchio AF. Type 1 transforming growth factor beta: amplified expression and secretion of mature and precursor polypeptides in Chinese hamster ovary cells. Mol Cell Biol 1987;7(10):3418-27.

120. Annes JP, Munger JS, Rifkin DB. Making sense of latent TGFbeta activation. J Cell Sci 2003;116(Pt 2):217-24.

121. Yu Q, Stamenkovic I. Cell surface-localized matrix metalloproteinase-9 proteolytically activates TGF-beta and promotes tumor invasion and angiogenesis. Genes Dev 2000;14(2):163-76.

122. Karsdal MA, Larsen L, Engsig MT, Lou H, Ferreras M, Lochter A, Delaisse JM, Foged NT. Matrix metalloproteinase-dependent activation of latent transforming growth factor-beta controls the conversion of osteoblasts into osteocytes by blocking osteoblast apoptosis. J Biol Chem 2002;277(46):44061-7.

123. Alfranca A, Lopez-Oliva JM, Genis L, Lopez-Maderuelo D, Mirones I, Salvado D, Quesada AJ, Arroyo AG, Redondo JM. PGE2 induces angiogenesis via MT1-MMP-mediated activation of the TGFbeta/Alk5 signaling pathway. Blood 2008;112(4):1120-8.

124. Thiolloy S, Edwards J, R., Fingleton B, Rifkin D, B., Matrisian L, M., Lynch C, C. An Osteoblast-Derived Proteinase Controls Tumor Cell Survival via TGF-beta Activation in the Bone Microenvironment. PLoS ONE 2012;7(1).

125. Worthington JJ, Klementowicz J, E., Travis M, A. TGFβ: a sleeping giant awoken by integrins. Trends in Biochemical Sciences 2011;36(1):47-54.

126. Unsold C, Hyytiainen M, Bruckner-Tuderman L, Keski-Oja J. Latent TGF-beta binding protein LTBP-1 contains three potential extracellular matrix interacting domains. J Cell Sci 2001;114(Pt 1):187-197.

127. Hyytiainen M, Penttinen C, Keski-Oja J. Latent TGF-beta binding proteins: extracellular matrix association and roles in TGF-beta activation. Crit Rev Clin Lab Sci 2004;41(3):233-64.

128. Annes JP, Chen Y, Munger JS, Rifkin DB. Integrin αVβ6-mediated activation of latent TGF-β requires the latent TGF-β binding protein-1. The Journal of Cell Biology 2004;165(5):723-734.

129. Munger JS, Huang X, Kawakatsu H, Griffiths MJ, Dalton SL, Wu J, Pittet JF, Kaminski N, Garat C, Matthay MA and others. The integrin alpha v beta 6 binds and activates latent TGF beta 1: a mechanism for regulating pulmonary inflammation and fibrosis. Cell 1999;96(3):319-28.

130. Wipff PJ, Rifkin DB, Meister JJ, Hinz B. Myofibroblast contraction activates latent TGF-beta1 from the extracellular matrix. J Cell Biol 2007;179(6):1311-23.

131. Shi M, Zhu J, Wang R, Chen X, Mi L, Walz T, Springer TA. Latent TGF-beta structure and activation. Nature 2011;474(7351):343-9.

132. Atti E, Gomez S, Wahl SM, Mendelsohn R, Paschalis E, Boskey AL. Effects of transforming growth factor-beta deficiency on bone development: a Fourier transform-infrared imaging analysis. Bone 2002;31(6):675-84.

133. Tang Y, Wu X, Lei W, Pang L, Wan C, Shi Z, Zhao L, Nagy TR, Peng X, Hu J and others. TGF-beta1-induced migration of bone mesenchymal stem cells couples bone resorption with formation. Nat Med 2009;15(7):757-65.

134. Choi JY, Lee BH, Song KB, Park RW, Kim IS, Sohn KY, Jo JS, Ryoo HM. Expression patterns of bone-related proteins during osteoblastic differentiation in MC3T3-E1 cells. J Cell Biochem 1996;61(4):609-18.

135. Maeda S, Hayashi M, Komiya S, Imamura T, Miyazono K. Endogenous TGF-beta signaling suppresses maturation of osteoblastic mesenchymal cells. EMBO J 2004;23(3):552-63.

136. Sowa H, Kaji H, Yamaguchi T, Sugimoto T, Chihara K. Activations of ERK1/2 and JNK by transforming growth factor beta negatively regulate Smad3-induced alkaline phosphatase activity and mineralization in mouse osteoblastic cells. J Biol Chem 2002;277(39):36024-31.

137. Ignotz RA, Massague J. Transforming growth factor-beta stimulates the expression of fibronectin and collagen and their incorporation into the extracellular matrix. J Biol Chem 1986;261(9):4337-45.

138. Centrella M, Casinghino S, Kim J, Pham T, Rosen V, Wozney J, McCarthy TL. Independent changes in type I and type II receptors for transforming growth factor beta induced by bone morphogenetic protein 2 parallel expression of the osteoblast phenotype. Mol Cell Biol 1995;15(6):3273-81.

139. Takeuchi Y, Nakayama K, Matsumoto T. Differentiation and cell surface expression of transforming growth factor-beta receptors are regulated by interaction with matrix collagen in murine osteoblastic cells. J Biol Chem 1996;271(7):3938-44.

140. Mohammad KS, Chen CG, Balooch G, Stebbins E, McKenna CR, Davis H, Niewolna M, Peng XH, Nguyen DH, Ionova-Martin SS and others. Pharmacologic inhibition of the TGF-beta type I receptor kinase has anabolic and anti-catabolic effects on bone. PLoS ONE 2009;4(4):e5275.

141. Alliston T, Choy L, Ducy P, Karsenty G, Derynck R. TGF-beta-induced repression of CBFA1 by Smad3 decreases cbfa1 and osteocalcin expression and inhibits osteoblast differentiation. EMBO J 2001;20(9):2254-72.

142. Graille M, Pagano M, Rose T, Ravaux MR, van Tilbeurgh H. Zinc induces structural reorganization of gelatin binding domain from human fibronectin and affects collagen binding. Structure 2010;18(6):710-8.

143. O'Dell BL, Browning JD. Zinc Deprivation Impairs Growth Factor-Stimulated Calcium Influx into Murine 3T3 cells Associated with Decreased Cell Proliferation. J Nutr 2011.

144. Yamaguchi M. Nutritional factors and bone homeostasis: synergistic effect with zinc and genistein in osteogenesis. Mol Cell Biochem 2012;366(1-2):201-21.

145. Fukada T, Civic N, Furuichi T, Shimoda S, Mishima K, Higashiyama H, Idaira Y, Asada Y, Kitamura H, Yamasaki S and others. The zinc transporter SLC39A13/ZIP13 is required for connective tissue development; its involvement in BMP/TGF-beta signaling pathways. PLoS ONE 2008;3(11):e3642.

146. Fukada T, Hojyo S, Furuichi T. Zinc signal: a new player in osteobiology. J Bone Miner Metab 2013;31(2):129-35.

147. Fukada T, Yamasaki S, Nishida K, Murakami M, Hirano T. Zinc homeostasis and signaling in health and diseases: Zinc signaling. J Biol Inorg Chem 2011;16(7):1123-34.

148. Nagata M, Kayanoma M, Takahashi T, Kaneko T, Hara H. Marginal zinc deficiency in pregnant rats impairs bone matrix formation and bone mineralization in their neonates. Biol Trace Elem Res 2011;142(2):190-9.

149. Cousins RJ, Liuzzi JP, Lichten LA. Mammalian Zinc Transport, Trafficking, and Signals. Journal of Biological Chemistry 2006;281(34):24085-24089.

150. Alcantara EH, Lomeda RA, Feldmann J, Nixon GF, Beattie JH, Kwun IS. Zinc deprivation inhibits extracellular matrix calcification through decreased synthesis of matrix proteins in osteoblasts. Mol Nutr Food Res 2011;55(10):1552-60.

151. Rossi L, Migliaccio S, Corsi A, Marzia M, Bianco P, Teti A, Gambelli L, Cianfarani S, Paoletti F, Branca F. Reduced growth and skeletal changes in zinc-deficient growing rats are due to impaired growth plate activity and inanition. J Nutr 2001;131(4):1142-6.

152. Aaseth J, Boivin G, Andersen O. Osteoporosis and trace elements--an overview. J Trace Elem Med Biol 2012;26(2-3):149-52.

153. Hall SL, Dimai HP, Farley JR. Effects of zinc on human skeletal alkaline phosphatase activity in vitro. Calcif Tissue Int 1999;64(2):163-72.

154. Hie M, Iitsuka N, Otsuka T, Nakanishi A, Tsukamoto I. Zinc deficiency decreases osteoblasts and osteoclasts associated with the reduced expression of Runx2 and RANK. Bone 2011;49(6):1152-9.

155. Lauffenburger DA, Linderman JJ. Receptors : models for binding, trafficking, and signaling. New York: Oxford University Press; 1996.

156. Cao Y, Chen J, Adeoye MO, Soboyejo WO. Investigation of the spreading and adhesion of human osteosarcoma cells on smooth and micro-grooved polydimethylsiloxane surfaces. Materials Science and Engineering: C 2009;29(1):119-125.

157. Bruckner-Tuderman L, von der Mark K, Pihlajaniemi T, Unsicker K. Cell interactions with the extracellular matrix. Cell and Tissue Research 2010;339(1):1-5.

158. Malizos KN, Papatheodorou LK. The healing potential of the periosteum: Molecular aspects. Injury 2005;36(3, Supplement):S13-S19.

159. Baksh D, Song L, Tuan RS. Adult mesenchymal stem cells: characterization, differentiation, and application in cell and gene therapy. J Cell Mol Med 2004;8(3):301-16.

160. Eghbali-Fatourechi GZ, Lamsam J, Fraser D, Nagel D, Riggs BL, Khosla S. Circulating osteoblast-lineage cells in humans. N Engl J Med 2005;352(19):1959-66.

161. Rumi MN, Deol GS, Singapuri KP, Pellegrini VD, Jr. The origin of osteoprogenitor cells responsible for heterotopic ossification following hip surgery: an animal model in the rabbit. J Orthop Res 2005;23(1):34-40.

162. Ichida M, Yui Y, Yoshioka K, Tanaka T, Wakamatsu T, Yoshikawa H, Itoh K. Changes in cell migration of mesenchymal cells during osteogenic differentiation. FEBS Lett 2011;585(24):4018-24.

163. Su WT, Yang JY, Lin CD, Chu IM. Control cell behavior on physical topographical surface. Japanese Journal of Applied Physics Part 1-Regular Papers Short Notes & Review Papers 2004;43(6B):3806-3809.

164. Lim JY, Dreiss AD, Zhou ZY, Hansen JC, Siedlecki CA, Hengstebeck RW, Cheng J, Winograd N, Donahue HJ. The regulation of integrin-mediated osteoblast focal adhesion and focal adhesion kinase expression by nanoscale topography. Biomaterials 2007;28(10):1787-1797.

165. Zahor D, Radko A, Vago R, Gheber LA. Organization of mesenchymal stem cells is controlled by micropatterned silicon substrates. Materials Science & Engineering C-Biomimetic and Supramolecular Systems 2007;27(1):117-121.

166. Wilkinson CDW, Riehle M, Wood M, Gallagher J, Curtis ASG. The use of materials patterned on a nano- and micro-metric scale in cellular engineering. Materials Science & Engineering C-Biomimetic and Supramolecular Systems 2002;19(1-2):263-269.

167. Ohara PT, Buck RC. Contact guidance in vitro : A light, transmission, and scanning electron microscopic study. Experimental Cell Research 1979;121(2):235-249.

168. Wojciak-Stothard B, Madeja Z, Korohoda W, Curtis A, Wilkinson C. Activation of macrophage-like cells by multiple grooved substrata - topographical control of cell behavior. Cell Biology International 1995;19(6):485-490.

169. Dickinson RB. A generalized transport model for biased cell migration in an anisotropic environment. J Math Biol 2000;40(2):97-135.

170. Ridley AJ, Schwartz MA, Burridge K, Firtel RA, Ginsberg MH, Borisy G, Parsons JT, Horwitz AR. Cell migration: integrating signals from front to back. Science 2003;302(5651):1704-9.

171. Boyan BD, Batzer R, Kieswetter K, Liu Y, Cochran DL, Szmuckler-Moncler S, Dean DD, Schwartz Z. Titanium surface roughness alters responsiveness of MG63 osteoblast-like cells to 1 alpha,25-(OH)2D3. J Biomed Mater Res 1998;39(1):77-85.

172. Taylor KM, Hiscox S, Nicholson RI, Hogstrand C, Kille P. Protein kinase CK2 triggers cytosolic zinc signaling pathways by phosphorylation. Sci Signal 2012;5(210):ra11.

173. Taylor KM, Kille P, Hogstrand C. Protein kinase CK2 opens the gate for zinc signaling. Cell Cycle. United States; 2012. p 1863-4.

174. Hojyo S, Fukada T, Shimoda S, Ohashi W, Bin BH, Koseki H, Hirano T. The Zinc Transporter SLC39A14/ZIP14 Controls G-Protein Coupled Receptor-Mediated Signaling Required for Systemic Growth. PLoS ONE 2011;6(3).

175. Inoue K, Matsuda K, Itoh M, Kawaguchi H, Tomoike H, Aoyagi T, Nagai R, Hori M, Nakamura Y, Tanaka T. Osteopenia and male-specific sudden cardiac death in mice lacking a zinc transporter gene, Znt5. Hum Mol Genet 2002;11(15):1775-84.

176. Fujita T, Azuma Y, Fukuyama R, Hattori Y, Yoshida C, Koida M, Ogita K, Komori T. Runx2 induces osteoblast and chondrocyte differentiation and enhances their migration by coupling with PI3K-Akt signaling. J Cell Biol 2004;166(1):85-95.

177. Hong SM, et al. Hydrophilic Surface Modification of PDMS Using Atmospheric RF Plasma. Journal of Physics: Conference Series 2006;34(1):656.

178. Prasad AS. Zinc in human health: effect of zinc on immune cells. Mol Med 2008;14(5-6):353-7.

179. Cho YE, Lomeda RA, Ryu SH, Lee JH, Beattie JH, Kwun IS. Cellular Zn depletion by metal ion chelators (TPEN, DTPA and chelex resin) and its application to osteoblastic MC3T3-E1 cells. Nutr Res Pract 2007;1(1):29-35.

180. Byrne H, Drasdo D. Individual-based and continuum models of growing cell populations: a comparison. J Math Biol 2009;58(4-5):657-87.

181. Rudolf E, Klvacova L, John S, Cervinka M. Zinc alters cytoskeletal integrity and migration in colon cancer cells. Acta Medica (Hradec Kralove) 2008;51(1):51-7.

182. Lymburner S, McLeod S, Purtzki M, Roskelley C, Xu Z. Zinc inhibits magnesium-dependent migration of human breast cancer MDA-MB-231 cells on fibronectin. The Journal of Nutritional Biochemistry 2013;24(6):1034-1040.

183. Wojciak-Stothard B, Curtis A, Monaghan W, Macdonald K, Wilkinson C. Guidance and activation of murine macrophages by nanometric scale topography. Experimental Cell Research 1996;223(2):426-435.

184. Chen SY. Studies on cell migration, adenylate cyclase and membrane-coating granules in the buccal epithelium of the zinc-deficient rabbit, including the influence of isoproterenol. Arch Oral Biol 1988;33(9):645-51.

185. Mehrotra S, Hunley SC, Pawelec KM, Zhang L, Lee I, Baek S, Chan C. Cell adhesive behavior on thin polyelectrolyte multilayers: cells attempt to achieve homeostasis of its adhesion energy. Langmuir 2010;26(15):12794-802.

186. Soboyejo W, Nemetski B, Allameh S, Marcantonio N, Mercer C, Ricci J. Interactions between MC3T3-E1 cells and textured Ti6Al4V surfaces. J Biomed Mater Res 2002;62(1):56-72.

187. Elineni KK, Gallant ND. Regulation of cell adhesion strength by peripheral focal adhesion distribution. Biophys J 2011;101(12):2903-11.

188. Ingber DE. Mechanical control of tissue morphogenesis during embryological development. Int J Dev Biol 2006;50(2-3):255-66.

189. Depoortere I. GI functions of GPR39: novel biology. Curr Opin Pharmacol 2012;12(6):647-52.

190. Cooper LF. A role for surface topography in creating and maintaining bone at titanium endosseous implants. J Prosthet Dent 2000;84(5):522-34.

191. Oh S, Brammer KS, Li YS, Teng D, Engler AJ, Chien S, Jin S. Stem cell fate dictated solely by altered nanotube dimension. Proc Natl Acad Sci U S A 2009;106(7):2130-5.

192. Dalby MJ, Gadegaard N, Tare R, Andar A, Riehle MO, Herzyk P, Wilkinson CD, Oreffo RO. The control of human mesenchymal cell differentiation using nanoscale symmetry and disorder. Nat Mater 2007;6(12):997-1003.

193. Thery M. Micropatterning as a tool to decipher cell morphogenesis and functions. Journal of Cell Science 2010;123(24):4201-4213.

194. Mizutani T, Haga H, Kawabata K. Cellular stiffness response to external deformation: Tensional homeostasis in a single fibroblast. Cell Motility and the Cytoskeleton 2004;59(4):242-248.

195. McBeath R, Pirone DM, Nelson CM, Bhadriraju K, Chen CS. Cell shape, cytoskeletal tension, and RhoA regulate stem cell lineage commitment. Dev Cell 2004;6(4):483-95.

196. Seo CH, Furukawa K, Montagne K, Jeong H, Ushida T. The effect of substrate microtopography on focal adhesion maturation and actin organization via the RhoA/ROCK pathway. Biomaterials 2011;32(36):9568-75.

197. Dorst K, Rammelkamp D, Hadjiargyrou M, Gersappe D, Meng Y. The Effect of Exogenous Zinc Concentration on the Responsiveness of MC3T3-E1 Pre-Osteoblasts to Surface Microtopography: Part I (Migration). Materials 2013;6(12):5517-5532.

198. Kim IS, Song YM, Hwang SJ. Osteogenic Responses of Human Mesenchymal Stromal Cells to Static Stretch. Journal of Dental Research 2010;89(10):1129-1134.

199. Ma ZJ, Misawa H, Yamaguchi M. Stimulatory effect of zinc on insulin-like growth factor-I and transforming growth factor-beta1 production with bone growth of newborn rats. Int J Mol Med 2001;8(6):623-8.

200. Sudo H, Kodama HA, Amagai Y, Yamamoto S, Kasai S. In vitro differentiation and calcification in a new clonal osteogenic cell line derived from newborn mouse calvaria. J Cell Biol 1983;96(1):191-8.

201. Hoemann CD, El-Gabalawy H, McKee MD. In vitro osteogenesis assays: influence of the primary cell source on alkaline phosphatase activity and mineralization. Pathol Biol (Paris) 2009;57(4):318-23.

202. Salasznyk RM, Klees RF, Williams WA, Boskey A, Plopper GE. Focal adhesion kinase signaling pathways regulate the osteogenic differentiation of human mesenchymal stem cells. Exp Cell Res 2007;313(1):22-37.

203. Wang D, Christensen K, Chawla K, Xiao G, Krebsbach PH, Franceschi RT. Isolation and characterization of MC3T3-E1 preosteoblast subclones with distinct in vitro and in vivo differentiation/mineralization potential. J Bone Miner Res 1999;14(6):893-903.

204. Tang N, Song WX, Luo J, Haydon RC, He TC. Osteosarcoma development and stem cell differentiation. Clin Orthop Relat Res 2008;466(9):2114-30.

205. Kanno S, Anuradha CD, Hirano S. Chemotactic responses of osteoblastic MC3T3-E1 cells toward zinc chloride. Biol Trace Elem Res 2001;83(1):49-55.

206. Soboyejo WO, Nemetski B, Allameh S, Marcantonio N, Mercer C, Ricci J. Interactions between MC3T3-E1 cells and textured Ti6Al4V surfaces. J Biomed Mater Res 2002;62(1):56-72.